PNPLA3 I148M drives ferroptosis due to decline of NAD+, predisposing to fatty liver disease

By

Kaitlyn Ashley Vitangcol

A dissertation submitted in partial satisfaction of the
Requirements for the degree of
Doctor in Philosophy
In
Metabolic Biology
In the
Graduate Division
Of the
University of California, Berkeley

Committee in charge:
Professor Andreas Stahl, Chair
Professor Dirk Hockemeyer
Professor James Olzmann
Professor Wally Wang

Spring 2026

Abstract

PNPLA3 I148M drives ferroptosis due to decline of NAD+, predisposing to fatty liver disease

By

Kaitlyn Ashley Vitangcol

Doctor in Philosophy in Metabolic Biology

University of California Berkeley

Professor Andreas Stahl, Chair

Metabolic dysfunction-associated steatotic liver disease (MASLD) has been the most prevalent liver disease over the past few decades, posing a substantial health concern due to its association with obesity, insulin resistance, and metabolic syndrome[1]. Genome-wide association studies (GWAS) have identified specific genetic variations that have been associated with an increased risk of MASLD, with one of the most common candidates being *Patatin-like phospholipase domain-containing 3* (*PNPLA3*).[2]

Although the I148M variant is suggested to promote MASLD through increased susceptibility ferroptosis (a non-apoptotic, iron-dependent form of cell death), the underlying causal mechanisms are not fully elucidated. Recent studies on wild-type *PNPLA3* indicate that it mediates the mobilization of polyunsaturated fatty acids (PUFAs) to phospholipids to promote very low-density lipoprotein (VLDL) secretion; however, PL-PUFA are known to promote ferroptosis susceptibility, creating a mechanistic discrepancy that makes the role of *PNPLA3* in ferroptosis unclear. To address this, we generated isogenic human induced pluripotent stem cells (hiPSCs) expressing either 148I or 148M *PNPLA3* variants and differentiated them into hepatocytes to investigate this link.

We discovered that 148M hepatocytes show significantly decreased NAPRT1 expression, leading to substantially suppressed NAD^+ biosynthesis. Because NAD^+ is essential for the antioxidant action of ferroptosis suppressor protein 1 (FSP1) and GPX4 action, diminished NAD^+ could compromise their activity. Therefore, we hypothesize that 148M hepatocytes are more susceptible to ferroptosis due to reduced NAD^+, GPX4 and FSP1 function, thereby driving the onset of MASLD. These findings provide a promising mechanistic framework allowing for potential therapeutics to be tested to target ferroptosis driving MASLD in I148M carriers.

Table of Contents

Table of Figures

Acknowledgements

This PhD would not have been possible without the incredible people in my life. I would first like to thank my parents. You both have been instrumental in my life, from having great expectations for me, while giving me the tools to meet that. I wouldn't have been able to achieve what I have today if it weren't for you both showing me as I've grown up how much dedication and work ethic can push you far in your career.

To my younger sisters, Alyssa, Lexi and Britney, you are all the strongest girls I know, and everything you have achieved has been so inspiring that it helped me keep pushing through. I'm so proud of you all for what you have done with your lives, and I hope you are proud of me as well as your Ate!

To my PI, Andreas, thank you for taking me into your lab and trusting me to take on this project head on. I've learned so much from my experience in your lab and feel as though I have become a better scientist under your guidance. It has been an honor to be a part of your lab over the past 6 years!

To my thesis committee, Wally, James and Dirk, thank you so much for taking the time to meet with me each year, giving me so much guidance. You all helped me gain confidence to defend my dissertation. This journey wouldn't have been possible without your advice.

To Hanqin, I wouldn't have been able to grow as fast as a scientist if it weren't for your help and guidance. This dissertation wouldn't have been possible at all if it weren't for you to give me the tools to generate these cells. My career trajectory has become so much clearer since working in your lab. Thank you for everything you have done for me!

To my lab, thank you all for being such a welcoming community. To Jessica, Amanda, Irene and Lu (Honorary Stahl lab member), I'm so grateful for all the times we had together, all the potluck dinners have been so much fun, each of those times has helped me keep sane. To Yuchen, thank you for all your help with putting together the finishing touches of this project! Grabbing coffee together each morning may have given me a new coffee addiction, but chatting with you has been so instrumental in the progress in my project! To Lin, thank you for your incredible wisdom, being the first to guide me through my projects, and helping me with analyzing data! I have learned so much from you. And thank you for all the recommendations for Columbus, Ohio, it has made my next new home feel exciting!

My best friends in the MBN department, Liza, Lindsey, Rachelle, Sophia, and Jinyu, you all have been my rock going through this entire process. I don't think I could have asked a better group of friends to go through this PhD process other than you all. From the girls' nights out to SF, to the chill Golden Bachelor watch parties, you have made my time here at UC Berkeley so incredible. I can't wait until it is your time to walk up the stage and finish this journey as well!

To my pole dancing community, my pole siblings Anna, Ella and Jeff, and my pole instructors Celia and Amelia, you have shown me that life can be joyous and whimsical. Whenever I was stressed out from working for hours on end in lab, you were always there to give me a proper

escape. Spinning on the pole, and dancing to my heart's content with you all has made me feel so strong and free. Thank you for giving me such an incredible community.

Lastly, I would like to thank the love of my life, Kenny. I don't think I would have been able to finish this PhD without your love and support. The long days and nights of us going on writing dates at Fieldwork Brewing were always the best. You edited and absolutely grilled my writing (which was desperately needed), you cooked me meals whenever I came home late from lab and gave me a shoulder to cry on whenever I felt as if I was not doing enough. You have been the force that helped hold me together as I went through this difficult process. Thank you for always cheering me on and giving me the support I needed. I love you so much.

I would like to dedicate this PhD to my younger self, who originally didn't believe that such an achievement could be possible for her. I would like to remind her that with so many people cheering her on, she can achieve anything.

Chapter 1: PNPLA3 role in MASLD progression

Contents in this chapter are modified from the following manuscript

1.1 Introduction Liver and MASLD: Clinical and Physiological Context

1.1.1 Liver Structure and Metabolic Function

The liver serves as one of the main central organs regulating whole body homeostasis. It maintains glucose and fatty acid metabolism to keep the body healthy. Blood glucose enters the liver via a plasma membrane transporter, GLUT2. In the liver, glucose is phosphorylated by glucokinase to glucose 6-phosphate. During the post-prandial state, glucose 6-phosphate is used for glycogen synthesize for glucose storage through the transfer of the phosphate between the 6- to the 1- carbon position by Phosphoglucomutase (PGM-1). The glucose 1-phosphate is then converted into UDP-glucose by UDP-glucose pyrophosphorylase to create the precursor of glycogen. The liver will build up the stores for glucose through glycogen generation to later be used for energy during fasting states.

Free fatty acids are emulsified in the GI tract by bile salts secreted from the bile duct to be packaged into micelles. They are absorbed in the brush border membrane of enterocytes via CD36 and FATP to be esterified into triglycerides (TAG). TAG is packaged into chylomicrons and transported out through the lymph. They are absorbed in the brush border membrane of enterocytes via CD36 and FATP, then bound by FABP to be trafficked over to the ER to be esterified into triglycerides (TAG). TAG is packaged into apolipoprotein (apo) B48-containing chylomicrons and transported over to the Golgi for further processing, then secreted out of the enterocyte through the lymphatic system[3]. Majority of the fatty acids are delivered to adipose tissue, the storage organ for fat via lipoprotein lipase (LPL).

Leftover triglycerides in the chylomicron are delivered to the liver through FATP4, FATP2, FATP5 and CD36. Most liver TAG sources come from the adipose tissue releasing FA through lipolysis. Intracellular fatty acids are bound by fatty acid binding proteins (FABP) to be transported to ER to be stored in lipid droplets (LD) esterified as TAG[4]. Intracellular fatty acids are bound by fatty acid binding proteins (FABP) to be transported to ER to be stored in lipid droplets (LD) esterified as TAG[4].

Liver acts as the central organ for fat metabolism via beta oxidation, having a constant flux of fat from adipose tissue, chylomicrons, and the endogenous generation of fatty acids through de novo lipogenesis (DNL). Medium chain fatty acids enter the liver via the portal vein, while chylomicron remnants carrying dietary fatty acids are delivered via the hepatic artery, then extracted out by lipoprotein lipase (LPL). Fatty acids are transported into the hepatocytes through fatty acid transport protein like FATP5 and CD36[5]. The liver can metabolize this accumulation of fatty acid through beta oxidation, secrete them out for circulation via very-low density lipoproteins (VLDL) or esterified to form phospholipids. This balance between influx and efflux of fatty acids is integral for maintaining the metabolic function of the liver[6]. Fatty acids are transported into the hepatocytes through fatty acid transport protein like FATP5 and CD36[5]. The liver can metabolize this accumulation of fatty acid through beta oxidation, secrete them out for circulation via very-low density lipoproteins (VLDL) or esterified to form phospholipids. This balance between influx and efflux of fatty acids is integral for maintaining the metabolic health of the liver[6] (Fig 2.).

The liver can also contribute to the accumulation of fatty acids by taking non-lipid precursors such as acetyl-CoA, and synthesizing into fatty acids, through de novo lipogenesis. Dietary glucose, or glycogen releasing glucose, will provide sources of acetyl-CoA for DNL. Insulin will stimulate the upregulation of SREBP1, which will increase the expression of DNL genes like fatty acid

synthase (FAS) and acetyl-CoA Carboxylase (ACC)[6,7]. Acetyl-CoA is carboxylated into malonyl-CoA, which inhibits CPT1 on the mitochondria to suppress fatty acid oxidation. The malonyl CoA is then elongated by FAS to form a fatty acid, the main product being 16-carbon palmitate. The fatty acid is then esterified onto a glycerol backbone to start the formation of TAG. Endogenous and exogenous TAG will enter the ER to initiate the formation of the lipid droplet for storage. A healthy liver will have less than 5% of hepatocytes with accumulated fatty acids[8]

During the fasted state, TAG is hydrolyzed by adipose triglyceride lipase (ATGL) bound on the surface of the lipid droplet activated by CGI-58 to release FFA and diacylglycerol. Diacylglycerol is then hydrolyzed by hormone-sensitive lipase (HSL) releasing FFA and monoacylglycerol (MAG). MAG is then fully hydrolyzed by MAG lipase (MGL) to release glycerol and FFA from the lipid droplet. FFA are transported by the FABP to the ER for packaging for VLDL-TG secretion. FFA is reesterified by diglyceride acyltransferase (DGAT) to synthesize TAG. In the ER, ApoB100 is folded by MTTP to form the nascent VLDL. TAG is supplied to the nascent VLDL and continues to be lipidated with the help of transmembrane 6 superfamily member 2 (TM6SF2). The lipidated VLDL is then transported to the Golgi for further VLDL maturation and secretion to the plasma[9].

The elevated flux of fatty acids from the adipose tissue to the liver also drives hepatic fatty acid oxidation. Fatty acids are transported the nucleus to activate to the nuclear receptor protein PPARalpha to promote fatty acid oxidation (FAO), increasing the expression of carnitine palmitoyl-transferases 1 and 2 (CPT1 and CPT2) in the mitochondria and to generate energy. This will allow for a balance between lipid uptake and breakdown[10,11]. The elevated flux of fatty acids from the adipose tissue to the liver or from DNL also exacerbates hepatic fatty acid oxidation.

The processes of lipid uptake and breakdown need to be maintained in a tight equilibrium to keep the function of the liver healthy. Dysfunction of the tightly regulated liver function predisposes to the development of metabolic dysfunction-associated fatty liver disease (MAFLD), through the over accumulation of fatty acids, driving lipotoxicity, and fibrosis.

1.1.2 Introduction to MASLD

The global prevalence of metabolic dysfunction-associated fatty liver disease (MAFLD) has affected up to 38% of the adult population[12–14]. It ranges from different stages of hepatic damage, starting from metabolic dysfunction-associated steatotic liver disease (MASLD), determined by >5% of hepatocytes containing fat[15], to metabolic dysfunction-associated steatohepatitis (MASH) diagnosed by inflammation and fibrosis[16], which then finally progresses to cirrhosis, hepatocellular carcinoma and mortality[17]. MASLD is associated with metabolic diseases such as obesity and type 2 diabetes, due to the significant increase in fatty acids accumulating in the liver (Fig 1).

MASLD and MASH are reversible, which can be treated with a healthy Mediterranean diet and 150 minutes of moderate physical activity. The Mediterranean diet consists of a larger quantity of plant-based foods, complimented with olive oil, healthy dairy products and fish. The goal for treatment is to lose around 3-10% of body weight, increased serum high-density lipoproteins, and substantially decrease serum triglycerides[18]. Surgical intervention may be considered, such as bariatric surgery if the patient wasn't able to treat themselves[15].

1.1.3 Lipid Dysregulation in MASLD

MASLD development begins when fat accumulates in more than 5% of hepatocytes. This can be exacerbated by obesity, since overeating leads to excess lipid storage in the adipose tissue. Once the storage capacity of the adipose tissue is exceeded, the remaining lipids are redirected to the liver. The presence of type 2 diabetes mellitus (T2DM) has also been a major determinant for the MASLD pathogenesis, with 85% of T2DM patients also being diagnosed with MASLD[19]. Insulin resistance is a hallmark of T2DM. Insulin resistant adipose tissue leads to excessive lipid storage in adipose tissue because insulin is no longer effectively suppressing lipolysis[20]. Excess fatty acids released from adipose tissue spill over into other organs, particularly the liver. This is beginning of lipotoxicity within the hepatocytes[21] (Fig 2).

Insulin resistance also leads to the promotion of de novo lipogenesis (DNL) and the reduction of FAO, which will elevate the accumulation of FFA, thus escalate the progression from MASLD to MASH[22]. Hyperinsulinemia due to insulin resistance will continue activate SREBP-1, which will activate genes that promote DNL, and hepatic steatosis[23–25]. DNL can make toxic fatty acids like diacylglycerides, which activate protein kinase C that results in inhibitory phosphorylation of the insulin receptor substrate, impairing insulin signaling.

The composition of the diet can also contribute to MASLD progression. Excessive consumption of carbohydrates such as glucose and fructose uptake from the Western diet also increases the risk of MASLD. Glucose and fructose enter the liver through GLUT2[26]. Fructose will stimulate SREBP1c and ChREBP, the major transcriptional regulator for DNL. Fructose bypasses phosphofructokinase-1, a critical regulatory step in glycolysis, promoting DNL and inhibiting FAO, thus leading to an influx of fatty acids[27]. The imbalance of fatty acid influx and metabolism leads to impaired function of liver cells, from mitochondrial dysfunction, lipotoxicity, ER stress, and production of reactive oxygen species [6,18].

Lipid accumulation activates Kupffer cells and recruited macrophages, which contribute to the release of pro-inflammatory factors, such as tumor necrosis factor alpha (TNF-a), Interleukin-1β (IL-1β), and nuclear factor kappa β (NF-kβ)[18]. Excessive lipotoxicity will accelerate hepatocyte death, which triggers the release of damage-associated molecular patterns (DAMPs) from its contents. This will elicit the activation of hepatic stellate cells (HSC). Activated HSC will differentiate into myofibroblast-like cells that produce collagen and extracellular matrix components, increasing fibrosis[28,29]. Increased accumulation of fatty acids from the imbalance of fatty acid influx and metabolism leads to impaired function of liver cells, from mitochondrial dysfunction, triggered ER stress, inflammation and production of reactive oxygen species [6,18]. Prolonged inflammation and fibrosis caused by Kupffer cell activation, DAMP release, and HSC activation can lead to cirrhosis and then eventually HCC[22].

1.1.4 MASLD Physiological Diagnosis

MASLD can be diagnosed by biomarkers that can be measured to determine the level of liver dysfunction, which are plasma levels of aspartate aminotransferase (AST) and alanine aminotransferase (ALT)[8]. This can be screened through a Liver Function Test (LFT). Liver damage causes the release of ALT and AST, with ALT being more specific for liver injury, and

AST can be also be released from extrahepatic organs such as the brain, heart and skeletal muscle[30,31].
Other noninvasive strategies to diagnose MASLD include serum biomarker tests and image-based elastography[32]. Hepatic Steatosis Index (HSI) is a scoring system for MASLD, analyzing the BMI, diabetes status, and the AST/ALT[33]. The fibrosis-4 index (FIB-4) is another score commonly used to detect MASLD in patients, normally tested first before further evaluation. The equation for this is FIB-4 = age x AST/(platelet count x √(ALT)) (age in years, ALT and AST in U/L and platelet count in 10^9/L). If the score is >1.3, then the patient has a high risk of fibrosis. But this score does have a low predictive value, so doctors would have their patients continue with additional testing to decrease the false positives[34]. Patients with a FIB-4 score between 1.3 and 2.67 will proceed to get tested with ultrasound devices, using vibration-controlled transient elastography (VCTE), liver stiffness measurement (LSM) and controlled attenuation parameter (CAP). MR elastography (MRE) can be used to determine liver stiffness, which has been known to help diagnose advanced fibrosis.
To determine more histological characteristics of hepatocytes, doctors require patients to have a liver biopsy done, to have a definite determination of trajectory of MASLD to MASH and rule out alternatives that cause the disease. It can be used to assess hepatocyte ballooning, lobular formation, and stages of fibrosis. Liver biopsies are more invasive compared to imaging, and serum-based diagnosis methods. However, they provide the most accurate detection of hepatic fibrosis[34]. Biopsies are performed using a 16-gauged needle and taken multiple times to improve the yield for diagnosis, which are done for patients that are in the later stages of fibrosis. There is a call for developing more non-invasive diagnostic techniques because taking liver biopsies is painful to the patient.

1.1.5 Prevention and Treatment for MASLD

Diets high in saturated fats, cholesterol, and sugar, on top of a sedentary lifestyle are closely linked to increased risk of MASLD. To prevent the progression of the disease, patients need to make lifestyle changes through a healthy diet and the incorporation of exercise. Weight loss of around 3-5% of total body weight can reduce MASLD progression. Patients with progressive liver disease with MASH would have to lose around 7-10% of body weight. The Mediterranean-style diet consisting of consuming whole grains, fruits, vegetables, fish and poultry will help reduce MASLD. Calorie deficits by 500-100 Calories help with reducing liver fat content. Both aerobic and resistance exercise have been known to help with weight loss and improve cardiovascular health. These lifestyle changes should be enough to have substantial benefit for these patients[35].
If the disease progresses to MASH, the patient will need pharmacological intervention. There currently a need for more elucidation and discovery for new drugs. It has become a challenge to run short-term clinical tests of MASH being such a slowly progressing disease, with no drugs completing a Phase 3 trial. The goal is to develop a drug intervention that can resolve steatohepatitis without progressing fibrosis or resolving fibrosis without the worsening of steatohepatitis.
Glucagon-like peptide (GLP-1) has been tested in a Phase II trial has seen benefits in resolution in MASH, however, there wasn't a significant suppression fibrosis. This would be due to the lack of GLP-1R in the liver, but it has helped MASH patients with diabetes or obesity.

In a recent Phase II clinical trial, Pan-PPAR agonist lanifibranor has been tested, resulting to be beneficial on insulin sensitivity, glucose metabolism, lipid metabolism, and reverse hepatic steatosis and fibrosis[36]. Pan-PPAR agonists target all major PPAR isoforms, PPARalpha/gamma/beta/delta. Compared to the placebo, patients treated with the lanifibranor drug saw significant decrease in hepatic glucose production, a reduction in the hepatic insulin resistance index, reduced A1c levels, increased serum HDL-C and restoration of muscle insulin sensitivity. Patients even had a significant increase in adiponectin secretion; an adipose tissue adipokine strongly associated with improved insulin sensitivity[36].

Sodium-glucose co-transporter-2 (SGLT2) inhibitors which are normally used for patients with Type 2 Diabetes, have been determined to be a treatment for MASH. SGLT2 inhibitors improve glycosuria, block glucose reabsorption from the renal tubes, which results in weight loss and reduce blood pressure. For MASLD patients, it has reduced in serum ALT and AST[37]. However, patients with severe renal impairment should refrain from taking these drugs[34].

If all else fails and the patient progresses to the final stages of liver disease of HCC, they would need to go through a liver transplant. This unfortunately comes with side effects, including weight gain and cardiovascular complications. To keep the patient from rejecting the liver, they need to take immunosuppressive medications. However, this could impair the patient's metabolic function. In a study looking over 150 patients who received liver transplants, within 5 years 86% had recurring metabolic syndrome, 80% had steatosis, 60% had steatohepatitis, and 20% had advanced fibrosis[38]. Managing weight and cardiovascular health is integral for long-term survival after a liver transplant.

1.2 Discovery of Genetic Susceptibility to MASLD

1.2.1 The Human Genome Project

The Human Genome Project was an international effort starting in 1990 to decode the entire human genetic code, to create a research tool to identify genes involved in disease. To decipher the human genome, scientists used a DNA sequencing method called Sanger Sequencing. Through this method, DNA was run through slab gel electrophoresis, with a mixture of a dideoxynucleotide triphosphates (ddNTPs), standard deoxynucleotides, and DNA polymerase. The gel was divided into 4 wells, each having their own chain determining ddNTP (ddATP, ddGTP, ddCTP, ddTTP) which terminated the DNA strand elongation. The DNA is separated by size by running through a denaturing polyacrylamide slab gel electrophoresis, each well separated by either by A, G, C, or T nucleotides, imaged through UV light, then tediously read the pattern of all 4 lanes[39].

The human genome consists of 3 billion nucleotides, mapping out all 23 chromosomes. Its sequence was completed in April 2003, after 13 years of collaborative effort, costing around $2.7 billion[40,41]. This was a phenomenal feat that has helped push for discovering the interplay between genetic and environmental influences This allowed for a more in-depth understanding of genetic prognosis for disease progression, providing an open-access genomic database. This research has been able to make major progress in genetic research in diseases such as diabetes, Alzheimer's Disease, heart disease, and fatty liver disease, which were connected through Genome Wide Associated Studies (GWAS).

1.2.2 GWAS

Genome Wide Associated Studies (GWAS) was developed to discover single nucleotide polymorphisms (SNPs), the most common form of DNA sequence variation. They need to build an entire catalog of SNPs to help with investigating the susceptibility of common diseases and genetic variation. The first population-specific database, the Japanese Single-Nucleotide Polymorphisms, was done in 2001 after the first draft of the Human Genome Project was published[42]. This provided both research and clinical analysis to help bridge the gap between genetic variation and prevalence of risk for disease progression. The first GWAS study done with this data led to the identification of the gene lymphotoxin-alpha linked to susceptibility to myocardial infarction[42]. This is done by scanning hundreds of thousands of SNPs across the human genome, identifying variants that occur more frequently with people with diseases compared to the controls.

1.2.3 *PNPLA3* Wild Type Function

With the advancement of GWAS, several genetic variants have been identified to increase susceptibility to MASLD progression. This highlighted the interaction between genetics and environmental factors in this complex disease. The risk of MASLD is strongly inheritable though generations, with studies showing that approximately 78% of children of parents with MASLD also have the increased risk, regardless of age, sex, race and BMI[43]. One of the most important genes associated with MASLD progression is *PNPLA3*.

PNPLA3 gene encodes for adiponutrin, a lipid droplet-associated protein involved in hepatic triglyceride metabolism. *PNPLA3* expression is regulated by sterol regulatory element binding protein 1c (SREBP-1c), which is activated during feeding and lipogenic conditions. Nutrients such as oleic acid stimulate SREBP1 to bind to intron 1 of *PNPLA3*, increasing translation of the protein, without significantly changing mRNA levels[44]. As a result, *PNPLA3* protein levels rise during the fed state when fatty acid uptake is high.

During feeding, *PNPLA3* accumulates on the surface of lipid droplets, where it binds CG1-58 and limits its interaction with adipose triglyceride lipase (*AGTL* otherwise known as *PNPLA2*) the rate limiting enzyme for lipolysis. This suppresses TAG breakdown and promotes TAG storage within hepatocytes. During fasting, *PNPLA3* is ubiquitinated and degraded through the proteasome pathway. This releases CGI-58, allowing it to bind and activate ATGL, which increases lipolysis and releases free fatty acids[45] (Fig 3). These fatty acids can then be repackaged into very-low-density lipoproteins (VLDL) and exported to peripheral tissues such as skeletal muscle, adipose tissue, and the heart[9,46].

Recent evidence suggests that wild-type *PNPLA3* also has an independent lipase function separate from ATGL. Rather than broadly hydrolyzing triglycerides, *PNPLA3* preferentially hydrolyzes triglycerides enriched in polyunsaturated fatty acids (PUFAs), particularly omega-3 and omega-6 fatty acids[47,48]. This releases PUFAs from triglyceride stores and promotes their incorporation into phospholipids, such as phosphatidylcholine (PC) and phosphatidylethanolamine (PE), which are important components of VLDL membranes. Wild-type *PNPLA3* helps maintain normal VLDL assembly and secretion by supplying PUFA-rich phospholipids required for lipoprotein formation. When *PNPLA3* is absent or dysfunction due to genetic variation, hepatocytes retain more

triglycerides and secrete less VLDL-triglyceride, contributing to the development of hepatic steatosis[47].

1.2.4 *PNPLA3* SNPs as the Central Variant for MASLD

The most well-characterized *PNPLA3* polymorphism associated with MASLD is rs738409 (chr22:43928847 C>G) which results in a isoleucine to methionine substitution at the 148th amino acid on the peptide chain (I148M)[49–52]. This variant is strongly associated with increased susceptibility to MASLD, even in individuals without obesity or metabolic dysfunction. In fact, lean individuals carrying the GG genotype may have a greater risk of MASLD progression than overweight or obese individuals without the variant. It has been particularly studied for the dysregulated suppression lipolysis in hepatocytes, promoting the accumulation of lipid droplets (LD) filled with triacylglycerol (TAG)[2,53] (Fig 3). The methionine allele has a minor allele frequency of approximately 35% and is considered the most common genetic risk factor of MASLD[51]. Interestingly, I148M has been found to reduce DNL[54], which paradoxically contrasts with the accumulation of lipids in the liver. This suggests that lipid droplet buildup is solely a result of lipolysis inhibition, impaired hepatic VLDL secretion[52], mitochondrial dysfunction[55].
The *PNPLA3* I148M variants promote hepatic steatosis by impairing normal lipid droplet turnover in hepatocytes. Under normal conditions, *PNPLA3* is ubiquitinated and degraded, allowing CGI-58 to activate ATGL and stimulate lipolysis. However, the I148M variant of PNPLA3 resists ubiquitination and remains persistently bound to CGI-58 on the lipid droplet surface[49,51,52,55]. This prevents CGI-58 from activating ATGL, leading to reduced lipolysis, enlargement of hepatic lipid droplets, and accumulation of TAG within the hepatocytes.
Notably, the *PNPLA3* gene harbors approximately 10,000 coding and non-coding SNPs, many of which have been reported in dbSNP and may be associated with MASLD (Table 1). Among these, rs738408 (chr22: 43928850 C>T) has received comparatively little attention despite it having a significantly high frequency. This variant is located 3 nucleotides downstream from rs738409 and is in strong linkage disequilibrium with the I148M variant[56]. Unlike the nonsynonymous I148M mutation, rs738408 is a synonymous SNP, meaning the nucleotide substitution does not alter the amino acid sequence of the *PNPLA3* protein. Despite this, Rs738408 has been highly associated with MASLD. Although its functional role remains unclear, in some cases synonymous SNPs can still influence mRNA splicing, stability, and even some rare cases, influence the in-vivo protein conformation[57–59].
In addition to reducing TAG breakdown, the I148M variant appears to impair the selective hydrolysis of PUFA-containing TAG. This promotes the accumulation of PUFA-rich TAG, particularly those enriched in omega-6 fatty acids relative to omega-3 fatty acids. The resulting increase of n-6/n-3 ratio may contribute to greater inflammation, liver injury, and progression of hepatic steatosis[60].

1.3 Lipid Remodeling in MASLD

1.3.1 PUFA

Polyunsaturated fatty acids (PUFAs) are essential fatty acids absorbed through the diet and cannot be synthesized endogenously by the human body. PUFAs contain two or more double bonds within their hydrocarbon chain structure. They are important structural components of the cell membrane, regulating the function of transmembrane proteins and peripheral membrane proteins[61]. These double bonds are typically in the cis configuration to increase the membrane flexibility when PUFAs are incorporated into phospholipids, giving the cell its rounded shape and helping maintain membrane fluidity[62]. The most important PUFAs for human health are omega-3 and omega-6 fatty acids[62].

Omega-3 PUFAs are found in walnuts, canola oil, and fatty fish. They are absorbed primarily as Alpha Linolenic Acid (ALA), which are converted into eicosapentaenoic acid (EPA) and docosahexaenoic acid (DHA). These are further metabolized into omega-3-derived mediators: resolvins and protectins. These help lead to reduce inflammation and maintain healthy lipid metabolism.

Omega-6 PUFAs are absorbed as Linoleic Acid (LA), converted into Arachidonic Acid, which can be consumed from seeds, corn oil, egg, and processed meats. They are used as substrates for lipoxygenase (LOX) and cyclooxygenase (COX) to produce pro-inflammatory eicosanoids such as leukotrienes, prostaglandins, and thromboxane. These will help with the protection against bacterial and viral infections by increasing the activation of immune cells, increasing vasodilation, and promoting blood coagulation.

Maintaining a balance between Omega-6 and Omega-3 is crucial for minimizing chronic inflammation. A high consumption of Omega-6 compared to Omega-3 is high, which is common in many Western Diets, it could risk the development of chronic inflammation[62] (Fig 4).

The Western diet often consists of sugar, red, processed meats, and dairy products. A high omega-6 to omega-3 ratio, which is common in Western diets, may contribute to excessive production of pro-inflammatory eicosanoids such as prostaglandins and leukotrienes[62]. Both Omega-6 and Omega-3 compete for the same desaturating enzymes, FADS1 and FADS2. A high consumption of Omega-6 compared to Omega-3 will result to Omega-6 outcompeting for the enzymes, leading to decreased conversion of anti-inflammatory eicosanoids. It is emphasized that patients should eat a diet rich in Omega-3 fatty acids to provide health benefits maintaining the inflammatory pathways.

1.3.2 PL-PUFA remodeling impacting membrane fluidity as protection against MASLD

Along with maintaining the inflammatory response, PUFAs are also critical in regulating the structural integrity and function of the cellular membrane. PUFAs are incorporated on the sn-2 position of phospholipid, either phosphatidylcholine (PC), phosphatidylethanolamine (PE), phosphatidyl serine (PS), phosphatidylglycerol, or phosphatidylinositol (PI). The incorporation of the PUFAs in the phospholipids is run by the Lands cycle, which is regulated by two enzymes, acyl-CoA synthase long chain 4 (ACSL4) and lysophoshatidylcholine acyltransferase 3 (LPCAT3).

Depending on the composition of PUFAs, MUFAs, and Saturated fatty acids incorporated on the phospholipid, it will impact their flexibility. A higher composition of PUFAs compared to MUFAs would increase the membrane's fluidity[61]. This is due to the multiple cis double bonds in the fatty acid chain, which prevents tight packing of the phospholipids. The fluidity of the membrane will affect the function of cellular signaling and metabolic regulation.
The composition of the phospholipid membrane is crucial for maintaining the function of the liver. Patients with MASLD had fewer PUFAs integrated into the hepatic PC. Fatty acid components of the ER membrane determine its functionality. ER stress is increased after an increase of SFAs into the phospholipid species, driving activation of the JNK pathway and promoting apoptosis[63]. The activation of the JNK pathway will lead to the impairment of insulin signaling, through the phosphorylation of the insulin receptor substrate. Enrichment of SFA in the mitochondrial membrane will also exacerbate mitochondrial dysfunction and lead to increased ROS[63].
Studies have shown that a supplementation of PUFAs is negatively correlated with the induction of ER stress through XBP1 splicing[64]. It has also been shown that supplementation of krill oil, which contains omega-3 PUFA bound to PL suppressed DNL, and activated fatty acid oxidation, which resulted in suppression in MAFLD progression in mice. The study also showed that PL-PUFA suppressed AST and ALT, two major markers of liver damage. The PL-PUFA has been shown to increase the secretion of adiponectin, an adipokine from adipose tissue that promotes insulin sensitivity [65]. Finally, PUFA integration into the phospholipid helps promote the secretion of VLDL, providing protection against MASLD[47,48]. This showcases the importance of the ratio of PUFA:SFA incorporation into the phospholipid, directly correlating to the metabolic function of the liver.

1.4 Molecular Mechanisms of Ferroptosis in MASLD

1.4.1 PL-PUFA increased risk in Ferroptosis and MASLD

The role of phospholipid-bound polyunsaturated fatty acids (PL-PUFAs) in MASLD is complex. On one hand, PL-PUFAs can be protective by improving very-low-density lipoprotein (VLDL) secretion, maintaining membrane fluidity, and reducing endoplasmic reticulum stress. On the other hand, their high degree of unsaturation makes them particularly vulnerable to lipid peroxidation, increasing susceptibility to ferroptosis[66]. Ferroptosis is an iron-dependent, non-apoptotic cell death that is induced by reactive oxygen species (ROS) and lipid peroxidation. Unlike apoptosis, ferroptosis does not initially rupture the plasma membrane or fragment organelles. Instead, it is characterized by the accumulation of oxidize phospholipids, particularly PL-PUFAs[67].
PL-PUFA are especially susceptible to oxidation because of the multiple double bonds in their structure contain bis-allylic hydrogens that are easily taken by hydroxyl radical (OH•). This initiates a chain reaction of lipid peroxidation, resulting in a phospholipid radical (PL•) formed. The lipid radical then reacts with oxygen, to form a phospholipid peroxyl radical (PLOO•). The newly formed PLOO• attacks neighboring PL-PUFAs, generating phospholipid hydroperoxide (PLOOH) and another PLOO• that will continue to react with oxygen. In the presence of a ferrous ion, PLOOH undergoes the Fenton reaction taking its electron to produce ferric and a highly reactive phospholipid hydroxyl radical (PLO•) that will amplify the lipid peroxidation of nearby PL-PUFA, promoting membrane damage and cell death.[67–69] (Fig 6).

Certain PUFAs are more prone to ferroptosis. Omega-6 fatty acids such as arachidonic are among the strongest substrates for lipid peroxidation, while highly unsaturated omega-3 fatty acids such as DHA can also increase ferroptosis susceptibility due to the double bonds with allylic hydrogens[68] As MASLD progresses and oxidative stress increases, the accumulation of the oxidized PL-PUFAs may further enhance hepatic injury and inflammation
PUFA incorporation into phosphorylation is regulated by acyl-CoA synthetase long-chain family member 4 (ACSL4), and lysophosphatidylcholine acyltransferase 3 (LPCAT3). ACLS4 activates free PUFA into PUFA-CoA species, while LPCAT3 incorporates them into the membrane phospholipids. Both ACSL4 and LPCAT3 promote the formation of ferroptosis-sensitive PL-PUFA. The expression of ACSL4 has been reported to increase in MASH, further predisposing hepatocytes to ferroptosis[70,71] (Fig 5).

1.4.2 Cellular Protection against Ferroptosis

Cells are protected from ferroptosis by two different pathways, glutathione peroxidases 4 (GPX4) and ferroptosis suppressor protein 1 (FSP1). These pathways work in parallel to prevent the accumulation of lipid peroxides within the cell membrane.
GPX4 suppresses ferroptosis by reducing phospholipid hydroperoxides into non-toxic phospholipid alcohols. This process depends on the synthesis of glutathione (GSH). GSH synthesis requires cystine, which is imported into the cell by an antiporter transporter that is comprised of two homodimers, SLC7A11 and SLC3A2 (system Xc^-). This transporter imports cystine into the cell in exchange for glutamate. Once inside the cell, Cystine is reduced into cysteine to be used for GSH, the substrate for GPX4 to neutralize phospholipid peroxides. The used GSH is oxidized into oxidized glutathione (GSSG). GSSG is then recycled back to GSH by Glutathione Reductase (GR) to continue the protection against ferroptosis. If GPX4 function decreases, the cells become more susceptible to ferroptosis. Drugs such as RSL3 directly inhibit GPX4, inducing ferroptosis in cells[67]. Drugs such as RSL3 directly inhibit GPX4, inducing ferroptosis in cells[67].
The second protective pathway against ferroptosis is mediated by regulated FSP[72]. FSP1 is localized to the membrane by N-myristoyltransferase 2 (NMT2), regulated by NADPH availability. From there, it prevents lipid peroxidation by reducing CoQ10 to CoQ10H2, which acts as an efficient radical-trapping antioxidant independently from GPX4[73]. Loss of FSP1 with iFSP1 treatment induced ferroptosis, demonstrating FSP1 strong protective effect against ferroptosis. Membrane PUFAs are protected from ferroptosis due to activation of GPX4 and FSP1, while depletion of these enzymes will lead to peroxidation and ferroptosis damage (Fig 5).

1.4.3 Reactive Oxygen Species (ROS)

Reactive Oxygen Species (ROS) are highly reactive molecules generated as byproducts of oxidative phosphorylation in the mitochondria. Major ROS include superoxide radicals (O2•−), hydrogen peroxide (H202), and hydroxyl radicals (OH•). O2•− is primarily produced by the electron leakage from mitochondrial complexes I, II, and III. superoxide dismutase 1 (SOD1) converts O2•− into H2O2 that contributes to oxidative stress.

In addition to the mitochondria, ROS can also be produced by NADPH oxidases (NOX). These enzymes transfer electrons from NADPH to oxygen, producing O2•−. The O2•− will subsequently be converted to H2O2 by SOD1. H2O2 can then participate in the Fenton reaction to oxidize ferrous (Fe2+) to Ferric (Fe3+), resulting in the generation of OH•. OH• are among the most damaging ROS because they rapidly oxidize nearby proteins, lipids, and DNA [74,75]
The liver is particularly susceptible to ROS-induced damage since each hepatocyte contain a high density of mitochondria, which occupy around 20% of its cell volume[76]. Mitochondrial dysfunction and disruption of redox homeostasis can lead to excessive ROS accumulation in the liver. Elevated ROS levels promote oxidative damage to lipids, proteins and DNA, contributing to hepatocyte dysfunction and cell death. Damaged hepatocytes release DAMPs driving inflammation and tissue injury to neighboring hepatocyte cells[75,76].
ROS is especially important for inducing ferroptosis because they initiate and propagate lipid peroxidation of PL-PUFA. In the presence of iron, ROS contribute to the formation of phospholipid radicals and phospholipid peroxides, ultimately leading to ferroptosis[77].

1.4.4 Iron Metabolism

Iron is an essential element for many functions in the body, used for oxygen transport through hemoglobin[78], a cofactor for enzymes in DNA repair and metabolism[79], with the liver being the main storage organ. Iron is absorbed from the diet from meat, fish or poultry.
Dietary iron is mainly absorbed from meat, fish and poultry. Iron absorption occurs primarily in the duodenum and upper jejunum. In the intestinal lumen, ferric iron (Fe3+) is reduced to the more soluble ferrous form (Fe2+) by duodenal cytochrome b (DCYTB) at the brush border of enterocytes. The low pH of gastric acid helps facilitate this conversion. Ferrous iron is then transported into the enterocytes through divalent metal transporter 1 (DMT1)[80].
Once inside the enterocyte, Fe2+ can either be stored temporarily in ferritin or exported into the bloodstream through ferroportin, the major iron export protein. During export, Fe2_ is oxidized back to Fe3+ by hephaestin, allowing it to bind to transferrin, the major iron transport protein in the blood. Cells take up transferrin-bound iron through the transferrin receptor 1 (TfR1)-mediated endocytosis. Within the acidic environment of the endosome, Fe3+ is reduced back to Fe2+ and released from transferrin. DMT1 then transports Fe2+ out of the endosome into the cytoplasm, where it can be used for cellular metabolism or stored in ferritin[80].
Although iron is essential, excessive accumulation of iron is toxic because it can participate in the Fenton reaction, generating highly reactive hydroxyl radicals from hydrogen peroxide[81]. The liver is particularly vulnerable to iron overload because it is the main iron storage organ. Increased hepatic iron accumulation promotes oxidative stress, lipid peroxidation, and ferroptosis, thereby contributing to the MASLD development.

1.4.5 Ferroptosis and MASLD

In recent years, ferroptosis has been increasingly recognized as a major contributor to the progression of MASLD to metabolic dysfunction-associated steatohepatitis (MASH) due to the liver's essential function in iron metabolism. In hepatocytes, iron overload and the accumulation

of PL-PUFA increase the susceptibility to ferroptosis, resulting to membrane damage and cell death. The ferroptotic hepatocytes release danger-associated molecular patterns (DAMPS) such as oxidized phospholipids, malondialdehyde (MDA), 4-hydroynoneal (4-HNE) and 4-hydroxyhexenal (4-HHE). These molecules increase inflammation, promote hepatocyte ballooning and contribute to the onset of MASLD to MASH.

The release of 4-HNE and MDA can also induce ER stress and injury in of neighboring hepatocytes, further propagating liver damage. 4-HNE has been shown to activate pro-inflammatory pathways, such as JNK. Elevated MDA release correlated with greater inflammation, steatosis, and fibrosis. Persistent fibrotic injury promotes hepatic stellate cell activation, extracellular matrix progression, and fibrogenesis, contributing to the progression of MASH. [70,82].

As MASLD progresses, the hepatic omega-6:omega-3 ratio increases significantly[63] Both omega-3 and omega-6 can increase risk of ferroptosis due to their double bonds being highly vulnerable to lipid peroxidation. However, omega-6 fatty acids are more potent substrates for ferroptotic lipid peroxidation than omega-3 fatty acids due to its pro-inflammatory role. As a result, a higher omega-6:omega-3 ratio may further increase oxidative stress, inflammation, and ferroptotic injury to the liver[83,84].

1.4.6 Ferroptosis and the link to *PNPLA3*

PNPLA3 I148M has been proposed to increase the susceptibility of ferroptosis, however the precise mechanism is still unclear. Recent studies showing that wild-type *PNPLA3* promotes the incorporation of PUFAs into phospholipids have created an apparent paradox[47,48,85]. Because phospholipid-bound PUFAs are highly susceptible to lipid peroxidation, greater PUFA incorporation into phospholipids would be expected to increase ferroptosis sensitivity. However, wild-type *PNPLA3* is generally considered protective against MASLD progression because it supports VLDL secretion and prevents hepatic triglyceride accumulation[47,48]. This suggests that the effect of wild-type *PNPLA3* on PUFA metabolism may be context dependent. Although increased phospholipid PUFA content can sensitize cells to ferroptosis, wild-type *PNPLA3* may still provide an overall protective effect by promoting efficient lipid export and preventing excessive lipid droplet accumulation. In contrast, I148M variant impairs the triglyceride hydrolysis function, reducing PUFA mobilization, VLDL secretion, and TAG turnover, leading to steatosis and a lipotoxic cellular environment that favors ferroptosis[48].

One recent study investigated the direct effects of *PNPLA3* in liver tissue and primary hepatocytes from individuals carrying the variant who had no prior liver disease diagnosis. The investigators found that hepatocytes carrying *PNPLA3* I148M exhibited greater ER stress, mitochondrial dysfunction, lower GPX4 expression and increased ferroptosis. Treatment with the ferroptosis inhibitor ferrostatin-1 or overexpression of GPX4 was sufficient to rescue the cells, suggesting that ferroptosis may be an important therapeutic target in *PNPLA3* I148M-associated MASLD[86].

Transcriptomic metabolomics data comparing wild-type and I148M hepatocytes also showed that NAD+ metabolism was significantly reduced in cells carrying the variant. NAD+ is important for maintaining cellular redox balance and supports antioxidant systems that suppress ferroptosis, including GPX4- and FSP1-dependent pathways. Reduced NAD+ availability may therefore further impair the ability of I148M hepatocytes to resist oxidative stress and lipid peroxidation, increasing susceptibility to ferroptosis[86].

1.5 NAD+ Deficiency in MASLD

1.5.1 NAD+ and NADP+ Biosynthesis

Nicotinamide adenine dinucleotide (NAD+) is essential for maintaining the function of metabolic pathways, DNA repair, and chromatin remodeling through redox reactions. NAD+ is distributed throughout cellular compartments such as the cytoplasm, mitochondria, and the nucleus. To maintain cellular energy balance, NAD+ biosynthesis, recycling and degradation are tightly regulated (Fig 7).

There are three primary pathways for NAD+ biosynthesis, the Preiss-Handler pathway, Kynurenine pathway, and the salvage pathway. The Preiss-Handler pathway utilizes dietary nicotinic acid (NA), which enters the cell via transporters SLC5A8 and SLC22A13. In the cytoplasm, NA is converted into nicotinamide mononucleotide (NAMN) by the enzyme nicotinic phosphoribosyl transferase (NAPRT). NAMN is the converted into nicotinic acid adenine dinucleotide (NAAD) by nicotinamide mononucleotide adenylyl transferase (NMNAT), which finally is transformed into NAD+ by NAD+ synthase (NADS).

The Kynurenine pathway generates NAD+ through de novo synthesis, taking dietary tryptophan that enters the cell via SLC7A5, and SLC6A4. The tryptophan is then converted NAMN through a cascade of reactions, which will then be transformed into NAD+ through the Preiss-Handler pathway.

NAD+ can also be regenerated through the salvage pathway by recycling nicotinamide (NAM), a byproduct of NAD+ consuming enzymes including sirtuins, poly(ADP-ribose) polymerases (PARPs) and cyclic ADP-ribose synthases (CD38, CD157, and SARM1). NAM is converted into nicotinamide mononucleotide (NMN) by nicotinamide phosphoribosyltransferase NAMPT. NMN is then transformed into NAD+ by nicotinamide mononucleotide adenylyltransferases (NMNAT) to replenish the NAD+ pool. Additional NAD+ precursors include nicotinamide riboside (NR) and nicotinamide mononucleotide (NMN), which can be absorbed from dairy, fruits, vegetables, and meat. These precursors also enter the salvage pathway to support NAD+ biosynthesis.

NADP+ and NADPH are important derivatives of NAD+ that are integral for the maintaining cellular redox balance. NADP+ is generated through the phosphorylation of NAD+, while NADPH is primarily produced through the pentose phosphate pathway. In this pathway, glucose-6-phosphoate is converted by glucose-6-phosphate dehydrogenase (G6PD) into 6-phosphogluconolactone, which is then converted by 6-phosphogluconolactonase (6PGL) into 6-phosphogluconate. NADPH plays a critical role in suppressing oxidative stress[87].

1.5.2 NAD+ Deficiency and MASLD

Beyond its role as a metabolic cofactor, NAD+ is a central regulator of cellular redox homeostasis. NAD+ and NADH participate in numerous redox reactions that maintain mitochondrial respiration, fatty acid oxidation, and ferroptosis defense. In hepatocytes, which perform extensive lipid metabolism, NAD+ availability is important for maintaining mitochondrial function and preventing oxidative stress. NADPH is critical for protecting cells against oxidative stress, one way by providing the reducing power needed to regenerate GSH from GSSG. This allows GPX4 to continue neutralizing phospholipid peroxides[88].

NAD+ decline has been studied to be a hallmark in aging and in the development of diseases such as MASLD. NAD+ consuming enzymes such as PARP1 and CD38 have been investigated to be the explanation of NAD+ decline. Low levels of NAD+ results in the inability to regulate the function of glucose metabolism, impairing mitochondrial function. This leads to the accumulation of proinflammatory macrophages M1, driving MASH. NAD+ is also integral for the protection against ferroptosis, FSP1 requiring it to reduce CoQ10, and Cystine to be converted into Cysteine for the protective function of GPX4[70]. Inhibition of these NAD+ Consuming enzymes or treatment of NAD+ have been shown to protect the liver from the development of MASLD, improve glucose and lipid homeostasis. This provides a clear direction of the potential therapeutics of NAD+ supplementation[89–91].

1.5.3 NAD+ Deficiency and *PNPLA3*

Paolini et al. reported that individuals carrying the *PNPLA3* I148M variant had lower dietary and circulating niacin levels, which is strongly exacerbated by obesity. Their generalized linear model suggested that *PNPLA3* I148M may be directly influence circulating niacin[92]. They also found that the genetic variation reduced the expression of hepatic enzymes involved in biosynthesis of NAD+, including NAPRT1, a key enzyme in the Preiss-Handler Pathway that converts NA to NAMN. This reduction occurred independently of steatosis, suggesting that *PNPLA3* I148M may directly impair hepatic NAD+ production

These findings raise the possibility that reduced niacin and NAD+ availability may contribute to the increased ferroptosis susceptibility observed in *PNPLA3* I148M hepatocytes. Both major ferroptosis defense systems, GPX4 and FSP1, depend on NADPH. FSP1 requires NADPH to reduce CoQ10 and for the activation of NMT2 for membrane localization[72,73].

GPX4 depends on NADPH to maintain glutathione in its reduced form. Cystine imported through the cystine/glutamate antiporter (system Xc^-) is reduced to Cysteine in a NADPH-dependent process, allowing for the synthesis of Glutathione (GSH) for GPX4 function. GPX4 then uses GSH to detoxify phospholipid peroxides, converting it to oxidized glutathione (GSSG). GSSG could be recycled back into GSH by Glutathione Reductase (GR), which also requires NADPH. Because the NAD+ pool supports NADPH generation through pathways, such as the pentose phosphate pathway and mitochondrial dehydrogenase pathways, reduced NAD+ biosynthesis in PNPLA3 I148M hepatocytes may ultimately limit NADPH production.

These findings suggest that *PNPLA3* I148M may impair ferroptosis resistance not only through altered lipid metabolism, but also by weakening NADPH-dependent antioxidant defenses. Reduced NADPH availability could impair both GPX4 and FSP1, increasing the vulnerability of lipid peroxidation and ferroptotic cell death[72].

1.6 Modeling *PNPLA3* MASLD Models through Stem Cells and Genome Editing

1.6.1 Limitations of Existing *PNPLA3* driven MASLD Models

Although MASLD has been extensively studied in mouse models, murine systems have been unable to fully recapitulate the effects of *PNPLA3* variants on disease progression. Human and

mouse *PNPLA3* differ substantially, particularly in the C-terminal region of the protein and in tissue-specific mRNA expression patterns. As a result, both knockout and overexpression of *PNPLA3* have shown minimal effects on triglyceride hydrolysis, triglyceride synthesis, glucose homeostasis, or hepatic steatosis[93].
These findings are inconsistent with numerous human in vivo and in vitro studies, which consistently demonstrate that *PNPLA3* variants, particularly I148M, promote lipid accumulation, steatosis, and advancement of MASLD pathology. Because of the species-specific differences, traditional mouse models may not be adequate for studying *PNPLA3*-driven liver disease[51,52,55,60].
To better investigate mechanisms of *PNPLA3*-associated MALD, human induced pluripotent stem cell (hiPSC)-derived models provide a more physiologically relevant system.

1.6.2 Stem Cell History

Stem cells are undifferentiated cells that can be both self-renew indefinitely and differentiate into multiple specialized cell types. There are several types of stem cells, including embryonic stem cells, somatic stem cells, and induced pluripotent stem cells (iPSCs). Embryonic stem cells are derived from the inner cell mass of blastocytes during the early stages of development, typically 4-7 days after fertilization. These cells are pluripotent, meaning they can differentiate into any cell type derived from the three embryonic germ layers: ectoderm, mesoderm, and endoderm. Because isolation of embryonic stem cells requires destruction of the embryo, their use has raised significant ethical concerns[94].
A breakthrough occurred in 2006 when Dr. Shinya Yamanaka developed a method to generate pluripotent stem cells directly from adult somatic cells. By introducing key transcription factors involved in maintaining pluripotency, differentiated cells such as fibroblasts could be reprogrammed into induced pluripotent stem cells. Important pluripotent factors include Oct3/4, Sox2, and Nanog, along with Klf4 and c-Myc[95].
iPSCs provide several advantages in disease modeling because they can be generated directly from patients and differentiated into relevant cell types, including hepatocytes. They also allow the creation of isogenic cell lines, in which cells are genetically identical except for a single mutation or genetic edit. This makes it possible to directly study the effects of specific variants on cellular phenotype. Isogenic stem cell lines can be generated using gene-editing technologies such as CRISPR-Cas9.

1.6.3 CRISPR-Cas9 Discovery

Clustered Regularly Interspaced Short Palindromic Repeats (CRISPR) was first discovered in 1987 by scientists led by Dr. Atsuo Nakata from in the Escherichia Coli[96,97]. CRISPR consists of short sequences that are found to be repeated in prokaryotes. These repeats are palindromic, which read the same from the forward and reverse directions. The CRISPR system was discovered to play an important role in adaptive immunity of bacteria and archaea. Between the repeated palindromic sequences are spacer sequences, which derived from foreign DNA from viruses that previously infected the prokaryote. These spacer sequences allow the organism to recognize and defend against infections after the foreign DNA infects the cell again[97].

When the bacteria encounter the virus, the CRISPR locus is transcribed to make the CRISPR-RNA (pre-crRNA). A trans-activating CRISPR RNA, which is a small RNA that recognizes the palindromic sequences of CRISPR, will bind to the pre-crRNA, and allow the Cas endonuclease to bind to the complex. The tracrRNA-pre-crRNA-Cas is then cleaved by RNAse III 10 nucleotides into the spacer sequences to release the mature tracrRNA-crRNA-Cas complex. The pre-crRNA has the sequence from the infection, and the palindromic CRISPR sequence[98]. During a subsequent viral infection, the crRNA guides the Cas enzyme to the complimentary viral DNA sequence, where Cas will cause a double-stranded break, thereby preventing viral replication.
The crRNA and tracerRNA normally exist as separate RNA molecules. However, one of the most important innovations done by Dr. Jennifer Doudna and Dr. Emmanuelle Charpentier[99] was to connect these two RNA with a linker loop while maintaining the secondary structure of the tracrRNA:crRNA duplex, thereby creating a single guide RNA (sgRNA). The sgRNA can direct Cas to nearly any target sequence with a 20-nucleotide sequence of a gene. This discovery demonstrated that synthetic RNA-programmed Cas9 could be used for targeted genome editing in a variety of organisms and allow for directed DNA cleaving.
Streptococcus pyogenes was also a bacteria used by Dr. Jennifer Doudna and Dr. Emmanuelle Charpentier which encodes RNA-guided Cas9 nuclease that creates double-stranded breaks in the DNA without overhangs. Cas9 recognizes conserved protospacer-adjacent motif (PAM) typically the sequence NGG located immediately downstream of the target DNA region[100,101]. Cas9 has been widely used in CRISPR mediated genomic editing in research. Cas9 has 2 nuclease domains that cleaves a few nucleotides upstream of the PAM. After cleavage, the DNA break then can be fixed through NHEJ, which is error-prone and often introduces insertions or deletions, or homology-directed repair (HDR), which uses a homologous DNA template, to lead precise genetic repair. This will help maintain uniformity and protect against the introduction of mutations. The cell can repair the DNA through 2 mechanisms: NHEJ and HDR. NHEJ repairs the DNA ends that have either 5' and 3' overhangs, or blunt ends. It is a more imprecise form of repair, taking around 30 minutes, which often leads to additions, or deletions of base pairs. HDR is a more complex mechanism that requires a donor DNA template that helps reduce the error of the DNA and allows to repair the DNA indistinguishable from the target DNA.

1.6.4 CRISPR-Cas9 HDR editing

CRISPR-Cas9 enables precise genetic editing by using a single guide RNA (sgRNA) to direct the Cas9 nuclease to a specific DNA sequence, where it introduces a double-strand break. This break can then be repaired through HDR and a donor template to direct changes. To enhance HDR efficiency and introduce precise edits, we use artificially synthesized single stranded oligodeoxynucleotides (ssODN) as donor templates. ssODN typically contain ~50-10 base pair homology arms flanking the desired edit, allowing precise incorporation of the mutation during DNA repair[101,102]. For optimal efficiency, the desired edit is placed close to the Cas9 cleavage site, as HDR efficiency decreases with increasing distance from the cut site[103]. HDR-mediated CRISPR editing is best used for introducing single nucleotide edits, short insertions, or small deletions. This approach is widely used to generate isogenic cell lines, allowing us to directly investigate specific SNPs affecting cellular phenotype.

1.7 Conclusion

The role of I148M variant in ferroptosis progression requires further investigation to better define how this mutation alters *PNPLA3* function. Current literature contains conflicting interpretations of wild-type *PNPLA3* activity, contributing to an incomplete understanding in its role in PL-PUFA-driven ferroptosis. Clarifying this mechanism is important, as it may inform the development of targeted therapies for individuals carrying the *PNPLA3* I148M variant.
To examine the direct effects of the SNP, we generated isogenic cell models by excising one *PNPLA3* allele in WTC11 cells to create locally haploid lines. We then mutagenized the remaining allele to create a low risk 148I clone (loHAP 148I), a high-risk 148M double mutant clone (loHAP 148M-DM) and a 148M clone single mutant unliked from rs738408 (loHAP 148M-SM). Each line was subsequently differentiated into hepatocytes

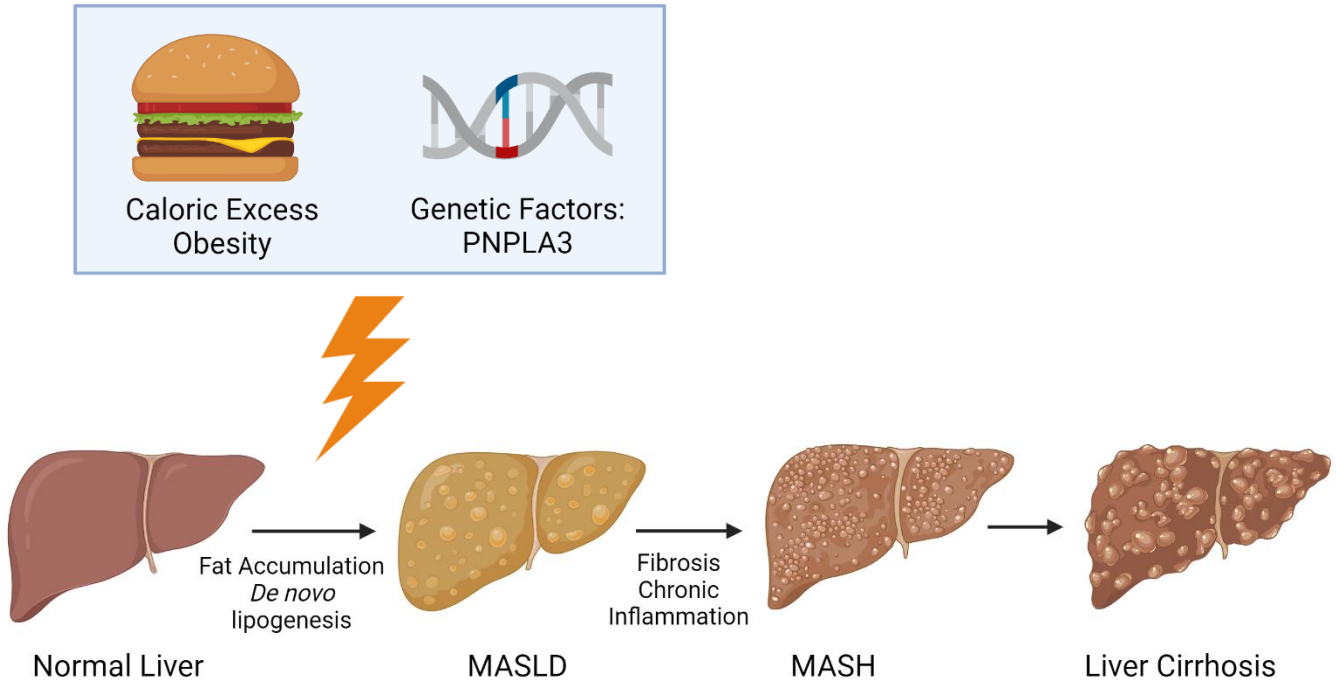

Figure 1: Metabolic Dysfunction Associate Fatty Liver Disease

MASLD development begins when fat accumulates in more than 5% of hepatocytes. This can be exacerbated by obesity, since overeating leads to excess lipid storage in the adipose tissue. Once the storage capacity of the adipose tissue is exceeded, the remaining lipids are redirected to the liver. The presence of type 2 diabetes mellitus has also been a major determinant for the MASLD pathogenesis, with 85% of T2DM patients also being diagnosed with MASLD[23]. Insulin resistance is a hallmark of T2DM. Insulin resistant adipose tissue leads to excessive lipid storage in adipose tissue because insulin is no longer effectively suppressing lipolysis[24]. Excess fatty acids released from adipose tissue spill over into other organs, particularly the liver. This is beginning of lipotoxicity within the hepatocytes[25].
Insulin resistance also leads to the promotion of de novo lipogenesis (DNL) and the reduction of FAO, which will elevate the accumulation of FFA, thus escalate the progression from MASLD to MASH[26]. Hyperinsulinemia due to insulin resistance will continue activate SREBP-1, which will activate genes that promote DNL, and hepatic steatosis[27–29]. DNL can make toxic fatty acids like diacylglycerides, which activate protein kinase C that results in inhibitory phosphorylation of the insulin receptor substrate, impairing insulin signaling. Created in https://BioRender.com courtesy of Dr. Kenneth Wilson

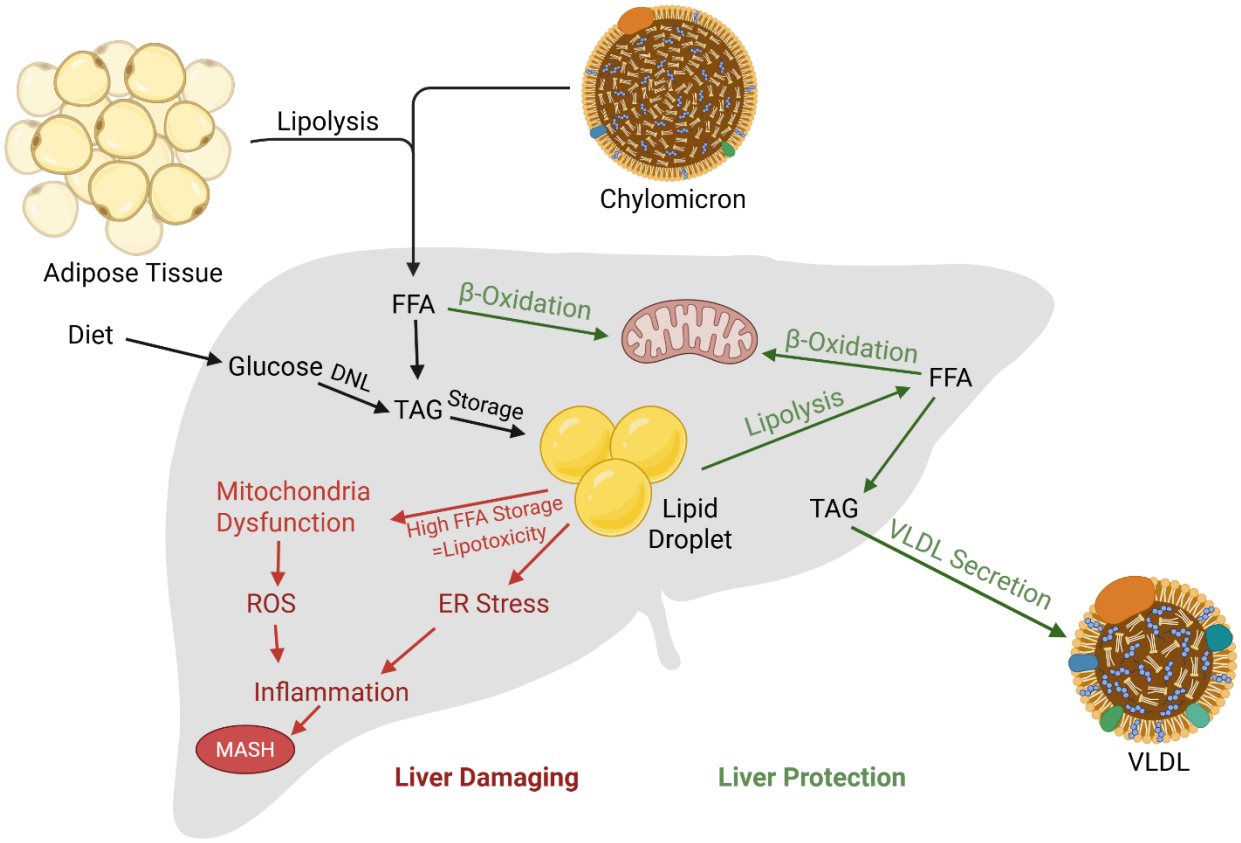

Figure 2: Cross talk between adipose tissue and liver

Liver acts as the central organ for fat metabolism via beta oxidation, having a constant flux of fat from adipose tissue, chylomicrons, and the endogenous generation of fatty acids through de novo lipogenesis (DNL). Medium chain fatty acids enter the liver via the portal vein, while chylomicron remnants carrying dietary fatty acids are delivered via the hepatic artery, then extracted out by lipoprotein lipase (LPL). Fatty acids are transported into the hepatocytes through fatty acid transport protein like FATP5 and CD36[9]. The liver can metabolize this accumulation of fatty acid through beta oxidation, secrete them out for circulation via very-low density lipoproteins (VLDL) or esterified to form phospholipids. This balance between influx and efflux of fatty acids is integral for maintaining the metabolic function of the liver[10]. Fatty acids are transported into the hepatocytes through fatty acid transport protein like FATP5 and CD36[9]. The liver can metabolize this accumulation of fatty acid through beta oxidation, secrete them out for circulation via very-low density lipoproteins (VLDL) or esterified to form phospholipids. This balance between influx and efflux of fatty acids is integral for maintaining the metabolic health of the liver[10]. Created in https://BioRender.com courtesy of Dr. Kenneth Wilson

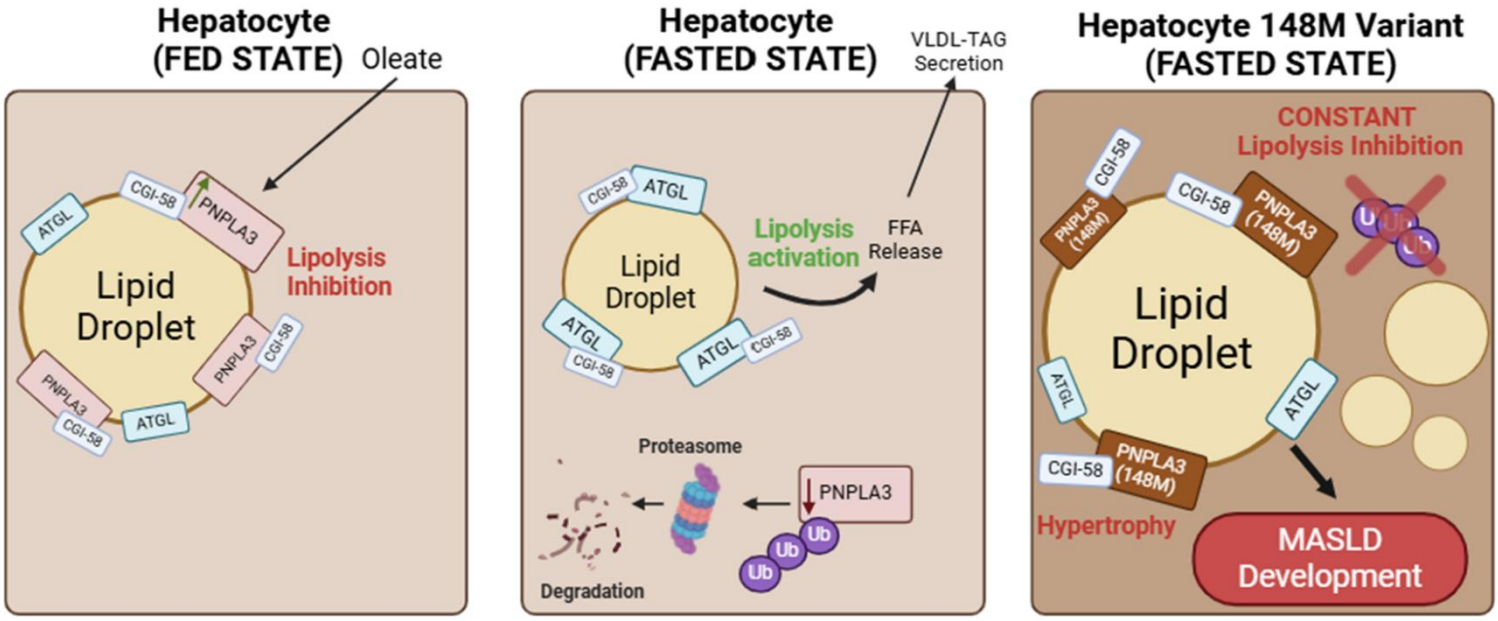

Figure 3: Mechanism of the PNPLA3 in fed vs fasted state

PNPLA3 is a protein encoded by the 22 chromosome that regulates lipolysis activity. In the fed state, *PNPLA3* is upregulated and sequesters the cofactor CGI-58 away from ATGL, the major enzyme activating lipolysis, leading to inactivation. In the fasted state, *PNPLA3* releases CGI-58 and is subsequently ubiquitinated and degraded, facilitating CGI-58 interaction with ATGL for activation of lipolysis. Free fatty acids (FFA) released from the lipid droplets are then packaged into VLDL and secreted out of the hepatocyte into circulation. A C>G substitution interferes with the ubiquitination of *PNPLA3*, resulting in inactivated lipolysis and elevated hepatic TAG, the main hallmark for MASLD progression. Created in https://BioRender.com courtesy of Dr. Kenneth Wilson

PNPLA3 SNP	Mutant	Position	Alleles	SNP Type	Minor Allele	Frequency	Disease	Clinical Significance	Notes
rs738408		43928850	C>A,G,T	Synonymous	T	0.2447	NAFLD	Strong	
rs738409	I148M	43928847	C>A,G,T	Missense	G	0.244815	NAFLD	Strong	
rs1810508		43947271	A>G,T	3 Prime UTR	G	0.216442	NAFLD	Benign	
rs2008451		43947089	T>C,G	3 Prime UTR	C	0.216514	NAFLD	Benign	
rs2076212		43927090	G>T	Missense	T	0.126664	NAFLD	Benign	
rs2076213		43927042	T>A,C,G	Missense	G	0.086681	NAFLD	Uncertain	
rs2294918	E434K	43946236	A>G	Missense	A	0.384009	NAFLD	Benign	
rs2294919		43946445	C>G,T	Missense	T	0.225929	NAFLD, HBV-Related HCC in Han Chinese	Benign	
rs6006460	S453I	43946294	G>T	Missense	T	0.033598	NAFLD	Likely Benign	
rs9626058		43947472	A>G	3 Prime UTR	G	0.047731	NAFLD	Likely Benign	
rs34179073		43932952	C>G,T	Missense	T	0.066408	NAFLD	Benign	
rs35726887		43933037	A>C	Missense	C	0.000144	NAFLD	Uncertain Significance	
rs41278871	G393C	43946775	G>A,C	3 Prime UTR	C	0.005773	NAFLD	Benign	MAF 0% in Hispanics and Puerto Rican
rs41278873	T429C	43946811	T>A,C	3 Prime UTR	C	0.048774	NAFLD	Benign	
rs62228000		43947129	T>A,C	3 Prime UTR	A	0.148088	NAFLD	Benign	
rs76510336		43946295	C>G,T	Missense	G	0.019748	NAFLD	Benign	MAF 0% in Hispanics and 1% in Puerto Rican
rs78730442		43937094	A>C	Missense	C	0.001832	N/A	Benign	
rs79118505		43927056	G>A,T	Synonymous	A	0.003937	NAFLD	Likely Benign	
rs115531341		43933070	G>A	Missense	A	0.003986	N/A	Benign	
rs116679026		43937265	C>G,T	Synonymous	T	0.004141	NAFLD	Likely Benign	
rs116795637		43924110	G>A,C	Intron Variant	A	0.012006	NAFLD	Benign	
rs138736228		43940139	G>A,C	Intron Variant	A	0.000091	NAFLD	Likely Benign	

rs140746182		43923744	C>A,T	2KB Upstream Variant	A	0.0112	NAFLD	Likely Benign	
rs141106484	B162M	43928887	G>A,C	Missense	A	0.002308	NAFLD, in Children metabolically unhealthy obesity	Benign/Uncertain	Contributed to MAFLD (metabolic associated fatty liver disease) in children
rs173392071	Y220C	43933050	A>C,G	Missense	G	0.00072	NAFLD	Likely Benign	Increased risk of NAFLD in the Japanese population, significantly increased MAFLD risk
rs144233415		43940005	A>G	Missense	G	0.005329	NAFLD, sleep disturbance	Likely Benign	Associated with sleep disturbances
rs144821153		43923872	C>G	5 Prime UTR Variant	G	0.007371	NAFLD	Likely Benign	
rs144872932		43939978	A>C	Intron Variant	C	0.006627	NAFLD	Likely Benign	
rs146578673		43947300	G>A	3 Prime UTR	A	0.001462	NAFLD	Uncertain	
rs147289545	R447G	43946276	G>A,C	Missense	A	0.000038	NAFLD	Uncertain	Potential association with increased risk of NAFLD in Japanese males
rs147412464		43926963	T>C	Synonymous	C	0.000162	NAFLD	Likely Benign	

rs148469440		43934601	C>A	Intron Variant, frame shift	A	0.000032	NAFLD	Uncertain	Disrupted regular splicing in 80% of transcript, decreasing PNPLA3, but did not decrease NAFLD susceptibility. Disrupted joining of PNPLA3 exons, causing exon skipping, suggesting a deleterious SNP for PNPLA3 function
rs148866299		43932948	C>A,T	Missense	A	0.00057	NAFLD	Uncertain	Associated with sleep disturbances
rs184910573		43944787	C>G,T	Synonymous	T	0.000537	NAFLD	Uncertain	
rs185208551		43933099	G>A,T	Intron Variant	A	0.002286	NAFLD	Uncertain	
rs190477302	T200M	43932990	C>G, T	Missense	T	0.000328	NAFLD	Uncertain	
rs200528261		43926982	C>T	Missense	T	0.000023	NAFLD	Uncertain	
rs201268858		43946273	C>T	Missense	T	0.000053	NAFLD	Uncertain	
rs202103609	I237M	43934620	A>G,T	Missense	G	0.000318	NAFLD	Uncertain	
rs370909367		43926996	C>G,T	Missense	T	0.0007	NAFLD	Likely Benign	
rs372749129		43937210	G>A	Missense	A	0.000094	NAFLD	Uncertain	
rs375286131		43934602	A>G,T	Intron Variant	G	0.00004	NAFLD	Uncertain	

rs376208148		43946355	C>T	Synonymous	T	0.000144	NAFLD	Uncertain	
rs529050829		43947557	A>C	3 Prime UTR	C	0.000876	NAFLD	Uncertain	
rs531789428		43923800	A>T	2KB Upstream Variant	T	0.012003	NAFLD	Likely Benign	
rs537338257		43946657	C>A,T	3 Prime UTR	T	0.000136	NAFLD	Likely Benign	
rs537933350		43946604	G>A,T	3 Prime UTR	T	0.0002	NAFLD	Uncertain	
rs545853993		43947142	T>C	3 Prime UTR	C	0.000129	NAFLD	Uncertain	
rs548897706		43923801	G>A	2KB Upstream Variant	A	0.01427	NAFLD	Likely Benign	
rs554000765		43946728	G>A,T	3 Prime UTR	T	0.002	NAFLD	Uncertain	
rs555962274		43946830	C>T	3 Prime UTR	T	0.000204	NAFLD	Uncertain	
rs564752977		43947008	A>G	3 Prime UTR	G	0.000007	NAFLD	Likely Benign	
rs569255289		43946401	T>G	3 Prime UTR	G	0.000952	NAFLD	Uncertain	
rs746140741		43926973	G>A	Missense	A	0.000057	NAFLD	Uncertain	
rs746640250		43947450	C>T	3 Prime UTR	T	0.000699	NAFLD	Uncertain	
rs749773774		43927153	G>A,C	Missense	C	0.000019	NAFLD	Uncertain	
rs753625728		43946274	G>A	Synonymous	A	0.000042	NAFLD	Uncertain	
rs753837923		43927030	C>T	Stop Gained	T	0.00011	NAFLD	Uncertain	
rs757406991		43946198	C>G,T	Missense	G	0.000008	NAFLD	Uncertain	

Table 1: dbSNP *PNPLA3* variant list *PNPLA3* gene harbors approximately 10,000 coding and non-coding SNPs, many of which have been reported in dbSNP and may be associated with MASLD.

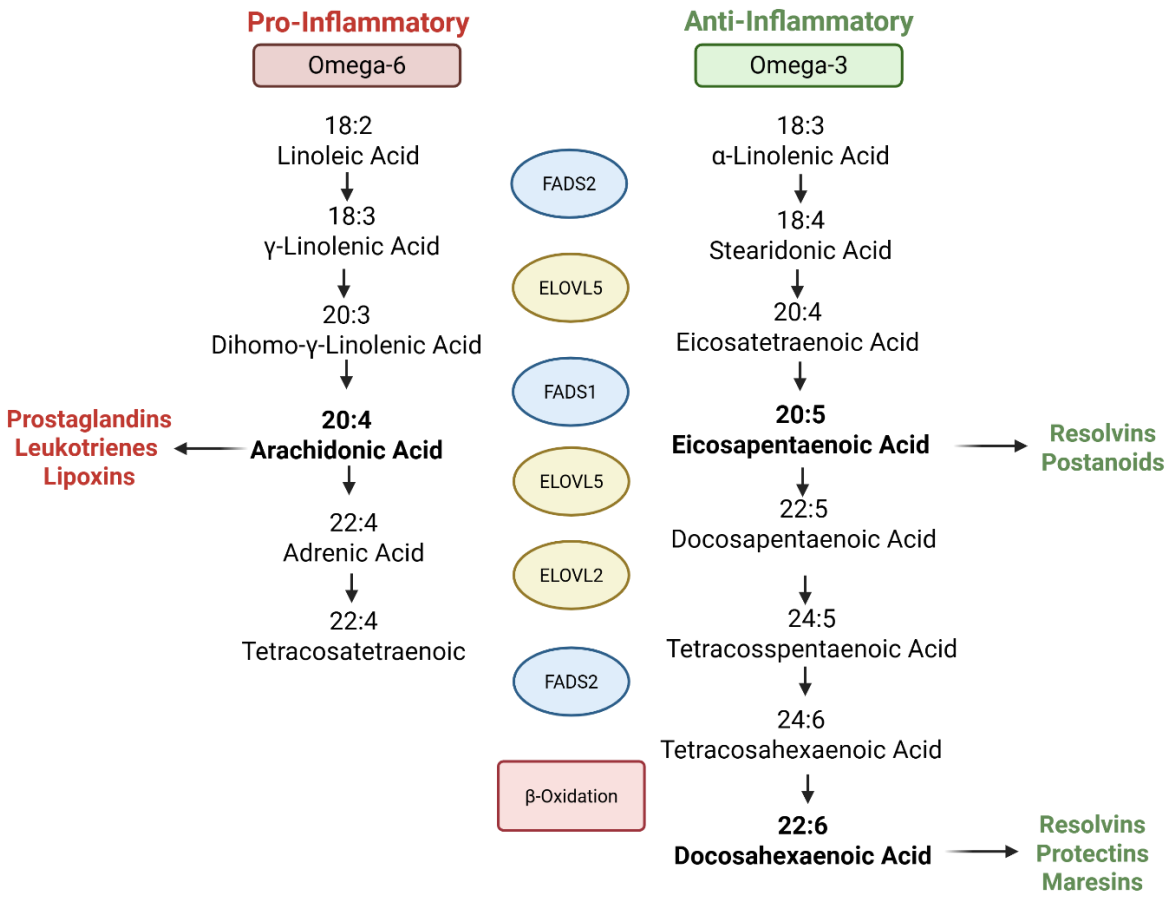

Figure 4: PUFAs Omega-6 and Omega-3 metabolism

Omega -6 PUFAs are absorbed as Linoleic Acid (LA), converted into Arachidonic Acid, which can be consumed from seeds, corn oil, egg, and processed meats. They are used as substrates for lipoxygenase (LOX) and cyclooxygenase (COX) to produce pro-inflammatory eicosanoids such as leukotrienes, prostaglandins, and thromboxane. These will help with the protection against bacterial and viral infections by increasing the activation of immune cells, increasing vasodilation, and promoting blood coagulation.
Omega-3 PUFAs are found in walnuts, canola oil, and fatty fish. They are absorbed primarily as Alpha Linolenic Acid (ALA), which are converted into eicosapentaenoic acid (EPA) and docosahexaenoic acid (DHA). These are further metabolized into omega-3-derived mediators: resolvins and protectins. These help lead to reduce inflammation and maintain healthy lipid metabolism. Created in https://BioRender.com courtesy of Dr. Kenneth Wilson

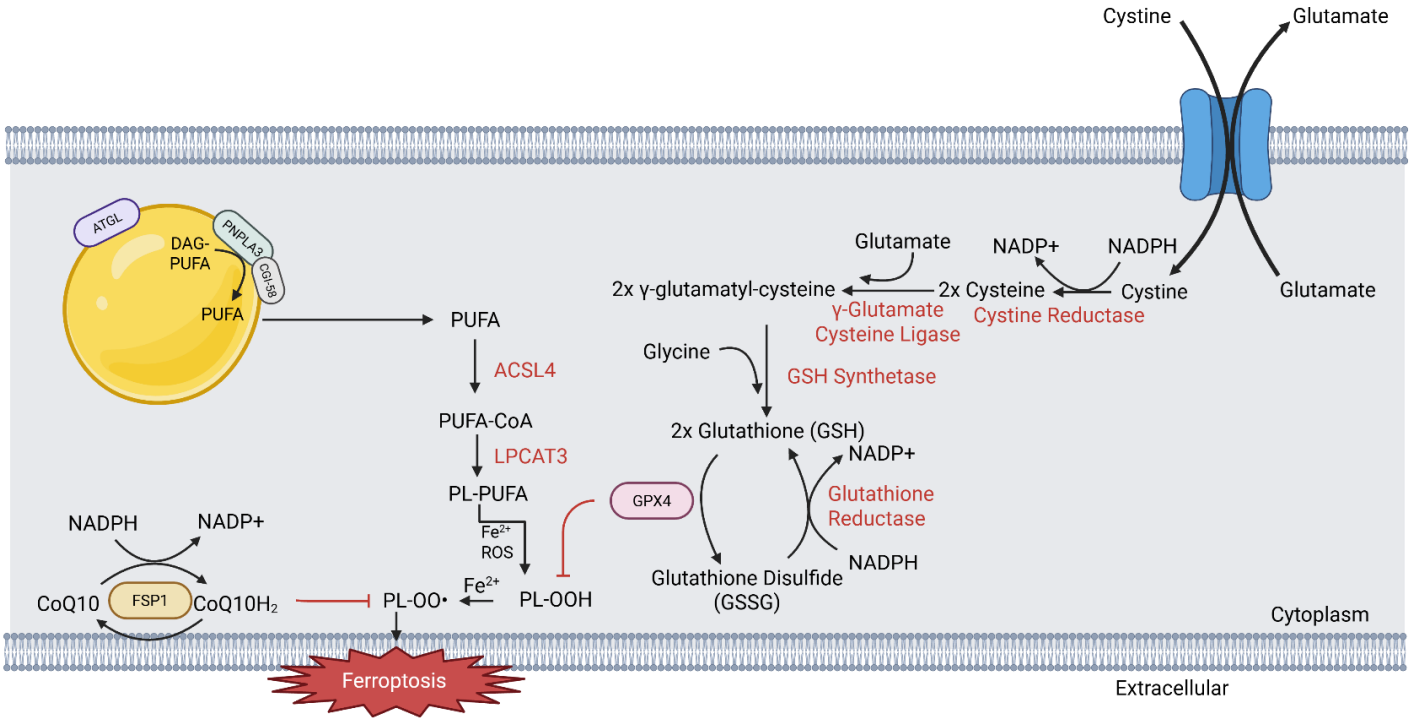

Figure 5: Ferroptosis Protection Pathway

GPX4 suppresses ferroptosis by reducing phospholipid hydroperoxides into non-toxic phospholipid alcohols. This process depends on the synthesis of glutathione (GSH). GSH synthesis requires cystine, which is imported into the cell by an antiporter transporter that is comprised of two homodimers, SLC7A11 and SLC3A2 (system Xc^-). This transporter imports cystine into the cell in exchange for glutamate. Once inside the cell, Cystine is reduced into cysteine to be used for GSH, the substrate for GPX4 to neutralize phospholipid peroxides. The used GSH is oxidized into oxidized glutathione (GSSG). GSSG is then recycled back to GSH by Glutathione Reductase (GR) to continue the protection against ferroptosis

The second protective pathway against ferroptosis is mediated by regulated FSP[73]. FSP1 is regulated by NADPH availability. From there, it prevents lipid peroxidation by reducing CoQ10 to CoQ10H2, which acts as an efficient radical-trapping antioxidant independently from GPX4[74].

PNPLA3 preferentially hydrolyzes triglycerides enriched in polyunsaturated fatty acids (PUFAs), particularly omega-3 and omega-6 fatty acids[51,52]. This releases PUFAs from triglyceride stores and promotes their incorporation into phospholipids, such as phosphatidylcholine (PC) and phosphatidylethanolamine (PE), which are important components of VLDL membranes. Wild-type *PNPLA3* helps maintain normal VLDL assembly and secretion by supplying PUFA-rich phospholipids required for lipoprotein formation. Created in https://BioRender.com courtesy of Dr. Kenneth Wilson

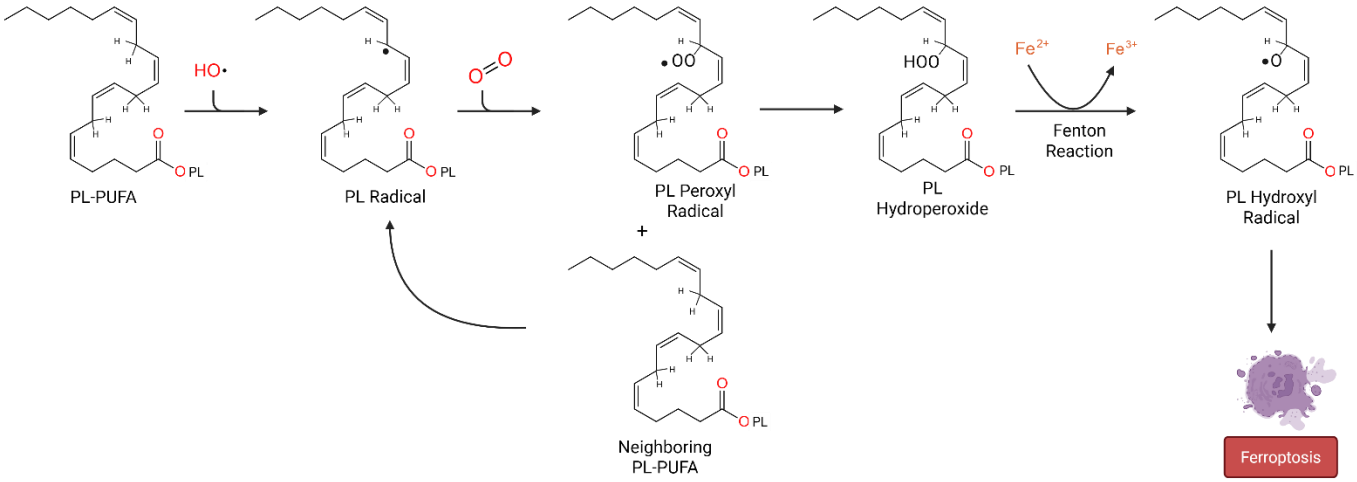

Figure 6: Lipid Peroxidation

Ferroptosis is an iron-dependent, non-apoptotic cell death that is induced by reactive oxygen species (ROS) and lipid peroxidation. PL-PUFA are especially susceptible to oxidation because of the multiple double bonds in their structure contain bis-allylic hydrogens that are easily taken by hydroxyl radical (OH•). This initiates a chain reaction of lipid peroxidation, resulting in a phospholipid radical (PL•) formed. The lipid radical then reacts with oxygen, to form a phospholipid peroxyl radical (PLOO•). The newly formed PLOO• attacks neighboring PL-PUFAs, generating phospholipid hydroperoxide (PLOOH) and another PLOO• that will continue to react with oxygen. In the presence of a ferrous ion, PLOOH undergoes the Fenton reaction taking its electron to produce ferric and a highly reactive phospholipid hydroxyl radical (PLO•) that will amplify the lipid peroxidation of nearby PL-PUFA, promoting membrane damage and cell death. Created in https://BioRender.com courtesy of Dr. Kenneth Wilson

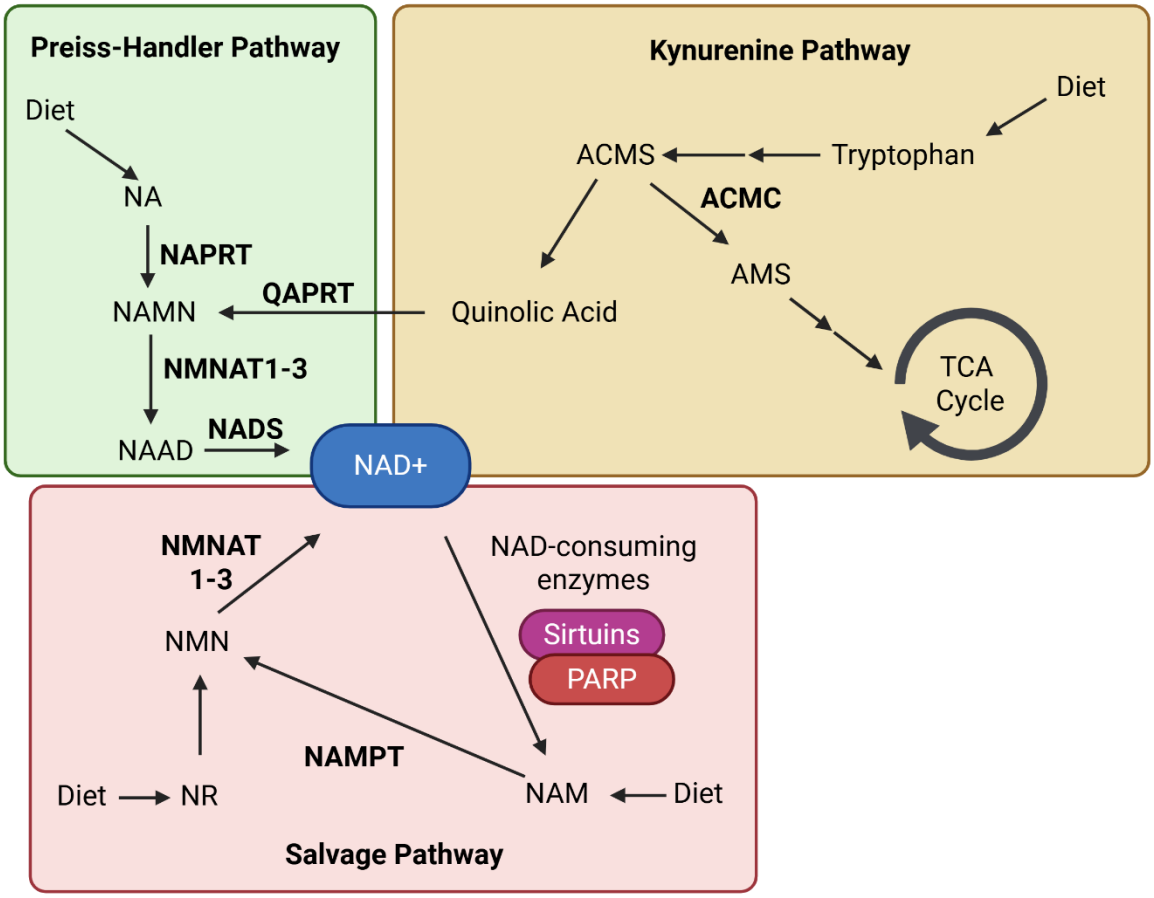

Figure 7: NAD Biosynthesis

There are three primary pathways for NAD+ biosynthesis, the Preiss-Handler pathway, Kynurenine pathway, and the salvage pathway. The Preiss-Handler pathway utilizes dietary nicotinic acid (NA), which enters the cell via transporters SLC5A8 and SLC22A13. NA is converted into nicotinamide mononucleotide (NAMN) by the enzyme nicotinic phosphoribosyl transferase (NAPRT). NAMN is the converted into nicotinic acid adenine dinucleotide (NAAD) by nicotinamide mononucleotide adenylyl transferase (NMNAT), which finally is transformed into NAD+ by NAD+ synthase (NADS).
The Kynurenine pathway generates NAD+ through de novo synthesis, taking dietary tryptophan that enters the cell via SLC7A5, and SLC6A4. The tryptophan is then converted NAMN through a cascade of reactions, which will then be transformed into NAD+ through the Preiss-Handler pathway.
Salvage pathway recycles nicotinamide (NAM), a byproduct of NAD+ consuming enzymes including sirtuins, poly(ADP-ribose) polymerases (PARPs) and cyclic ADP-ribose synthases (CD38, CD157, and SARM1). NAM is converted into nicotinamide mononucleotide (NMN) by nicotinamide phosphoribosyltransferase NAMPT. NMN is then transformed into NAD+ by nicotinamide mononucleotide adenylyltransferases (NMNAT) to replenish the NAD+ pool. Created in https://BioRender.com courtesy of Dr. Kenneth Wilson

Chapter 2: Creation of PNPLA3 locally haploid human induced pluripotent stem cells

Contents in this chapter are modified from the following manuscript

2.1 Introduction

The functional roles of *PNPLA3* genetic variants other I148M in MASLD progression remain poorly understood. Generating locally haploid cells with defined genetic changes allows for controlled screening of variant-specific effects. Using this approach, we can directly investigate how the nonsynonymous SNP rs738409 influences MASLD progression independently of synonymous SNP rs738408. To directly elucidate the relationship between rs738409 and rs738408, we generated isogenic human induced pluripotent stem cells (hiPSC) lines in which the linkage between rs738409 and rs738408 was uncoupled using CRISPR/Cas9 based genetic editing. This strategy enables direct comparison of each variant in isolation, providing a clearer understanding of their impact on the MASLD disease mechanism.

Traditional homology directed repair (HDR)-mediated editing in diploid cells often produces compound heterozygosity, where the desired GWAS variant is introduced on one allele while the second allele acquires unintended insertions or deletions through non-homologous end joining (NHEJ)-mediated repair. These undefined additional mutations can confound the interpretation of a risk-variant, particularly those with small effect sizes.

To address this limitation, we collaborated with the Hockemeyer lab to generate locally haploid cells (loHAPs) in which one copy of the gene of interest is excised[104]. This ensures that any engineered mutation introduced on the remaining allele directly determines the phenotype without the interference from a second allele[104]. Using the WTC11 iPSC line, we created *PNPLA3* loHAP cells by introducing an approximately 35 kb deletion on chromosome 22. WTC11 is particularly well suited for this approach because it is a well-characterized iPSC line and is heterozygous for the *PNPLA3* I148M variant. This enabled us to generate 3 allelic combinations, *PNPLA3* C/C (low risk 148I), *PNPLA3* G/C (high risk 148M-SM single mutant uncoupled from synonymous SNP), and PNPLA3 G/T (high risk 148M-DM double mutant coupled with synonymous SNP) for rs738409 (chr22:43928847 C>G) and rs738408 (chr22: 43928850 C>T). This chapter will lay out the editing strategy of the loHAP cells and the further characterization of the different clones (Fig 8).

2.2 Result

2.2.1 Generating loHAP cells

We generated loHAP cells from the WTC11 iPSC line through CRISPR-Cas9 mediated editing. Guide RNAs were designed to target regions approximately 13 kbp upstream the 5' end and 1.3 kbp downstream from the *PNPLA3* genomic locus (**Fig 2**). For genome editing, 300 pmol sgRNAs were delivered as ribonucleoprotein (RNP) complexes via nucleofection, (see Methods). Following nucleofection, cells were plated in 6 well plates for expansion. Colonies were then subcloned into 96 well plates at a low density, (~100 cells per plate) to ensure single cell derived population and avoid mixed clones. Edited clones were expanded and cryopreserved. The high efficiency of loHAPs editing was around 5% for the PNPLA3 23kb (Fig 9).

To determine the successful loHAP deletion of the allele, primers were designed around 200 bp upstream from the designed sgRNA binding sites, in which the de novo junctions were detected by PCR. Primer designs are laid out on Table 1. Negative control wells had the unedited WTC11,

primers and PrimeSTAR GXL DNA Polymerase, resulting in no clear band. This is because the designed primers are over 23 kilobases from each other. Without the CRISPR-Cas9 determined edit by the designed sgRNAs, the DNA polymerase would forward and reverse primers The positive control determined the depicted by the bands at around 500 bp (Fig 10a). Primers were designed to flank the I148M SNP for PCR amplification (Fig 10b). Successful deletions are identified using polymerase chain reaction (PCR) detecting the 500bp of the floxed junctions. The remaining allele is determined through Sanger Sequencing (Fig 10d). Cell clones are genotyped using primers flanking the deletion region. The F2 clone was confirmed to be the loHAP 148I from present loHAP and I148M bands, and the sequenced low risk allele through Sanger Sequencing. However, the F2 clone was multiclonal, meaning it had many different expressions of off target gene edits. To overcome this, we did a second limited dilution of the expanded F2 clone (Fig 10c). After running a limited dilution, we ran the genotyping for the loHAP deletion and the I148M allele again. This resulted in 28 clones successful with the single allele deleted. We excised the bands from the I148M gel and extracted the DNA for each clone, in which the genomic DNA was sent over to the Hockemeyer laboratory for NGS. From the sequencing, we were able to confirm that the F1 well clone had the remaining functional allele on the loHAP. The F1 well clone was determined to be I148M, which was then expanded and frozen for stocks.
To generate isogenic clones, the 148I was mutagenized to introduce the 148M high risk allele linked (loHAP 148M double mutation 148-DM) and unlinked with rs738408 SNP (loHAP 148M single mutation 148M-SM). The variants were edited through HDR-mediated CRISPR editing. Single-stranded oligonucleotides (ssODN) were designed to create the 148M-SM and 148M-DM (Table 2). The F1 148I loHAP was nucleofected with RNP containing CRISPR and the ssODNs, the 4 ssODNs notated in Table 1. The mutagenized clones were identified for loHAP and I148M primers (Fig 11 a). We were successful in genetically editing the remaining 148I allele into the 148M single mutation (loHAP 148M-SM) without rs738408, and the loHAP 148M double mutation (loHAP 148M-DM) with the rs738408 SNP (Fig 11b). Importantly, the haploinsufficient WTC11 lines and isogenic clones did not impact their ability to proliferate, nor change their morphology (Fig 11c).

2.2.2 Karyotyping and pluripotency determination

Before proceeding with the clones for further experimentation, each clone was assessed for pluripotency by staining for stem cell markers such as OCT4, and SSEA4. Because CRISPR-Cas9 editing can impair the hiPSCs pluripotency efficiency, this validation step was critical. After staining, we observed no difference in pluripotency markers in the loHAP 148I, 148M-DM, and 148M-SM clones, indicating the genome editing did not compromise the stem cell identity (Fig 13).
CRISPR-based editing can cause off-target mutations, leading to chromosomal instability. If there are differences within the karyotyping of the clones, it would not be reliable to compare the clones. hiPSC clones were then sent out for karyotyping. We discovered that the parental clone had a loss in Chromosome 18, and gain in chromosome 20, but the genetically edited clone only had a gain in Chromosome 20. From the limited dilution, the cells may have expanded out only one of the impacted chromosomes, while the other clones had both. This led to the issue of driving the original parental clone cannot be compared to the edited clones. However, the loHAP 148I, 148M-DM and 148M-SM clones each have the same karyotype, with the gain in chromosome 20. Thus,

we decided to move forward and continue the research with the main comparisons being between the loHAP cell line with the gain on chromosome 20 (Fig 12, 15).
The gain in chromosome 20 is the most frequent genetic lesions seen in hiPSCs. An increased copy of chromosome 20 plays a role in the cancer progression, leading to the result of fast proliferation and reduced cell-cycle time[105]. These mutations can lead to increase in genes such as *IDI BCL21L TPX2 DNMT3B* and *POFUT*. Enzymatic passaging is only minimally done for the monolayer passage for hepatocyte differentiation. This process can cause cleavage of receptors and proteoglycans, which in turn diminishes the responsiveness to growth factors. This is likely due to enzymatic passaging promoting genetic abnormalities[105]. To reduce the impact of this mutagenesis of these cells, the cells are picked through mechanical passaging, which will diminish the differentiated cells from transferring to the next passage.

2.3 Discussion

We established an efficient method to generate haploid isogenic cell lines that can be used for the direct investigation of the genetic variants and the uncoupled SNPs for I148M (Fig 10-11). This has not been done previously focusing on rs738408's effect on rs738409 impact on the progression of MASLD. The *PNPLA3* non-synonymous polymorphism I148M is robustly associated with MASLD development, impairing its ubiquitination, resulting in significantly decreases hepatocyte lipolysis and contributing to an accumulation of fatty acids in the liver (Fig. 3)[1,2,53,106]. Rs738408 has a high linkage disequilibrium to rs738409, and within the literature it has been determined to be Rs738408 is a synonymous genetic variant that has a high linkage disequilibrium with I148M, 3 nucleotides downstream, and is also associated with increased risk MASLD (Table 1). Although synonymous SNPs do not change the amino acids, they can still cause deleterious effects. This may cause premature splicing of the mRNA, potentially leading to altered expression of *PNPLA3*. The rs738408 SNP is highly associated with 148M but is often overlooked, so it holds importance and needs to be elucidated.
Each colony generated had the desired genotype needed, with the pluripotency markers unchanged. The staining of all pluripotency markers remained unchanged, indicating that the clones can still maintain their stem cell identity after the CRISPR edit.
The karyotyping issues were since the parental line that was used in the initial editing contained gains in Chromosome 20 and losses in Chromosome 18. The gain in the chromosome 20 was carried out to the next generations of loHAP cells, which then were able to be confirmed to all have the same karyotype. Other diploid WTC11 cells either did not have the chromosome 18 loss and the Chromosome 20 gain or had both. To maintain the comparisons between cell types with the same karyotype, we opted to continue the project with the cells with the chromosome 20 gain since it is the most investigated karyotype in hiPSCs (Fig 12). If experiments are to be redone, it is encouraged to run the generation of the loHAPs again with a WTC11 cell line previously karyotyped and continuously karyotyped throughout the editing process. That way we could mitigate the impact of any genetic aberrations impacting the data.
Despite those issues, this protocol can be scaled up to investigate many different SNPs and their direct role in MASLD. With the loHAP cells, we could mutagenize around 100 different SNPs and scale up the investigation of each edit. The advantages of this are to generate a high throughput method that can test out the 10,000 SNPs direct impact in the lipid generation, steatosis, and ferroptosis driven MASLD (Table 1). In future projects, the goal would be to expand the SNP

editing library and make the top 100 most frequent clones and run high throughput screening on their impact on liver metabolism.

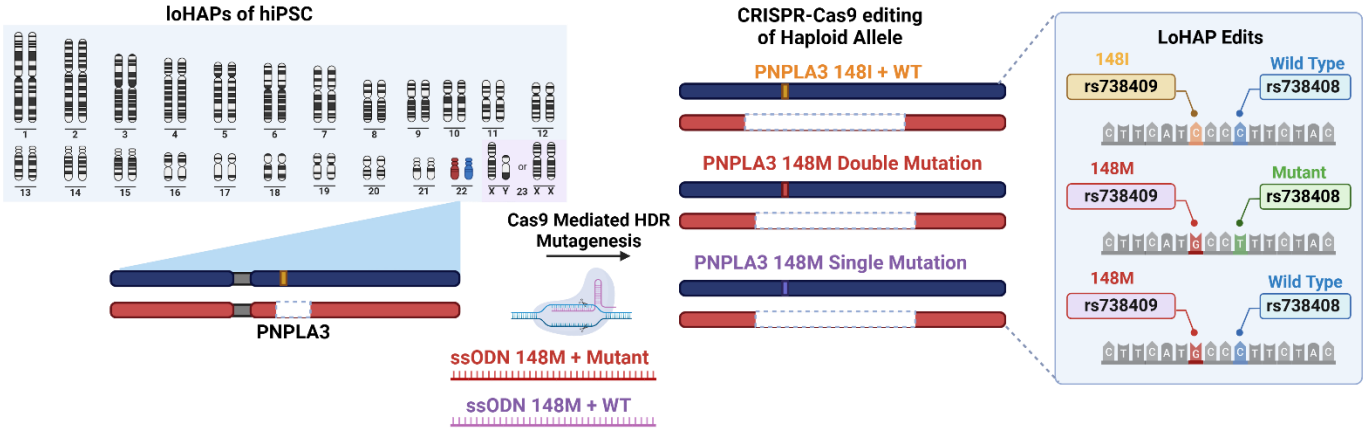

Figure 8: Layout of locally haploid edits

WTC11 cells were mutagenized to delete one copy of the PNPLA3 gene through CRISPR-Cas9. Locally Haploid clones are determined through PCR and NGS. High risk 148M allele deleted, with the remaining low risk 148I allele mutagenized with a single stranded oligodeoxynucleotide as a donor template for CRISPR-Cas9 mediated HDR. Created in https://BioRender.com courtesy of Dr. Kenneth Wilson

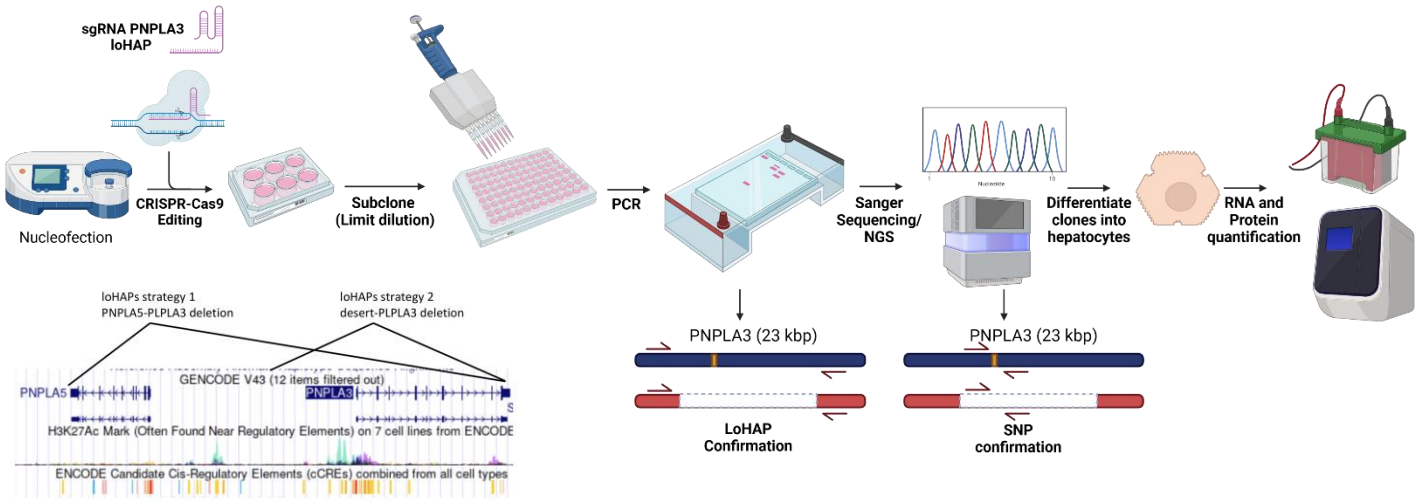

Figure 9: Outline of locally haploid cell generation

One allele of *PNPLA3* will be excised out via CRISPR-Cas9 editing. 300 pmol sgRNA designed using loHAP strategy 2 flanking PNPLA3 were delivered to WTC11 as RNPs via nucleofection. After nucleofection, cells are plated onto 6 well plates for expansion. Once colonies form, they will be subcloned into 96 well plates, 100 cells per plate, to ensure a single cell attaches in each well to avoid mixed clones. Created in https://BioRender.com courtesy of Dr. Kenneth Wilson

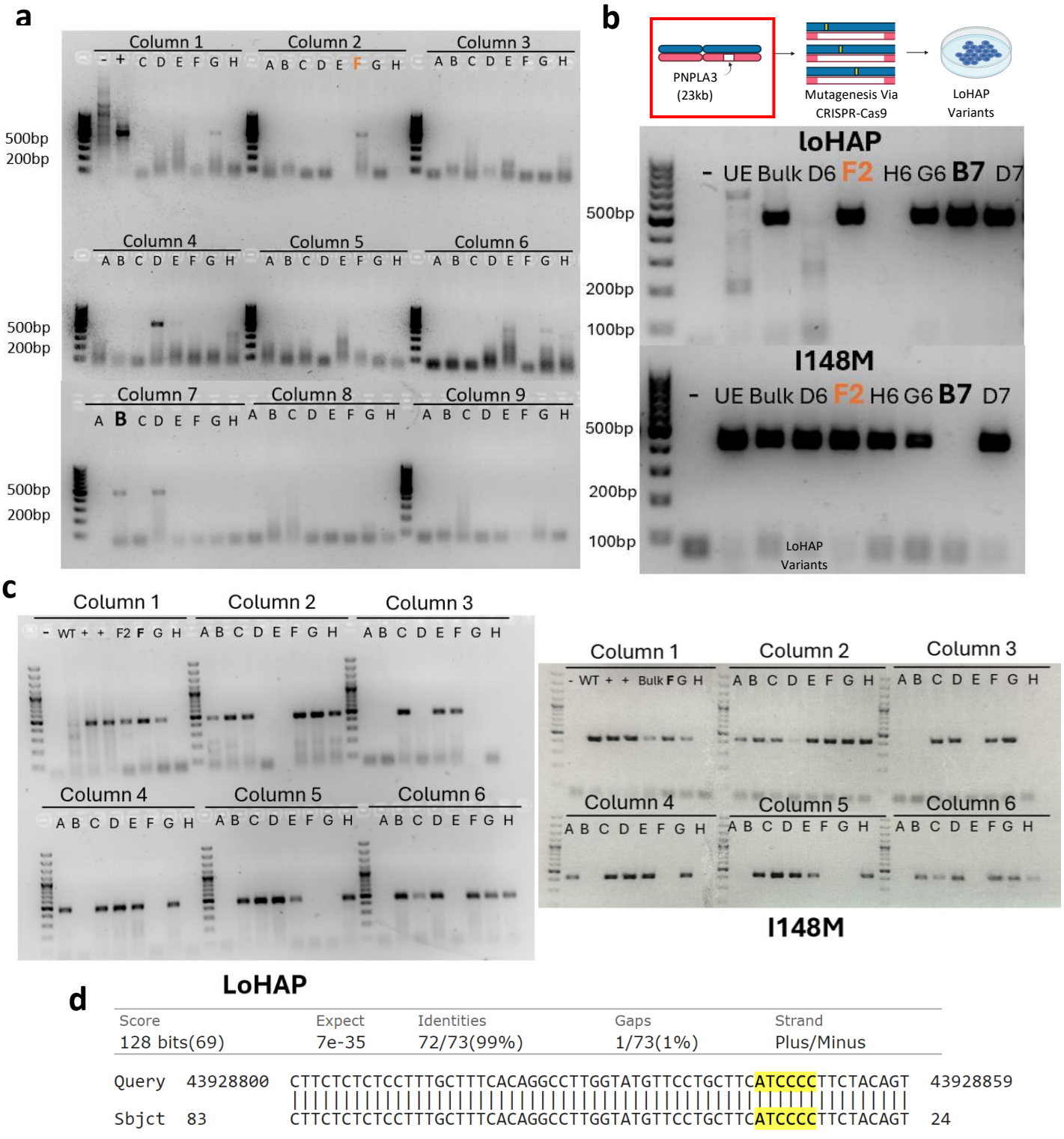

Figure 10: Generation of PNPLA3 loHAPs

a. PCR gel electrophoresis band determines loHAP b. PCR gel confirmed loHAP clones with I148M expression
c. F2 clone limited dilution PCR gels d. Confirmation of genotype through Sanger Sequences

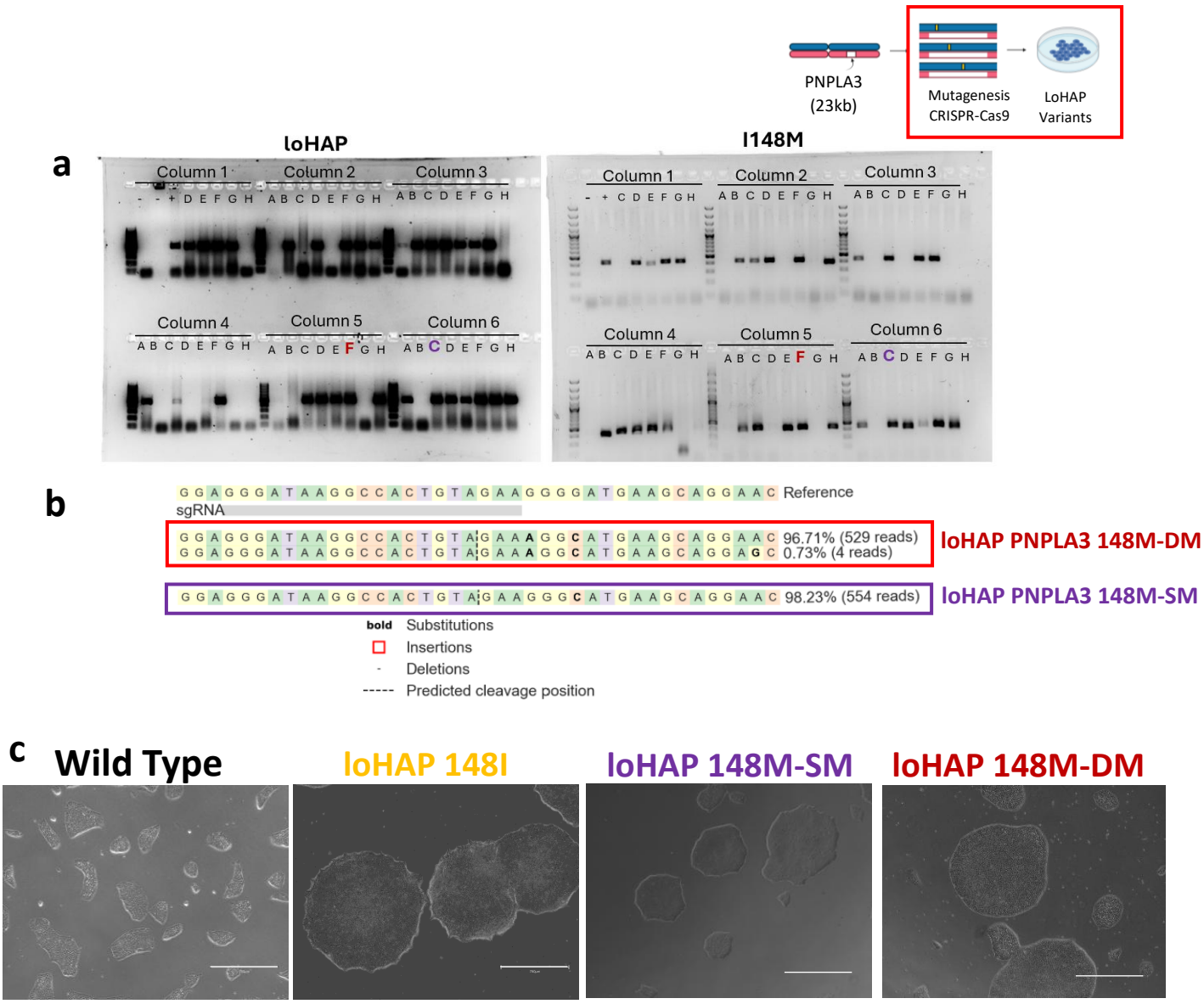

Figure 11: Mutagenesis of remaining loHAP 148I allele to 148M

a. Mutagenesis of loHAP 148I to make 148M-SM and 148M-DM b. NGS data of low-risk 148I, high-risk single mutant (148M-SM) and high-risk double mutant (148M-DM) c. loHAP hiPSC morphology images at 4x scale bar 750um

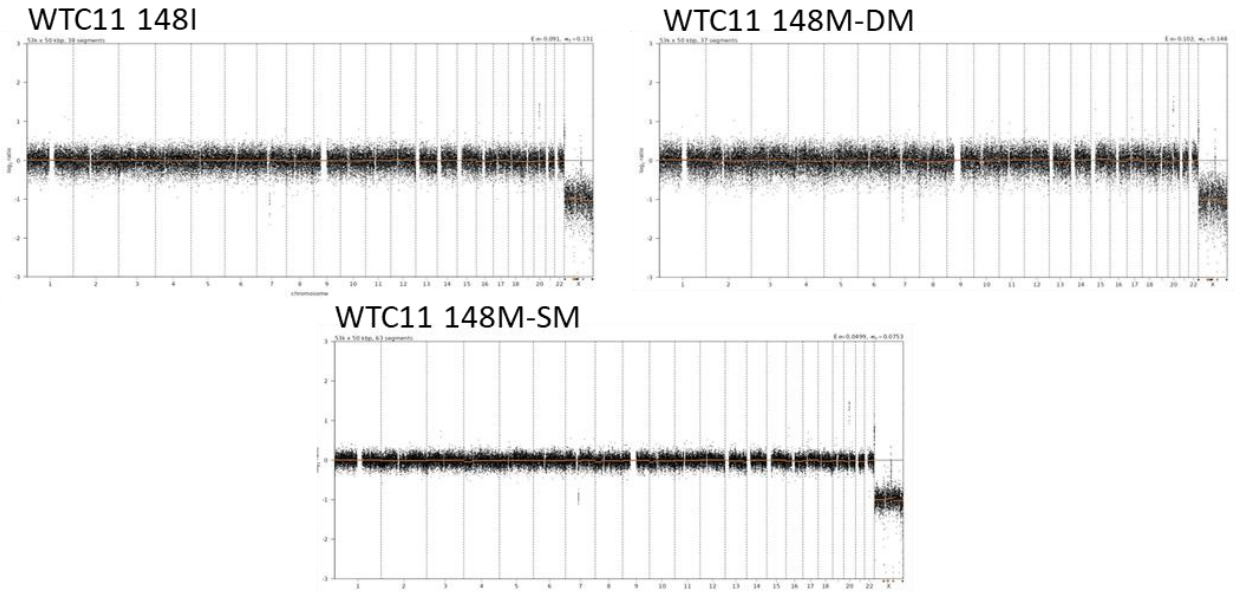

Cell Edit	Chrom	Start Position	End Position	Size	Cytoband	Copy Number	Status	Log2 Ratio
WTC11 148I	20	26,100,001	30,500,000	4.4 Mb	P11.1 - q11	4.6913	Gain	1.23
	X	88,450,001	92,350,000	3.9 Mb	q21.31	1.572	Gain	-0.35
WTC11 148M-DM	20	26,100,001	30,500,000	4.4 Mb	P11.1 - q11	4.9249	Gain	1.3
	X	88,450,001	92,350,000	3.9 Mb	q21.31	1.6133	Gain	-0.31
WTC11 148M-SM	20	26,100,001	30,500,000	4.4 Mb	P11.1 - q11	4.8142	Gain	1.2673
	X	88,450,001	92,350,000	3.9 Mb	q21.31	1.4918	Gain	-0.4229

Figure 12: Karyotyping results of cell clones

Done by the Human Stem Cell and Genomic Engineering Center at UCLA David Geffen School of Medicine.

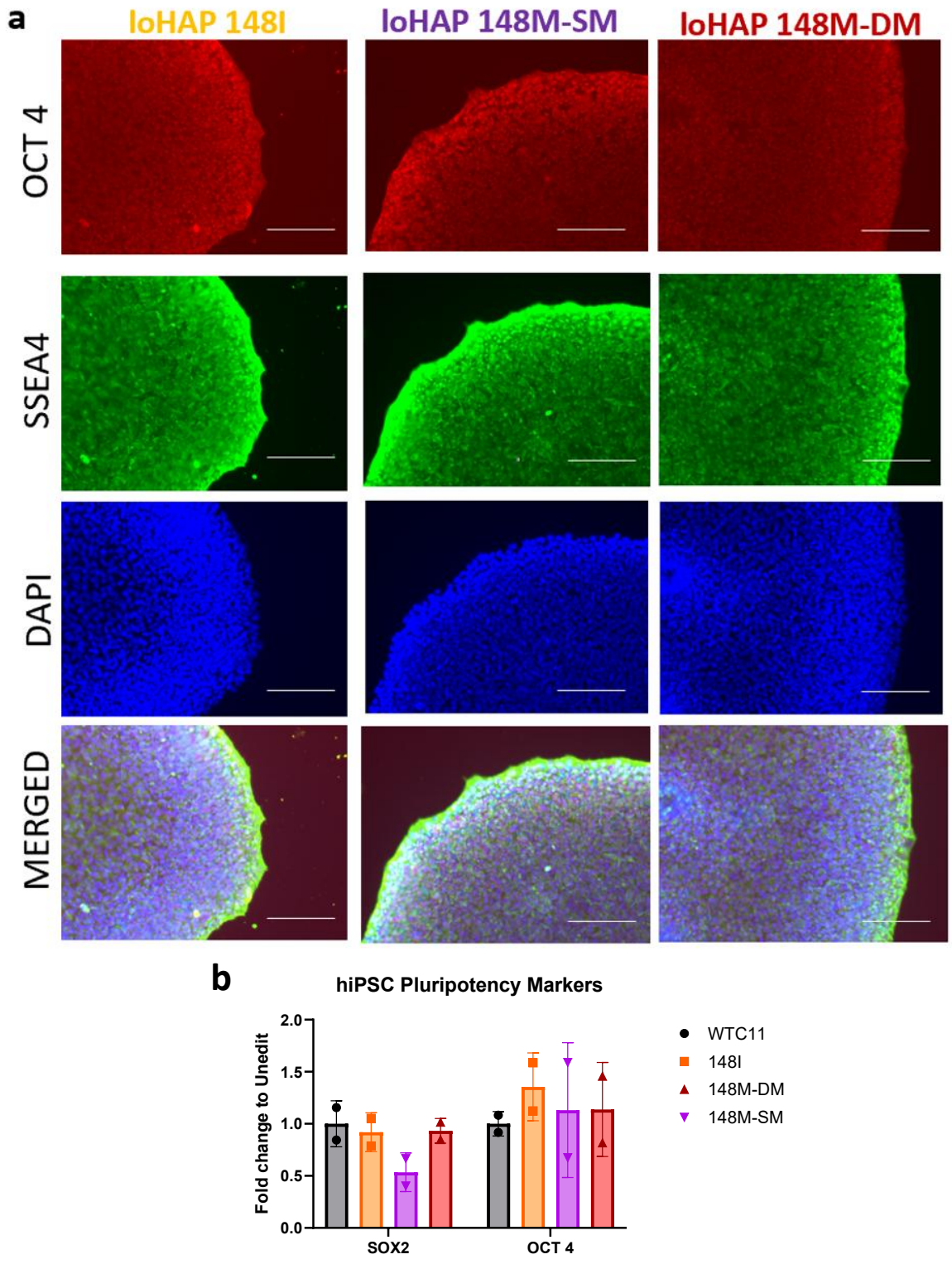

Figure 13: Pluripotency marker staining

a. loHAP clones stained with pluripotency markers OCT4 and SSEA4. Images taken at 10x, scale bar 300um
b. mRNA expression of pluripotent markers

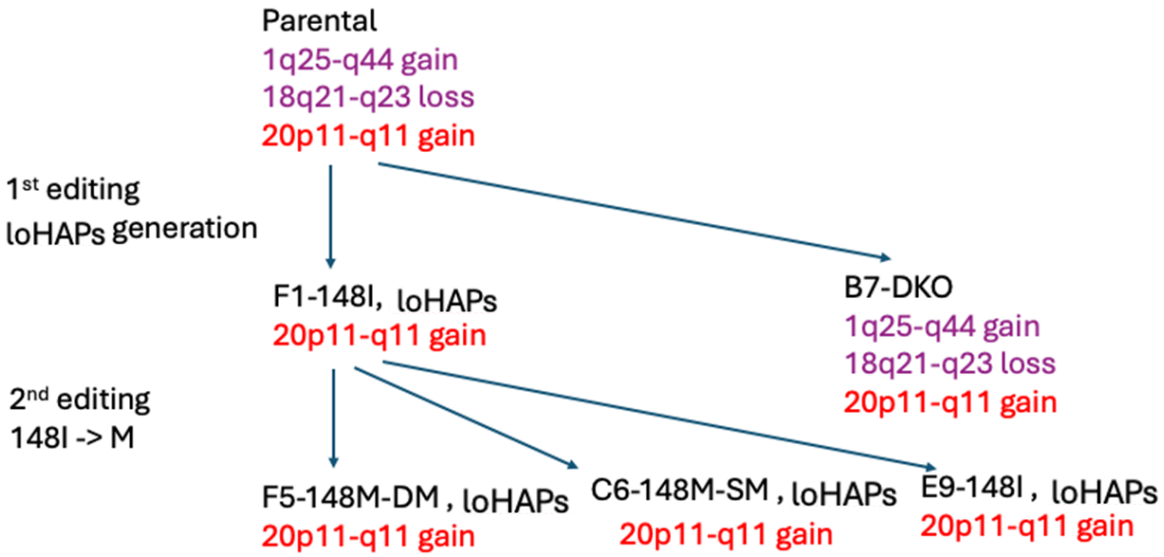

Figure 14: Karyotyping Generation Results

Layout of Karyotype between generations of loHAP cells

Chapter 3: Differentiation of PNPLA3 variants into functional hepatocytes

Contents in this chapter are modified from the following manuscript

3.1 Introduction

The *PNPLA3* loHAP 148I, loHAP 148M-SM and loHAP 148M-DM lines generated from the CRISPR-Cas9 edit were subsequently differentiated into hepatocytes. hiPSCs were first differentiated towards the definitive endoderm germ layer, the common progenitor for internal organs such as liver, pancreas and intestinal cells. After they were differentiated into the endoderm germ layer, the cells were differentiated to the posterior foregut. Lastly, the cells begin to generate and mature into the liver bud[107]. Our protocol produced hepatocytes in 27 days, which worked in WTC11[108]. The genetically edited cell lines will be differentiated using the protocol optimized by my lab, and their differentiation efficiency will be compared to unedited WTC11 hiPSCs (labeled as "Wild Type") differentiated into hepatocytes. Lastly, the cells begin to generate and mature into the liver bud[107]. Our protocol produced hepatocytes in 27 days, which worked in WTC11[108]. The genetically edited cell lines will be differentiated using the protocol optimized by my lab, and their differentiation efficiency will be compared to unedited WTC11 hiPSCs (labeled as "Wild Type") differentiated into hepatocytes.

We differentiated the wild type, loHAP 148I, 148M-SM, and 148M-DM clones to hepatocytes using our optimized hepatocyte protocol[108]. To determine differentiation efficiency, the expression of the following markers for mature hepatocytes were assessed: HNF-alpha, Albumin, and ApoB. HNF-alpha is a nuclear receptor highly conserved in liver, that promotes transcription of target genes such as ApoB[109]. Albumin is synthesized and secreted by mature hepatocytes and served as a carrier for hydrophobic molecules such as fatty acids through the bloodstream [110,111]. All the mentioned genes were used as markers to determine efficiency of hepatocyte differentiation. *PNPLA3* RNA expression was also measured to determine the impact of excising one copy of *PNPLA3*.

3.2 Results

3.2.1Differentiation of loHAPs into hepatocytes

The morphology of the hepatocytes between the different clones also remained unchanged. Hepatocytes have a hexagonal morphology along with lipid droplets accumulating inside. Images of the hepatocyte morphology across all the clones showed no difference, except for the increase of lipid droplet accumulation from Oleic Acid treatment. The loHAPs had a similar efficiency in differentiation into hepatocytes because they had no impact on the hiPSC morphology on the loHAP 148I nor the *PNPLA3* 148M. There was no difference in the expression on *PNPLA3*, nor the hepatocyte markers, other than ALB. ALB is a hepatocyte maturity marker. Despite the 148M-DM cells having a significantly higher expression of ALB than the other clones, their markers for *HNF4 alpha*, *PNPLA3*, and *ApoB* remain non-significantly different. We successfully differentiated the loHAP 148I, 148M-DM and 148M-SM clones. Wild type and loHAP 148I hepatocytes appear morphologically similar showing cells with large droplets (Fig 15a). 148M-SM had less lipid droplets and did not have any cells that had large lipid droplets. The hepatocyte markers expression in loHAP 148I is closely comparable to the unedited wild type cells, with having a significant increase in expression in hepatocyte markers (Fig 15b). In fact, loHAPs had

better efficiency in differentiating into hepatocytes compared to diploid cells, and no impact on *PNPLA3* mRNA expression.

3.2.2 LoHAP edited hiPSCs efficiently differentiated into hepatocytes and recapitulated MASLD progression

PNPLA3 inhibits lipolysis induced lipolysis by sequestering CGI-58 from ATGL, which increases the size of the lipid droplets in the hepatocytes. *PNPLA3* is inhibited during fasting through ubiquitination, allowing for ATGL to be activated by CGI-58 and drives the hydrolysis of triglycerides in the lipid droplet, depleting the triglyceride stores and shrinking the lipid droplet size. The high risk *PNPLA3* 148M cells are expected to have an impaired ubiquitination, leading to the constant binding of *PNPLA3* to CGI-58, leading to the inhibition of lipolysis in both post prandial and fasting state, resulting in enlarged and multiple lipid droplets accumulating in the hepatocytes. To determine the function of *PNPLA3* on the hydrolysis of triglycerides, we did a treatment with 500uM of Oleic Acid and stained with BODIPY (Fig 16 a).
In the low-risk cell lines, *PNPLA3* 148I had smaller lipid droplets, due to the functionality of ATGL driving lipolysis (Fig 16 b, c). For the high risk, the hepatocytes are expected to have larger lipid droplets, because of the impaired lipolysis activity of PNPLA3. On day 25 of differentiation, cells are treated with 500 uM of Oleic Acid and stained with BODIPY. 148M-DM and 148M-SM hepatocytes exhibited larger total amount of lipid droplets, and size of lipid droplets were significantly larger compared to the low risk and diploid cell lines. This confirms the editing of the cell line has been able to recapitulate the progression of *PNPLA3* facilitating MASLD development, through the increased accumulation of lipid droplets, along with the enlarged lipid droplets.
Western blots of *PNPLA3* showed a slight decrease in the expression of *PNPLA3* in loHAP (Fig 17). However, the function of *PNPLA3* in the loHAP cells was not impacted, due to the size of the lipid droplets being significantly higher in the 148M-DM and 148M-SM cells compared to the WTC11 and loHAP 148I (Fig 16).
We ran functional experiments on the differentiated hepatocytes of all the loHAP edited cells. Lipolysis will be measured by a lipolysis colorimetric assay measuring glycerol release. To determine if the enlarged lipid droplets and the increased amount of lipid droplets were due to the impairment of lipolysis, we analyzed the release of glycerol. After treatment of Oleic acid, isoproterenol and forskolin to induce lipolysis, 148M-DM and 148M-SM clones had significantly blunted lipolysis compared to 148I hepatocytes (Fig 18). This significant decrease in glycerol release was seen in all treatments of 148M-DM and 148M-SM. This means that the triglycerides are contained inside the lipid droplets and the lipid droplets were enlarged through hypertrophy. This shows that our isogenic cell system has been able to recapitulate the worsening of MASLD.

3.3 Discussion

For the loHAP cell lines to be used for further characterization of the impact of *PNPLA3* to MASLD, confirming their efficiency of differentiation into hepatocytes along with the ability to recapitulate the phenotype of *PNPLA3* is integral. From our tests, we have been able to see that

despite the deletion of one allele of PNPLA3, the differentiation efficiency of the loHAPs to hepatocytes remained unchanged. Compared to the diploid cell lines, there was no impairment in their hepatocyte differentiation markers, nor their morphology. We did see a slight decrease in the expression of the PNPLA3 protein. However, when observing the function of the lipid droplet size after oleic acid treatment, we determined that the decrease in *PNPLA3* protein did not have significant impact on the overall function. Despite the decrease in *PNPLA3* expression, we still see no difference in the lipid droplet size and amount of lipid droplets in the diploid WTC11 hepatocytes to the loHAP 148I cell lines. We also saw a significant increase in the lipid droplet size and amount in the mutagenized 148M-DM and 148M-SM cell lines, meaning the introduction of both the synonymous SNP and unlinking the synonymous SNP resulted in progression of MASLD (Fig 16, 17). Further optimization needs to be done for the western blot protocol, due to *PNPLA3* being notoriously difficult protein to probe due to the many off target binding of the antibody.

Furthermore, we discovered that the unlinking of the synonymous rs743408 SNP from the rs743409 resulted in no significant difference in the impaired function of *PNPLA3* 148M-DM. Both the *PNPLA3* 148M-DM and the 148M-SM resulted in increased lipid droplet size and overall lipid droplet amount. Despite there being no difference, this is a first look into the function of *PNPLA3* rs743409 independent from the SNP with the high linkage disequilibrium. In the future we would generate another cell line that just has the rs743408 SNP to further elucidate the function of it independently from rs743409.

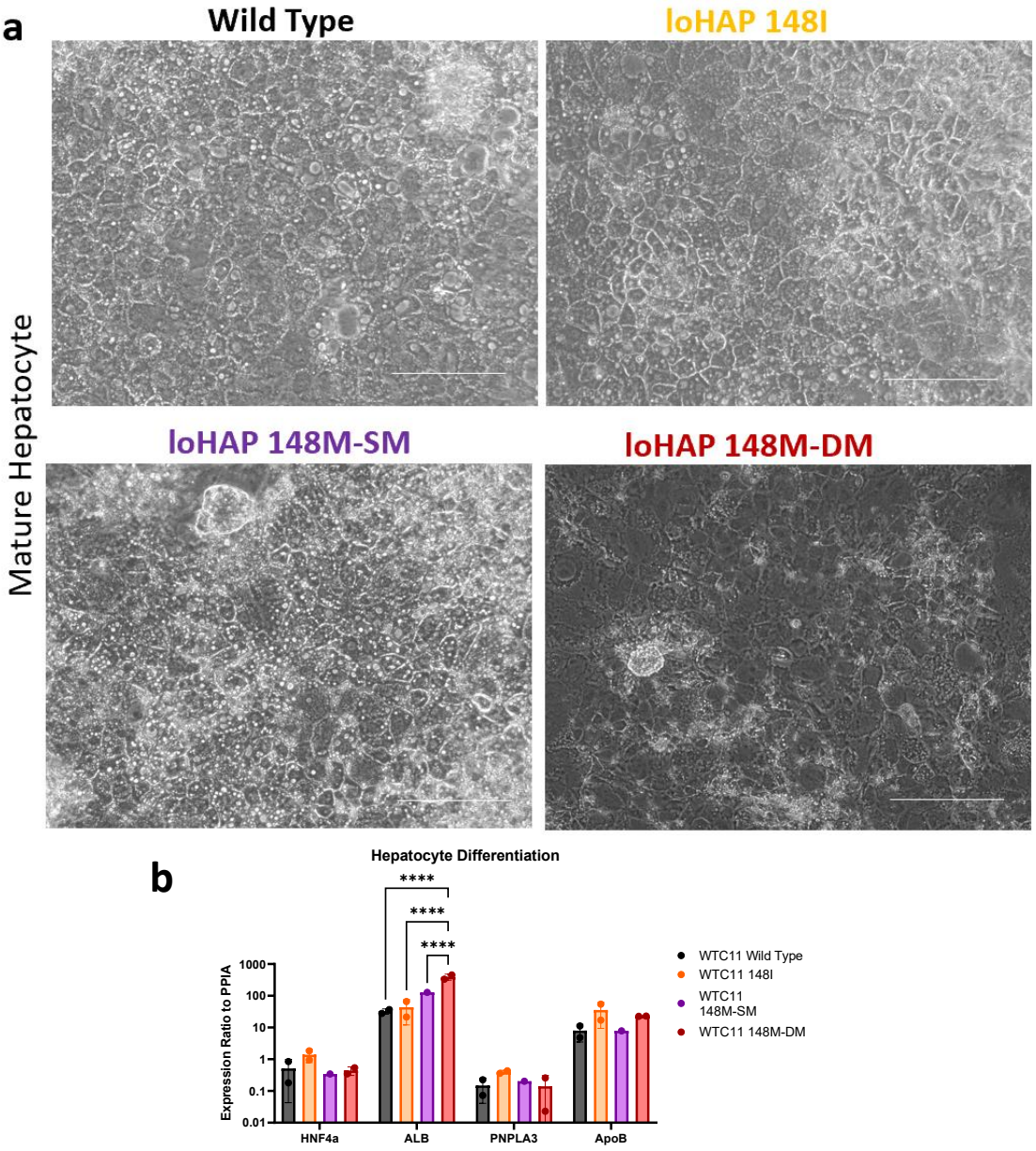

Figure 15: loHAP clone differentiation into hepatocytes

a. Diploid wild type compared to loHAP *PNPLA3*, differentiated to mature hepatocytes after 27 days images 10x scale bar 300um b. RNA expression of hepatocyte markers and *PNPLA3*

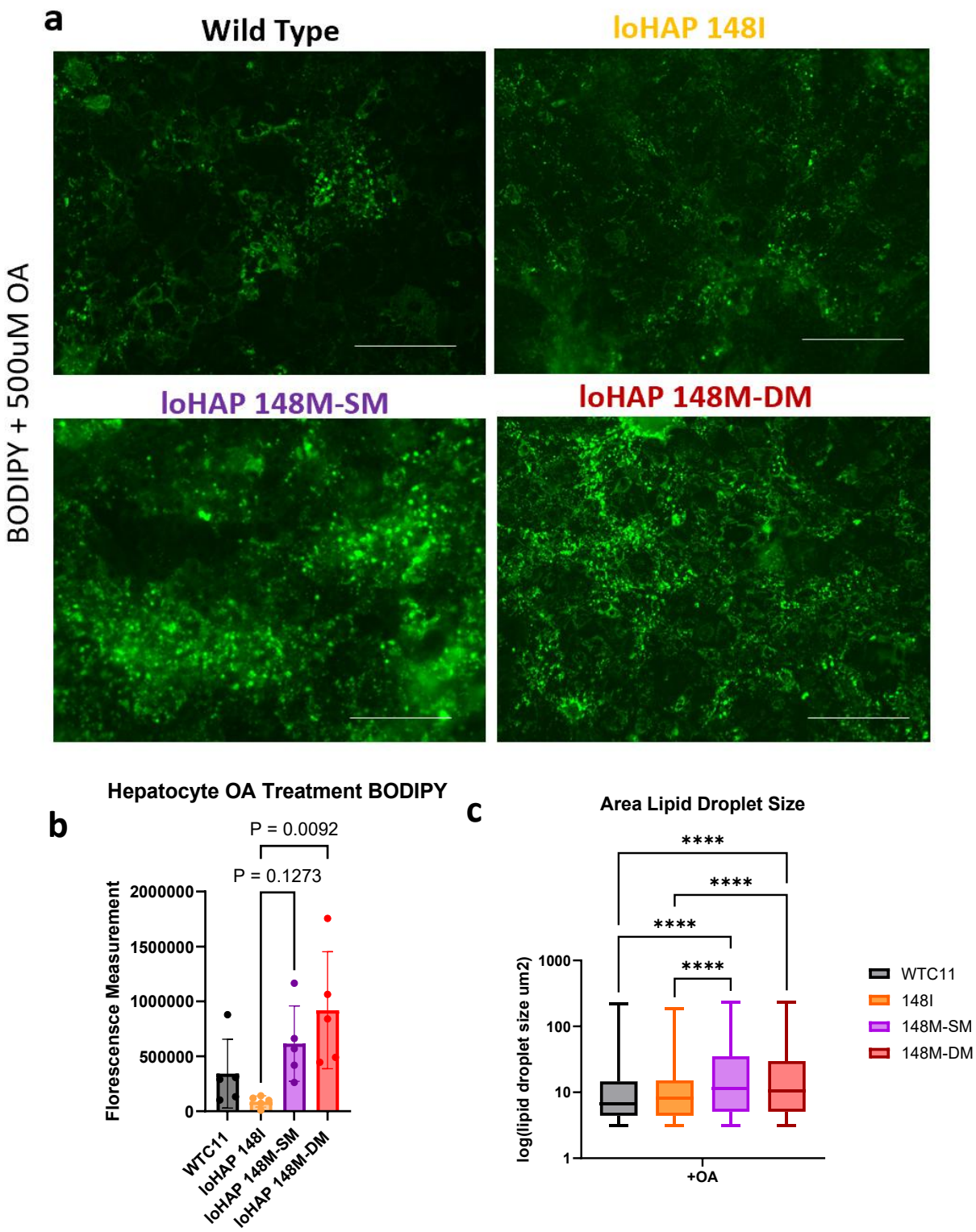

Figure 16: loHAP Hepatocyte fatty acid uptake

a. Functional impact of PNPLA3 a. loHAP clones and Wild Type cells treated with 500uM of Oleic Acid for 48 hours, lipid droplets stained with BODIPY. Images taken 10x, scale bar 300um b. Lipid Droplet accumulation analyzed using ImageJ c. Lipid droplet size analyzed using ImageJ

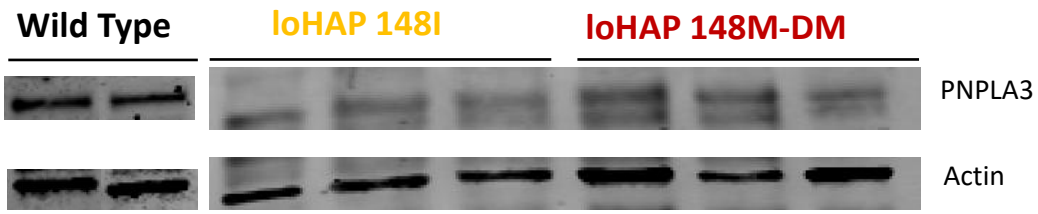

Figure 17: PNPLA3 Protein expression

Western blot of PNPLA3 of wild type and loHAP Day 27 hepatocytes treated with 500uM OA.

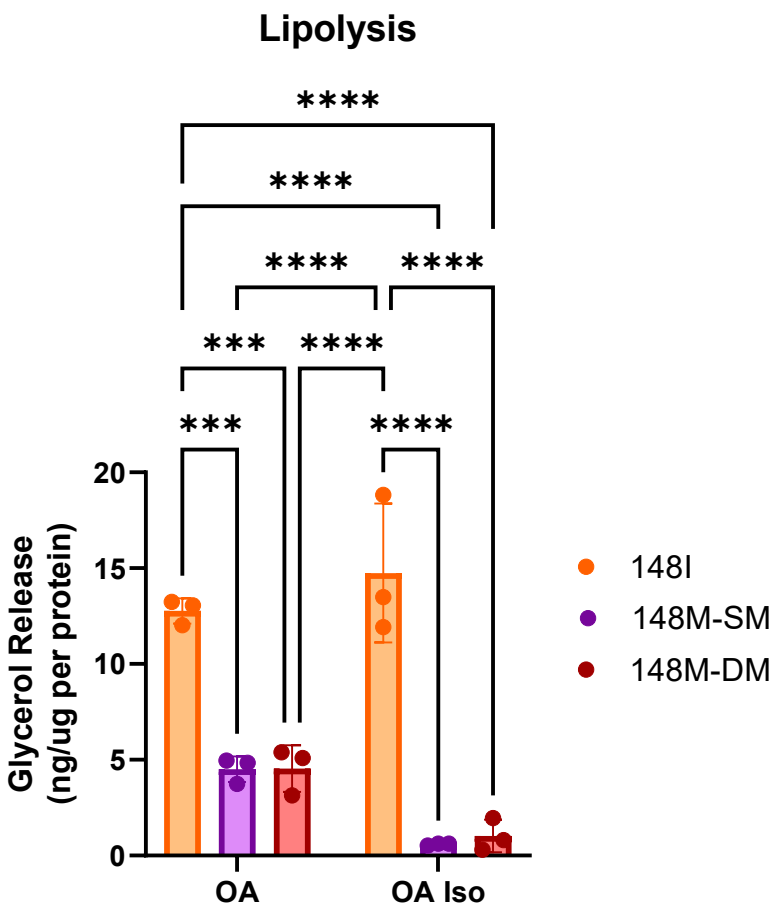

Figure 18: 148M-DM and 148M-SM high risk clones show impaired lipolysis

Free Glycerol measured from media after treatment with Isoproterenol and Forskolin to induce lipolysis, normalized to protein measured through BCA

Chapter 4: PNPLA3 drives Ferroptosis

Contents in this chapter are modified from the following manuscript

4.1 Introduction

Ferroptosis has recently emerged as hallmark of MASLD. The liver serves as a central organ maintaining lipid and iron homeostasis. Disruption of with any imbalance driving the progression of MASLD. Hepatocytes become ferroptotic due to increased imbalance of iron, and the increased uptake of PUFA in the phospholipid. After an excess of fatty acid uptake exceeds the metabolic capacity of the liver, this leads to lipotoxicity. The overload of free fatty acids will trigger ER stress and exacerbate mitochondrial ROS accumulation due to the increased mitochondrial beta-oxidation. All this compounded will induce ferroptosis and contribute to MASLD.
The role of *PNPLA3* in ferroptosis is still a confounding question that has yet to be fully answered. Within the literature, *PNPLA3* I148M variant has been determined to be a compounding factor in the exacerbation of ferroptosis. However, recent discoveries of the individual role of *PNPLA3* have elucidated that *PNPLA3* preferably hydrolysizes PUFA-TG, leading to the free PUFA to be integrated into the phospholipids. Increased PL-PUFA is integral for the lipid homeostasis of the liver, through the secretion of VLDL-TG. This raises questions about the role of ferroptosis, because the increase in PL-PUFA should increase ferroptosis sensitivity. The biallelic hydrogens are more prone to being removed from the PUFA, initiating the start of lipid peroxidation. If there was more PL-PUFA from the wild type *PNPLA3* would exacerbate the cell sensitization to ferroptosis. But if not, then there is a compensatory mechanism that is helping protect the cell from lipid peroxidation, despite the increase in PL-PUFA.
To first investigate the individual role of the 148M genetic variant with the progression of ferroptosis, we confirmed that our loHAP cell system can recapitulate the increased sensitivity of lipid peroxidation. To test this, we induced cell death through inhibiting the GPX4 ferroptosis protector with RSL3.

4.2 Results

4.2.1 The high-risk cell 148M-DM exhibited enhanced ferroptosis sensitization by RSL3, recapitulating ferroptosis driven MASLD

loHAP 148I, 148M-DM, and 148M-SM hiPSC-derived hepatocytes were differentiated on 96-well plates, with two cell lines cultured per plate to minimize plate-to-plate variability and ensure the same treatment conditions. By day 25 of differentiation, hepatocyte-like cells displayed mature morphology and were subsequently subjected to ferroptosis induction using RSL3, a selective inhibitor of glutathione peroxidase 4 (GPX4). GPX4 is a critical antioxidant enzyme responsible for reducing lipid hydroperoxides within phospholipid membranes, and its inhibition promotes the accumulation of lipid reactive oxygen species, ultimately triggering ferroptotic cell death.
Cells were treated with increasing concentrations of RSL3 ranging from 50nM to 10 μM for 24 hours to assess the susceptibility of each PNPLA3 genotype to ferroptosis.
The difference became most pronounced at the highest concentration of 10 μM RSL3, indicating that cells carrying the homozygous I148M mutation possess heightened sensitivity to GPX4 inhibition and ferroptotic stress. These findings support previous evidence linking the PNPLA3 I148M variant to dysregulated lipid remodeling and increased vulnerability to lipid peroxidation.

Interestingly, hepatocytes carrying the synonymous SNP in combination with the I148M variant (148M-SM) demonstrated a modest reduction in ferroptotic cell death relative to the 148M-DM cells. Although the synonymous mutation does not alter the amino acid sequence of PNPLA3, this observation suggests that the variant may still influence cellular function through alternative mechanisms such as altered mRNA stability, translation efficiency, codon usage bias, or transcriptional regulation. The reduced susceptibility observed in the 148M-SM cells raises the possibility that the synonymous SNP modulates the pathological effects of the I148M mutation and may contribute to differences in ferroptosis sensitivity between PNPLA3 haplotypes (Fig. 19a).

4.2.2 Gene expression of protective Ferroptosis genes were not impacted compared to loHAP 148I, 148M-DM and 148M-SM

As mentioned in Chapter 1, cells have protective enzymes that are integral for protecting the phospholipid membrane from lipid peroxidation. Ferroptosis is driven from lipid accumulation of oxidized PL-PUFA, making the regulation of the membrane structure crucial for the protection against ferroptosis. One of the primary protective enzymes is GPX4, which reduces toxic phospholipid hydroperoxides into non-toxic lipid alcohols. Inhibition of GPX4 through RSL3 disrupts its ability to protect, resulting in uncontrolled accumulation of lipid peroxidation and ultimately ferroptotic cell death. Because GPX4 is a central protective enzyme against ferroptosis, alterations in its expression or its compensatory antioxidant pathway FSP1 have been proposed to influence the ferroptosis sensitivity in PNPLA3 MASLD models.
However, analysis of our differentiated hepatocytes showed no significant differences of GPX4 or FSP1 between the isogenic cells loHAP 148I, 148M-DM, and 148M-SM cell lines (Fig 19). These findings suggest that the increased ferroptosis sensitivity observed in the PNPLA3 risk variants is not driven by reduced baseline expression of these enzymes like the findings reported by Florentino[86]

4.3 Discussion

After treating the hepatocytes with RSL3 ferroptosis sensitizer, we were able to successfully recapitulate the progression of ferroptosis in 148M-DM, proving that the genetic variant does increase the risk of ferroptosis. From 100nM-10uM of RSL3, 148M-DM exhibited exacerbated Interestingly, we also discovered that without the synonymous SNP resulted in less cell death compared to the 148M-DM with the synonymous SNP linked. This calls for further investigation into the function of the synonymous SNP in its role in ferroptosis. As mentioned in chapter 1, Rs738408 has been highly associated with MASLD, but there has been little investigation into its role in relation to I148M. This may be because it is a synonymous SNP, so there is no change in amino acid with the nucleotide substitution. However, there is evidence showing that synonymous SNPs can affect mRNA splicing, stability, and even some rare cases, influence the in-vivo protein conformation[57–59]. The role of rs738408 in I148M must be further investigated, so we can have a better understanding of it which influences the function of I148M.

A paper investigating the influence of *PNPLA3* 148M on the progression of ferroptosis revealed that 148M had decreased expression of GPX4. They hypothesized that the SNP is directly responsible for the progression of ferroptosis due to the lack of GPX4. However, they investigated two different cell types, one being homozygous for 148I and the other homozygous for 148M.
The direct link of *PNPLA3* and the cell death of hepatocytes through ferroptosis was investigated through our findings. Our system utilizes isogenic cell lines, with the only difference between each line being the change in SNP. This gives us an advantage to investigate how the change in nucleotide directly impacts the sensitivity of hepatocytes to ferroptosis, which led us to the leading experiments to investigate I148M and the impairment of NAD+ metabolism.

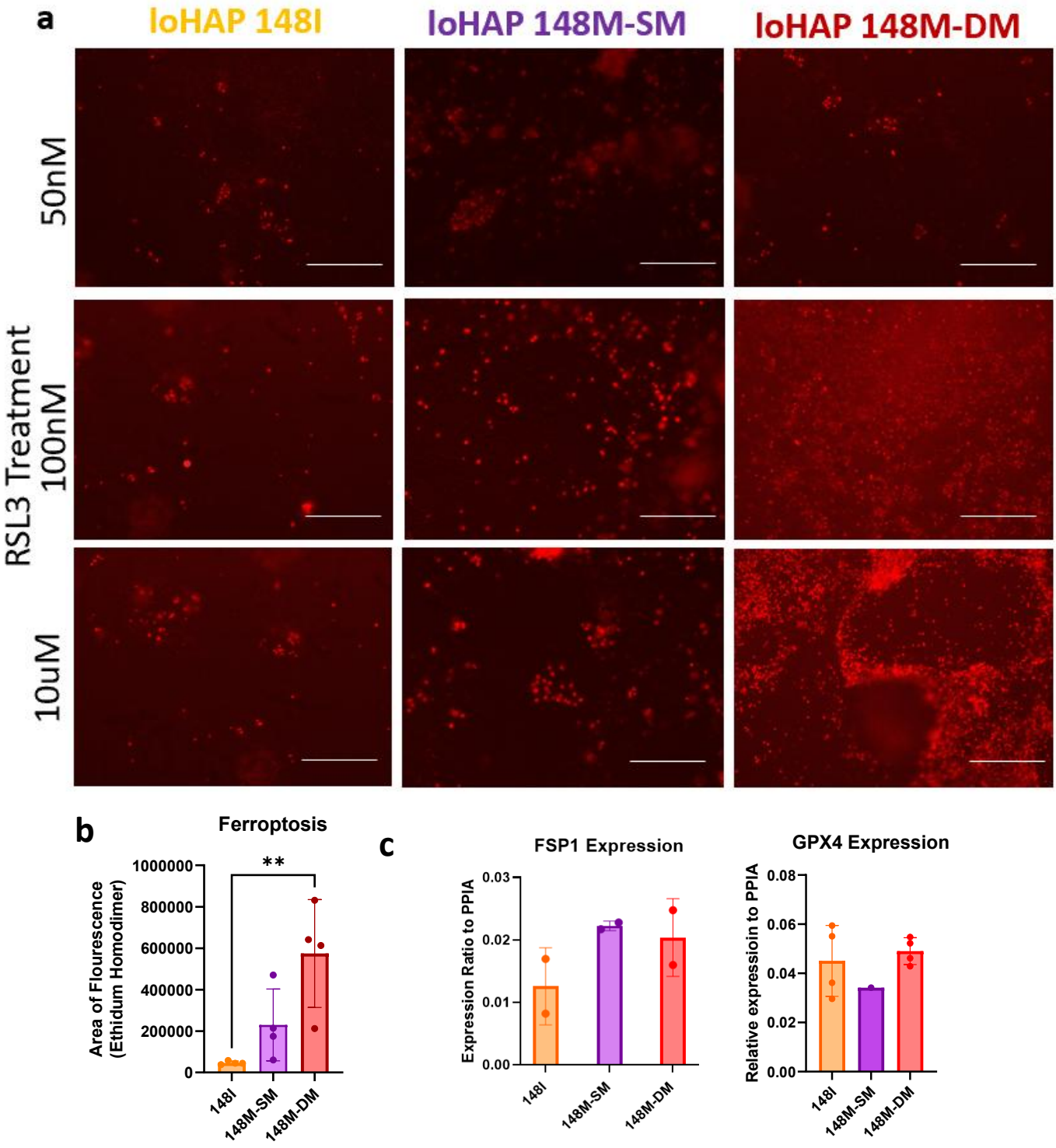

Figure 19: loHAP 148M-DM ferroptosis induced cell death

Hepatocytes differentiated on 96 well plate were treated with RSL3 from 50nM-10uM for 24 hours, stained with Ethidium Homodimer, images taken at 10x, scale bar 300um b. Image J analysis f Area Fluorescence of Ethidium Homodimer c. mRNA expression of FSP1 and GPX4

Chapter 5: *PNPLA3* drives NAD+ dysfunction

Contents in this chapter are modified from the following manuscript

5.1 Introduction

Intracellular NAD+ in hepatocytes plays a critical role in cellular metabolism. Research on supplementation of NAD+ has been shown to ameliorate fatty liver disease. A decline of NAD+ content contributes to the development of liver steatosis and fibrosis[112]. Emerging evidence suggests that *PNPLA3* I148M impairs NAD+ biosynthesis through the reduced expression of NAPRT1, part of the Preiss-Handler pathway, which converts nicotinic acid into NAD+[92]. Transcriptomic analysis confirmed these findings revealing that hepatocytes expressing wild-type *PNPLA3* exhibit higher NAD+ metabolic activity compared to those expressing the I148M variant[86].

NAD+ availability is also critical for ferroptosis defense pathways. Antioxidant enzymes such as GPX4 and FSP1 depend on cellular redox balance maintained by NADPH. GPX4 activity requires cysteine, derived from cystine uptake via the cystine-glutamate antiporter and subsequent NADPH-dependent reduction. Cysteine is then used to synthesize glutathione, the essential substrate for GPX4-mediated detoxification the lipid peroxides. Oxidized glutathione is recycled by NADPH-dependent glutathione reductase to be reutilized by GPX4. In parallel, FSP1 functions as a radical-trapping antioxidant following its myristoylation by NMT, attaching it to the plasma membrane[72,113]. It reduces coenzyme Q10 (CoQ10) to CoQ10H2 to ameliorate lipid peroxidation. Both GPX4 and FSP1 pathways are tightly coupled to NADPH availability linking NAD+ to cellular protection against ferroptosis.

The link between *PNPLA3* and ferroptosis lies in the impairment of NAD+ biosynthesis. Our isogenic stem cell system enables direct investigation of the link between the I148M genetic variant and NAD+ metabolism. In this chapter, we observe the phenotypic changes to be specifically attributed to the genetic variant.

5.2 Results

5.2.1 qPCR results of the loHAP cells confirm the decrease of NAD+ biosynthesis due to the genetic variation

The differentiated hepatocytes of loHAP 148M-DM line exhibited significantly reduced expression of NAPRT, consistent with the findings reported by Paolini et al[92]. In contrast, no significant differences were observed in NMNAT1 expression between the loHAP cell lines, suggesting that the downstream enzymatic machinery required for NAD+ synthesis remains intact. These results indicate a more specific defect in the Preiss-Handler pathway rather than a complete disruption of overall NAD+ biosynthesis, while the NAD+ salvage pathway may remain at least partially functional. NAPRT serves as the rate-limiting enzyme of the Preiss-Handler pathway, catalyzing the conversion of nicotinic acid (NA) into nicotinic acid mononucleotide (NAMN), the first committed step in NAD+ synthesis from dietary niacin. NAMN is subsequently converted by NMNAT enzymes into nicotinic acid adenine dinucleotide (NAAD), which is then amidated to form NAD+. Because NMNAT expression was unchanged, the observed reduction in NAD+ levels is likely driven primarily by limited substrate entry into the pathway due to decreased NAPRT expression rather than impaired downstream conversion. This reduction in NAPRT may therefore restrict hepatocyte capacity to replenish NAD+ pools under conditions of metabolic

stress, increasing susceptibility to mitochondrial dysfunction, oxidative stress, and lipid peroxidation. Since NAD+ is required for multiple redox reactions, mitochondrial β-oxidation, and antioxidant defense systems, impaired NAD+ biosynthesis may contribute to the progression of MASLD in *PNPLA3* I148M hepatocytes by weakening cellular resilience to lipotoxicity and ferroptotic stress (Fig. 20a,b).

5.2.2 NAD+ accumulation after Nicotinamide Riboside Treatment in both 148I and 148M-DM loHAP cells

Basal intracellular NAD+ levels were measured in the 148I and 148M-DM hepatocyte lines and revealed a significant reduction in total NAD+ content in the 148M-DM cells. Despite this decrease, no corresponding change was observed in the NAD+/NADH redox ratio, suggesting that while the overall NAD+ pool is diminished (Fig. 20c). The relative balance between oxidized and reduced nicotinamide cofactors remained maintained under basal conditions. However, a lower total NAD+ pool may still compromise the capacity of hepatocytes to respond to metabolic stress, particularly during conditions requiring increased mitochondrial respiration, lipid oxidation, and antioxidant defense.

To determine whether NAD+ depletion could still be rescued through the salvage pathway, hepatocytes were supplemented with 10 mM nicotinamide riboside (NR) for 48 hours. NR is a precursor of the NAD+ salvage pathway and bypasses the Preiss-Handler pathway by entering NAD+ biosynthesis through conversion to nicotinamide mononucleotide (NMN), which is then converted to NAD+ by NMNAT enzymes. Following NR treatment, NAD+ measurements showed a trend toward increased intracellular NAD+ accumulation in both the 148I and 148M-DM cell lines, indicating that the salvage pathway remains functionally active. However, the 148M-DM cells continued to exhibit lower NAD+ levels compared to the 148I cells, suggesting that NR supplementation only partially restores the NAD+ pools.

These findings support the hypothesis that reduced NAPRT expression impairs the Preiss-Handler pathway in *PNPLA3* I148M hepatocytes, while the salvage pathway retains partial capacity to compensate for this loss. The ability of NR to elevate NAD+ levels suggests a potential therapeutic strategy for improving hepatocyte resistance to ferroptosis. Restoring NAD+ availability may help protect 148M-DM hepatocytes from lipid peroxidation and ferroptotic cell death during MASLD progression.

5.2.3 Rescue of NR protected against ferroptosis

To determine whether nicotinamide riboside (NR) supplementation was sufficient to protect hepatocytes against ferroptosis, the ferroptosis induction experiments described in Chapter 4 were repeated using hepatocytes differentiated on Revvity PhenoPlates optimized for high-content imaging with the Opera Phenix imaging system. This platform allowed for improved quantitative assessment of cell viability and fluorescent marker analysis across multiple fields per well. Hepatocytes were first pretreated with 10 mM NR for 24 hours to allow intracellular NAD+ pools to increase prior to ferroptotic challenge. Following pretreatment, cells were exposed to RSL3 in the presence or absence of continued NR supplementation.

After treatment, cells were stained and imaged using the Opera Phenix high-content screening system, and fluorescence intensity and cell viability were quantified using the Harmony image analysis software. Consistent with previous findings, the high-risk 148M-DM hepatocytes exhibited a slightly higher percentage of cell death compared to the low-risk 148I hepatocytes following RSL3 treatment, further supporting the increased susceptibility of PNPLA3 I148M cells to ferroptotic stress.

Importantly, a trend toward rescue from RSL3-induced cell death was observed in both cell lines following NR supplementation, with the effect appearing more biologically relevant in the 148M-DM hepatocytes. Although the rescue was modest, these findings suggest that restoration of NAD+ availability may improve cellular resistance to ferroptosis. NR likely supports this protection by improving NADPH production indirectly, which is critical for maintaining reduced glutathione and supporting GPX4-mediated detoxification of lipid peroxides.

These results provide preliminary evidence that targeting NAD+ metabolism may represent a potential therapeutic strategy for reducing ferroptotic vulnerability in *PNPLA3*-driven MASLD. While further validation is needed to confirm the magnitude and mechanism of protection, the observed trend supports the concept that NAD+ depletion contributes functionally to ferroptosis sensitivity and that NR supplementation may help restore hepatocyte function under lipotoxic conditions.

5.3 Discussion

We were able to confirm that the increase in ferroptosis driving MASLD progression is associated with impaired NAD+ biosynthesis in the PNPLA3 148M-DM high risk hepatocytes. Specifically, a paper found that the PNPLA3 I148M genetic variant was associated with a statistically significant decrease in expression of NAPRT, a finding that was confirmed in our isogenic loHAP hepatocyte cells. NAPRT is the rate-limiting enzyme of the Preiss-Handler pathway and is responsible for converting NA into NAMN. Reduced NAPRT expression impairs NAD+ production and contributes to lower NAD+ availability. We confirmed this by measuring the basal NAD+ levels, which showed a significant reduction in high risk 148M-DM and 148M-SM hepatocytes compared to low risk 148I hepatocytes.

Notably, supplementation with NR, the precursor of the NAD+ salvage pathway, increased intracellular NAD+ levels in both 148I and 148M-DM hepatocytes. Because NR bypasses the Preiss-Handler pathway and enters NAD+ synthesis through the conversion to NMN, this result indicates that the salvage pathway remains functional and can compensate for reduced NAPRT activity. After treatment with both NR and RSL3, a trend toward partial rescue from ferroptosis in both the low risk 148I and high risk 148M-DM hepatocytes. RSL3 directly inhibits GPX4, the central enzyme responsible for reducing lipid peroxidation. This suggests that NR supplementation may help with protection against ferroptosis, through the increase in NAD+, thus indirectly supporting NADPH synthesis and FSP1 directed protection. These findings provide mechanistic insight into how the *PNPLA3* I148M variant increases susceptibility to ferroptosis and promotes the progression for MASLD, through the disruption of NAD+ metabolism.

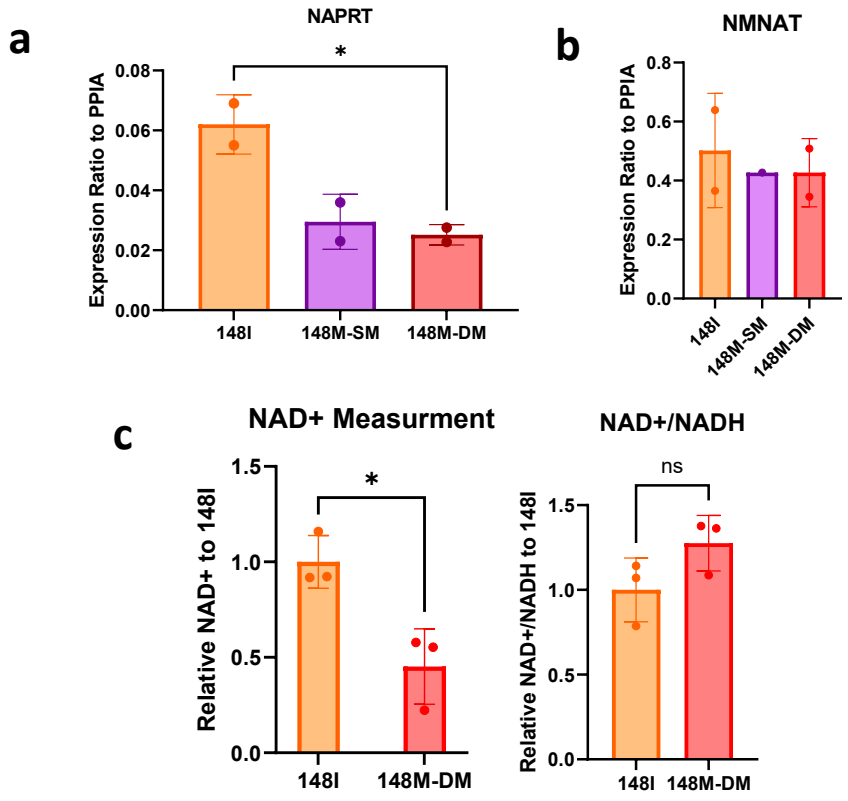

Figure 20: NAD+ Metabolism impaired in high risk 148M-DM hepatocytes

a. mRNA expression of Preiss-Handler NAD+ biosynthesis enzyme NAPRT b. mRNA expression of Salvage Pathway NAD+ recycling enzyme c. NAD+ and NAD+/NADH ratio measured through NAD+/NADH Promega kit

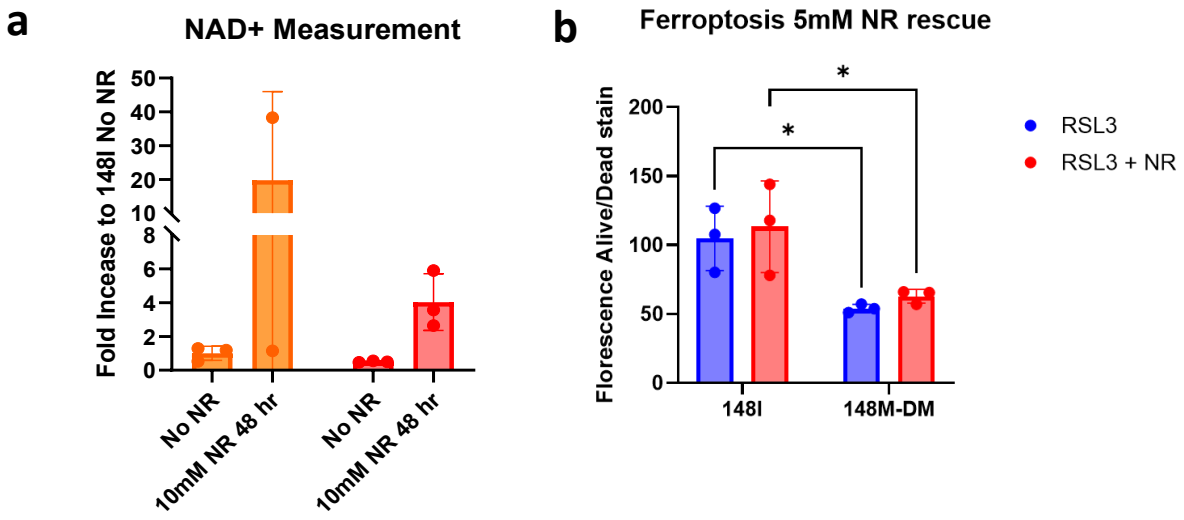

Figure 21: Nicotinamide Riboside treatment trended rescue from ferroptosis induction

a. Low risk loHAP 148I and high risk loHAP 148M-DM treated with 10mM of nicotinamide riboside showed increase in NAD+ biosynthesis, measured with ProMega NAD+/NADH Glo Kit. b. loHAP low risk and high-risk cells treated with 10uM RSL3 and rescued with 10mM NR

5.4 Conclusion

This dissertation started investigation into the direct role of the *PNPLA3* genetic variant I148M and rs738408 in promoting ferroptosis, which contributes to the progression of MASLD. We took advantage of the locally haploid cell editing strategy optimized by the Hockemeyer laboratory using CRISPR-Cas9 editing generating loHAP isogenic cell lines. We made 3 cell lines, each expressing different genetic variants from the low risk 148I, high risk 148M-DM linked with synonymous SNP, and 148M-SM unlinked from synonymous SNP. These loHAP clones were able to successfully differentiate into functioning hepatocytes, showcasing the progression of MASLD through increased lipid accumulation and impairment of lipolysis. From there, we ran ferroptosis assays that recapitulated the increased sensitivity of ferroptosis in the 148M genetic variant.

Questions were raised about the progression of ferroptosis with *PNPLA3* I148M because of its wild type function to release PUFA from TG and initiate the incorporation of PUFAs into the phospholipid membrane. Increase PL-PUFA exacerbates the sensitivity of ferroptotic cell death due to its susceptibility to lipid peroxidation compared to PL-MUFA. To figure out how wild type *PNPLA3* protects the cell from ferroptosis despite the increased accumulation of PL-PUFA, we decided to investigate the impact of NAD+ biosynthesis. Both ferroptosis protective enzymes GPX4 and FSP1 are reliant on the NAD+ pools. We discovered that *PNPLA3* 148M-DM and 148M-SM both have significant decrease in *NAPRT*, a NAD+ biosynthesis gene that is important for the Preiss-Handler Pathway. Rescue treatment with nicotinamide riboside showed improvement in *PNPLA3* 148M-DM NAD+ biosynthesis. This shows the potential of *PNPLA3* 148M being rescued from ferroptosis induction with the supplementation of NAD+.

PNPLA3 I148M drives the impairment of NAD+ metabolism, causing cellular redox mechanisms to be dysregulated and the function of ferroptosis radical-trapping antioxidant processes to be ablated. NAD+ supplementation could be a beneficial treatment to protect patients with the variant from MASLD progression, reducing inflammation from lipid peroxidation.

Overall, this study identifies NAD+ deficiency as a previously underappreciated contributor to ferroptosis in PNPLA3-driven MASLD and suggests that therapeutic strategies aimed at restoring NAD+ homeostasis, such as NR supplementation, may offer a potential approach to reduce hepatocyte injury and slow disease progression. Further studies are needed to determine the long-term efficacy of NAD+ restoration and whether combination therapies targeting both lipid remodeling and redox metabolism may provide stronger protection against ferroptosis.

6.1 Methods and Materials

6.1.1 Tissue Culture

WTC11 is an induced pluripotent stem cell generated by Dr. Bruce Conklin as a control for diseased iPSCs. The stem cell line was generated from the skin of a healthy Japanese 30-year-old male. WTC11 has been genotyped to be heterozygous for PNPLA3 I148M. Cells were recovered from frozen in mTSER Plus supplemented with 10uM Y27632 on Matrigel coated plates. After 24 hours of plating, cells have media replaced with mTSER Plus, then changed every other day.

6.1.2 Generation of loHAPs

To generate the loHAPs, we designed of guide RNAs 200 bp upstream from the PNPLA3 end site of the gene of interest, avoiding potential off-target effects. After nucleofection, cells were seeded at 1k, 10k, and 30k cells per well in a 6 well for recovery and expansion for viable cells. After nucleofected cells proliferate into colonies, cells are seeded onto 3 vitronectin coated 96 well plates at seeding densities of 100, 300, and 1000 cells per plate, to optimize low seeding densities for single cell attachment in each well. Remaining cells were frozen into vials labeled as bulk edits. After 1 day for attachment, each well was checked to determine single cell attachment. Wells with only one cell attached were circled on the plate lid and notated on notebook. mTSER Plus media with 10uM Y27632 was changed after 3 days of plating, then mTSER Plus media was changed every other day. On day 10 when the single cells have proliferated into colonies, cells are washed with PBS once then treated with 25uL of Accutase. Accutase was neutralized with 25uL of mTSER Plus supplemented with 10 uM Y27632. Cells were carefully resuspended and 25uL of suspension was dispensed in a new vitronectin coated 96 well plate loaded with 75uL of mTSER Plus supplemented with 10uM Y27632 to be cultured for 7 days. The remaining 25uL of suspension was transferred in a 96-well PCR plate with 25uL of 2x lysis buffer (100 mM KCl, 4mM MgCl2, 0.9% NP-40, 0.9% Tween-20, and 500 ug ml-1 protease K, in 20 mM Tris ph8). Cell lysate in 96-well PCR plate was incubated at 50*C for 1 hour, then heated to 95*C for 10 minutes to inactivate proteinase K. Cell clones were genotyped by using primer pairs flanking the deleted region, around 100 bp away from the CRISPR cut site to capture the extended deletion. Touch Down PCR was run for optimal binding of primers. Amplicons were visualized by agarose gel electrophoresis, then extracted through DNA gel extraction kits (NEB). Extracted DNA was sequenced by NGS. Primers contained NGS barcode attachment sites (GCTCTTCCGATCT). NGS data were analyzed using CRISPResso to identify the remaining allele. Cells identified as loHAP were subcloned by low-density seeding and genotyped to establish clonal loHAP cell lines.

6.1.3 CRISPR-mediated mutagenesis

To introduce Rs738409 and unlink from rs738408, 300 pmol sgRNA and 80 pmol ppurified Cas9 protein were delivered as RNP as described above. Targeted designer mutations were introduced with a 150 nt ssODN HDR template centered around the I148M site. HDR templates were designed

on Benchling, then sent over to IDT to be made. sgRNA sequences are sent over to Synthego for development.

6.1.4 Cas9/sgRNA RNP assembly

Designed sgRNA was ordered from Synthego. Cas9 protein from QB3 MacroLab from UC Berkeley. RNP was assembled with 300 pmol sgRNA (designs shown above) and 80 pmol Cas9 mixed in nuclease-free water to a final volume of 10uL. RNP is incubated at room temperature for 5-10 minutes before nucleofection.

6.1.5 Genomic DNA Extraction

Cells are washed with DPBS, then harvested with Accutase. Cells are pelleted, then resuspended with 100uL cold PBS in 1.5mL Eppendorf tube. Sample lysis follows the NEB Genomic DNA extraction protocol (NEB Monarch Genomic DNA Extraction T3010), but lysates are incubated at 56-degree Celsius heat block for 45 minutes, at 5-minute intervals. After each 5-minute interval, samples are vortexed for 10-15 seconds, then placed back onto the heat block. Genomic DNA Binding and Elution protocol is then followed with the prepared lysis.

6.1.6 Nucleofection

hiPSCs cultured on either vitronectin or Matrigel coated plates. hiPSC were washed with 1x PBS and then detached from plates with Accutase (SCR005, Millipore Sigma) for 5-7 minutes at 37*C. Accutase were neutralized with DMEM/F12 then cells were subsequently pelleted, spun down at 300 rcf for 5 minutes, then counted. 500k cells were pelleted and resuspended in 20 uL Lonza P3 primary nucleofection reagent, mixed with pre-assembled Cas9/sgRNA RNP (protocol described above). Generation of LoHAP nucleofection mixed without 100 pmol of ssODN HDR donor (ssODN HDR design shown above). Cells nucleofected using program CA137 on Lonza nucleofector 4D. For nucleofection of the loHAP cells for mutagenesis of remaining allele, cells were mixed with pre-assembled Cas9/sgRNA flanking the I148M SNP and ssODN HDR donor designed to change the G to C, and T to an A for the double mutant. Followed the same nucleofection protocol.

6.1.7 NGS Genomic DNA Extraction

Bands imaged after gel electrophoresis are sliced out with a blade, while being visualized under a UV light box. Slices are cut to less than 150mg. Each gel slice is weighed and then melted following the protocol of the NEB Genomic DNA extraction kit.

6.1.8 PCR

hiPSCs genomic DNA are harvested with 2× lysis buffer (100 mM KCl, 4 mM MgCl2, 0.9% NP-40, 0.9% Tween-20 and 500 µg ml−1 proteinase K, in 20 mM Tris pH 8) for DNA extraction. Cell lysis was incubated at 50*C for one hour, then heated to 95*C to inactivate proteinase K. Amplicons were expanded using PrimeSTAR GXL Tanaka kit. PCR touchdown protocol. Primers designed on Benchling, made by IDT.

Touch Down PCR

Step	Temperature	Time
1	98*C	3:00
2	98*C	0:30
3	70*C (-1*C Per cycle)	0:30
4	72*C	0:30
5	GOTO Step 2 16x	
6	98*C	0:30
7	54*C	0:30
8	72*C	0:30
9	GOTO Step 6, 23x	
10	72*C	7:00
11	4*C	Infinity

6.1.9 Western Blot Cell Lysate Harvest and Protein Concentration Analysis

Cell lysates are washed with cold PBS twice. On ice, lysates are harvested with RIPA buffer and 100x phosphatase and protease inhibitor. Lysates are spun down at 12,000 rpm and in a 4 degree Celsius refrigerated centrifuge for 10 minutes. Supernatant was collected in a separate tube, and protein concentration was determined by following protocol of Pierce BCA Protein Assay (Thermo Fisher A55864).

6.1.10 Hepatocyte Differentiation

hiPSCs are grown up to 80% confluency, which are then seeded 1:1 on a new 24 well plate.1 day after seeding, cells will undergo three phases of differentiation to turn the hiPSCs into definitive endoderm, hepatocyte specific, then mature hepatocytes. Day 1, basal media consists of RPMI with no phenol red, 1% Anti-anti/Pen Strep, 10mL of B27 supplement -insulin, 1% NEAA, and 25mM HEPES. Day 1 treated with 100ng/mL Activin A, 20ng/mL FGF2, 10ng/mL BMP4, 25nM PI103, 4uM CHIR99021, 1uM Doxycycline, and 2uM Y-27632. Day 2 has same composition as day 1 but CHIR99021 was removed. Day 3, same composition as Day 2, but FGF2 and BMP4 removed. Day 4-7, same composition as day 3 but PI103 removed. Day 8-17, basal media consists of IMDM without phenol red, 1% NEAA, 1% Anti-Anti, and 10mL B27 Supplement with insulin. Day 8-12 consists of 20ng/mL FGF2 and 10ng/mL BMP4. Day 13-17 is the same as Day 8-12 but

with 20ng/mL of HGF. Day18-28 base media is the Lonza HCM with all growth factors that come with the kit except for hEGF. Day 18-23 consists of 20ng/mL Onconstatin M, and 20ng/mL of HGF. Day 24-27 consists of just 20ng/mL of HGF.

6.1.11 Lipolysis

On day 25 of hepatocyte differentiation, cells were treated with 500uM of Oleic Acid diluted in 5% BSA and with 2uM BODIPY 493/503 (3822 Thermo Fisher Scientific) for 48 hours. After the treatment, cells were washed twice with 1x PBS, then media replaced with HBSS with 1% BSA. 500uL of HBSS in each well for 12 well plates, or 250uL in 24 well plates. With 3 conditions on the plate, treat with 10uM Isoproterenol (I6504 Sigma), 400uM Forskolin, or basal in the HBSS media. Collect the HBSS media at 0 Hour and after 4 hours. Remaining cells were washed with PBS and harvested for western blot with RIPA and 1:100 Protease and phosphatase inhibitor. For glycerol analysis, standards were made with Glycerol Standard Solution (G7793 Sigma). 100uL of standard and HBSS sample from hours 0 and 4 were loaded on 96 well plate. 100uL of Free Glycerol Reagent (F6428 Sigma) was added, plate is then placed in the 37 degree Celsius Incubator for 5 minutes. Read absorbance at 540 nm. Use Plate Reader SpectraMax i3. Glycerol released was normalized to protein amount, measured by BCA.

6.1.12 Live Dead Staining Ferroptosis

On day 25 of hepatocyte differentiation, cells are treated with RSL3 (Cayman Cat. No.S8155) from dilutions of 5nM-25uM. Wells are treated 10mM of Nicotinamide Riboside (NR) for the rescue of ferroptosis. Cells were treated for 48 hours. After 48 hours, cells are washed once with 1x PBS except for the positive control wells. The positive control wells have 0.1% Saponin added to incubate at RT for 10 minutes. After the saponin treatment, positive control wells are washed with PBS. Live Dead stain is made in 10mL DPBS, 4uM Ethidium Homodimer, and 2uM Calcenin AM, and Hoechst. Incubated plate in the dark for 30 minutes at Room Temperature. Images are taken on the Opera Phenix and analyzed through Horizon.

6.1.13 NAD+/NADH Kit

Hepatocytes differentiated up to day 23 are treated with 1mM nicotinamide riboside chloride for 24-48 hours treatment remade and changed out the beginning of each day. Hepatocytes are then washed and harvested with Accutase. Cells are resuspended in 150uL of PBS then added 150uL of 1% DTAB in NaOH to lyse the cells. Follow protocol of NAD/NADH-Glo from Promega (Cat# G9071).

6.1.14 Opera Phenix High Throughput Imaging

Hepatocytes were differentiated in 96-well Revvity Opera Phenix PhenoPlates for high-content imaging. Images were acquired using the PhenoVue Fluor 594, Alexa Fluor 488, and Hoechst channels. For each well, 12 fields of view were captured with Z-stack imaging ranging from −10 µm to +10 µm. Fluorescence analysis was performed using Harmony software.

6.1.15 Table 2: sgRNA and Oligonucleotides

sgRNAs		
Experiments	Name	Protospacer
PNPLA3 loHAPs generation	loHAP PNPLA3 _R1	TCTAGGGACAAACTCTACGT
	loHAP PNPLA3 _R2*	TGCTAATAGATTATCACACC
	loHAP PNPLA3 _F1*	GTGGTTGACAACACCCTTTG
	loHAP PNPLA3_F2	ACAACCCCACTAAACTTCTT
PNPLA3 exon 3 edit	sg_PNPLA3_e3	GGATAAGGCCACTGTAGAAG
Primers		
Experiments	Name	Sequences
PNPLA3 loHAPs genotyping	PNPLA3 Deletion Detection FWD	GCACCATCCACACCTGTCC
	PNPLA3 Deletion Detection REV	CACTGACGGAGCAACCACTG
	I148M SNP FWD	GCCCCTTTCAGTCCATGAGC
	I148M SNP REV	GAAAGCCGACTTACCACGC
ssODN HDR template		
Experiments	Name	Sequences
PNPLA3 exon 3 edit	KV_PNPLA3_I148M_opool_01	gcttatgaaggatcaggaaaattaaaagggtgctctcgcct ataacttctctcctttgctttcacaggccttggtatgttcctg cttcatGcccttctacagtggccttatccctccttccttcaga ggcgtggtaagtcggctttctctgctagcgctgagtcctgggg gcctctgaagtgtgctcacacatctcct
	KV_PNPLA3_I148M_opool_02	gcttatgaaggatcaggaaaattaaaagggtgctctcgcct ataacttctctcctttgctttcacaggccttggtatgttcctg cttcatGccTttctacagtggccttatccctccttccttcaga ggcgtggtaagtcggctttctctgctagcgctgagtcctgggg gcctctgaagtgtgctcacacatctcct
	KV_PNPLA3_I148M_opool_03	aggagatgtgtgagcacacttcagaggcccccaggactca gcgctagcagagaaagccgacttaccacgcctctgaagga aggagggataaggccactgtagaaAggCatgaagcagga acataccaaggcctgtgaaagcaaaggagagagaagttat aggcgagagcacccttttaattttcctgatccttcataagc
	KV_PNPLA3_I148M_opool_04	aggagatgtgtgagcacacttcagaggcccccaggactca gcgctagcagagaaagccgacttaccacgcctctgaagga aggagggataaggccactgtagaagggCatgaagcagga acataccaaggcctgtgaaagcaaaggagagagaagttat aggcgagagcacccttttaattttcctgatccttcataagc

6.1.16 Table 3: Hepatocyte Reagents

Growth Factor	Company	Cat Number	Dose Concentration
Activin A	Gibco	12014P100UG	100 ng/ml
FGF2	Gibco	10018B1MG	20 ng/ml
BMP4	Gibco	12005ET500UG	10 ng/ml
P1103	Sigma	528101-2MG	25nM
CHIR	Sigma	361571-5MG	2uM
RI	Sigma	#688001	2uM
HGF	Gibco	10039H500UG	20 ng/ml
Oncostatin	Gibco	30010H100UG	20 ng/ml
1-Thiglycerol	Sigma	M6145-100ML	0.5mM
dexamethasone	Sigma	D4902-25MG	100nM
Doxycycline	Sigma	D5207-1G,	1uM
Knockout Serum	Gibco	10828010-100ML	1-2%
Media	**Company**	**Cat Number**	**Media Additives**
RPMI 1640 Medium, no phenol red	Gibco	11835030	B27 Supplement, Minus Insulin, 1% MEM NEAA, 1% Pen Strep, 25mM HEPES
IMDM, no phenol red	Gibco	21056023	B27 Supplement, 1% MEM NEAA, 1% Pen Strep
HCM Hepatocyte Culture Medium Kit	Lonza	CC-3198	All contents included except for FGF
Media Additives	**Company**	**Cat Number**	**Dose Concentration**
B27 Supplement, minus Insulin	Gibco	A1895601	50x
B27 Supplement, serum free	Gibco	17504044	50x
MEM Non-Essential Amino Acids Solution (100X)	Gibco	11140076	1%
HEPES (1M)	Gibco	15630130	25mM
Penicillin-Streptomycin (5,000 U/mL)	Gibco	5070063	1%

References

1. Powell, E. E., Wai-Sun Wong, V. & Rinella, M. Non-alcoholic fatty liver diseases. *Lancet* **397**, 2212–2224 (2021).

2. Jonas, W. & Shurmann, A. Genetic and epigenetic factors determining NAFLD risk. *Mol. Metab.* **50**, 1–14 (2021).

3. Iqbal, J. & Hussain, M. Intestinal lipid absorption. *Am. J. Physiol. Endocrinol. Metab.* **296**, 1183–1194 (2009).

4. Rui, L. Energy Metabolism in the Liver. *Compr. Physiol.* **4**, 177–197 (2014).

5. Trefts, E., Gannon, M. & Wasserman, D. The liver. *Curr. Biol.* **27**, 1147–1151 (2017).

6. Smith, K., Dennis, K. & Hodson, L. The ins and outs of liver fat metabolism: The effect of phenotype and diet on risk of intrahepatic triglyceride accumulation. *Exp. Physiol.* **110**, 936–948 (2025).

7. Jones, J. Some paradoxes and unresolved aspects of hepatic de novo lipogenesis. *NPJ Metab. Health Dis.* **18**, (2024).

8. Badmus, O., Hillhouse, S., Anderson, C., Hinds, T. & Stec, D. Molecular mechanisms of metabolic associated fatty liver disease (MAFLD): functional analysis of lipid metabolism pathways. *Clin. Sci.* **136**, (2022).

9. Zwol, W. van, Sluis, B. van de, Ginsberg, H. N. & Kuivenhoven, J. A. VLDL Biogenesis and Secretion: It Takes a Village. *Circ. Res.* **134**, (2024).

10. Kersten, S. Integrated physiology and systems biology of PPARα. *Mol. Metab.* **3**, 354–371 (2014).

11. Choi, J., Smith, D., Scafidi, S., Riddle, R. & Wolfgang, M. Carnitine palmitoyltransferase 1 facilitates fatty acid oxidation in a non-cell-autonomous manner. *Cell Rep.* **43**, (2024).

12. Tilg, H., Petta, S. & Stefan, N. Metabolic Dysfunction–Associated Steatotic Liver Disease in Adults. *JAMA Netw.* **335**, 163–174 (2025).

13. Pouwels, S., Sakran, N. & Graham, Y. Non-alcoholic fatty liver disease (NAFLD): a review of pathophysiology, clinical management and effects of weight loss. *BMC Endocr. Disord.* **22**, 1–9 (2022).

14. Stefan, N., Yki-Järvinen, H. & Neuschwander-Tetri, B. A. Metabolic dysfunction-associated steatotic liver disease: heterogeneous pathomechanisms and effectiveness of metabolism-based treatment. *The Lancet* **13**, 134–148 (2025).

15. Younossi, Z., Kalligeros, M. & Henry, L. Epidemiology of metabolic dysfunction-associated steatotic liver disease. *Clin. Mol. Hepatol.* **31**, 32–50 (2024).

16. Friedman, S. Fat, fibrosis, and the future: navigating the maze of MASLD/MASH. *J. Clin. Investig.* **135**, (2025).

17. Cusi, K. *et al.* Metabolic Dysfunction–Associated Steatotic Liver Disease (MASLD) in People With Diabetes: The Need for Screening and Early Intervention. A Consensus Report of the American Diabetes Association. *Diabetes Care* https://doi.org/10.2337/dci24-0094 doi:https://doi.org/10.2337/dci24-0094.

18. Liu, J. *et al.* Special correlation between diet and MASLD: positive or negative? *Cell Biosci.* **15**, (2025).

19. Maldonado-Rojas, A. del C., Zuarth-Vázquez, J. M., Uribe, M. & Barbero-Becerra, V. J. Insulin resistance and Metabolic dysfunction-associated steatotic liver disease (MASLD): Pathways of action of hypoglycemic agents. *Ann. Hepatol.* **29**, 101182 (2024).

20. Morigny, P., Houssier, M., Mouisel, E. & Langin, D. Adipocyte lipolysis and insulin resistance. *Biochimie* **125**, 259–266 (2016).

21. Konige, M., Wang, H. & Sztalryd, C. Role of adipose specific lipid droplet proteins in maintaining whole body energy homeostasis. *Biochim. Biophys. Acta* **1842**, 393–401 (2014).

22. Dua, A. *et al.* Metabolic Dysfunction-Associated Steatotic Liver Disease (MASLD): the interplay of gut microbiome, insulin resistance, and diabetes. *Front. Med.* **12**, (2025).

23. Xu, X., So, J.-S., Park, J.-G. & Lee, A.-H. Transcriptional control of hepatic lipid metabolism by SREBP and ChREBP. *Semin. Liver Dis.* **33**, 301–311 (2013).

24. Harmancey, R., Haight, D. L., Watts, K. A. & Taegtmeyer, H. Chronic Hyperinsulinemia Causes Selective Insulin Resistance and Down-regulates Uncoupling Protein 3 (UCP3) through the Activation of Sterol Regulatory Element-binding Protein (SREBP)-1 Transcription Factor in the Mouse Heart. *J. Biol. Chem.* **290**, 30947–30961 (2015).

25. Moon, Y.-A. *et al.* The Scap/SREBP Pathway Is Essential for Developing Diabetic Fatty Liver and Carbohydrate-Induced Hypertriglyceridemia in Animals. *Cell Metab.* **15**, 240–246 (2012).

26. Geidl-Flueck, B. & Gerber, P. A. Fructose drives de novo lipogenesis affecting metabolic health. *J. Endocrinol.* **257**, e220270 (2023).

27. Sanders, F. W. B. & Griffin, J. L. De novo lipogenesis in the liver in health and disease: more than just a shunting yard for glucose. *Biol. Rev. Camb. Philos. Soc.* **91**, 452–468 (2016).

28. Raza, S. *et al.* Sterile inflammation in MASH: emerging role of extracellular RNA and therapeutic strategies. *NPJ Metab. Health Dis.* **3**, (2025).

29. Kim, H. Y. *et al.* Multi-modal analysis of human hepatic stellate cells identifies novel therapeutic targets for metabolic dysfunction-associated steatotic liver disease. *J. Hepatol.* **82**, 882–897 (2025).

30. Lala, V., Zubair, M. & Minter, D. Liver Function Tests. *StatPearls* htthttps://www.ncbi.nlm.nih.gov/books/NBK482489/ (2023).

31. Oh, R., Hustead, T., Ali, S. & Pantsari, M. Mildly Elevated Liver Transaminase Levels: Causes and Evaluation. *Am. Fam. Physician* **96**, 709–715 (2017).

32. Girish, V. & John, S. Metabolic Dysfunction-Associated Steatotic Liver Disease (MASLD). in *StatPearls* (StatPearls Publishing, Treasure Island (FL), 2026).

33. Tantu, M. T. *et al.* Pathophysiology, noninvasive diagnostics and emerging personalized treatments for metabolic associated liver diseases. *Npj Gut Liver* **2**, 18 (2025).

34. Tacke, F. *et al.* EASL–EASD–EASO Clinical Practice Guidelines on the management of metabolic dysfunction-associated steatotic liver disease (MASLD). *J. Hepatol.* **81**, 492–542 (2024).

35. Zeng, J., Fan, J. & Francque, S. M. Therapeutic management of metabolic dysfunction associated steatotic liver disease. *United Eur. Gastroenterol. J.* **12**, 177–186 (2024).

36. Barb, D. *et al.* Pan-PPAR agonist lanifibranor improves insulin resistance and hepatic steatosis in patients with T2D and MASLD. *J. Hepatol.* **82**, 979–991 (2025).

37. Suki, M. *et al.* SGLT2 Inhibitors in MASLD (Metabolic Dysfunction-Associated Steatotic Liver Disease) Associated with Sustained Hepatic Benefits, Besides the Cardiometabolic. *Pharmaceuticals* **18**, 1118 (2025).

38. Vallin, M. *et al.* Recurrent or de novo nonalcoholic fatty liver disease after liver transplantation: natural history based on liver biopsy analysis. *Liver Transplant. Off. Publ. Am. Assoc. Study Liver Dis. Int. Liver Transplant. Soc.* **20**, 1064–1071 (2014).

39. Karger, B. & Guttman, A. DNA Sequencing by Capillary Electrophoresis. *Electrophoresis* **30**, 196–202 (2009).

40. Collins, F. & Fink, L. The Human Genome Project. *Alcohol Health Res. World* **19**, 190–195 (1995).

41. Briney, E. The International Human Genome Project. *Hum. Mol. Genet.* **30**, 161–163 (2021).

42. Ikegawa, S. A Short History of the Genome-Wide Association Study: Where We Were and Where We Are Going. *Genomics Inform.* **10**, 220–225 (2012).

43. Pei, Y. & Goh, G. Genetic Risk Factors for Metabolic Dysfunction-Associated Steatotic Liver Disease. *Gut Liver* **19**, 8–18 (2025).

44. Huang, Y., He, S., Li, J. Z. & Hobbs, H. H. A feed-forward loop amplifies nutritional regulation of PNPLA3. *PNAS* **107**, (2010).

45. Yu, L., Li, Y., Grisé, A. & Wang, H. CGI-58: Versatile Regulator of Intracellular Lipid Droplet Homeostasis. *Adv. Exmerimental Med. Biol.* **1276**, (2020).

46. Minehira, K., Young, S. G. & Villanueva, C. J. Blocking VLDL secretion causes hepatic steatosis but does not affect peripheral lipid stores or insulin sensitivity in mice. *J. Lipid Res.* **49**, 2038–2044 (2008).

47. Johnson, S. *et al.* PNPLA3 is a triglyceride lipase that mobilizes polyunsaturated fatty acids to facilitate hepatic secretion of large-sized very low-density lipoprotein. *Nat. Commun.* **15**, (2024).

48. Sherman, D. *et al.* PNPLA3-I148M is a neomorph that interferes with two primary hepatic triglyceride clearance pathways. *Cell Rep.* **44**, (2025).

49. BasuRay, S. PNPLA3-I148M: a problem of plenty in non-alcoholic fatty liver disease. *Adipocyte* **8**, 201–208 (2019).

50. Petta, S., Armandi, A. & Bugianesi, E. Impact of PNPLA3 I148M on Clinical Outcomes in Patients With MASLD. *Liver Int.* **45**, (2024).

51. Chen, L.-Z. *et al.* PNPLA3 I148M variant in nonalcoholic fatty liver disease: Demographic and ethnic characteristics and the role of the variant in nonalcoholic fatty liver fibrosis. *World J. Gastroenterol.* **21**, 794–802 (2015).

52. Pirazzi, C., Adiels, M. & Burza, M. A. Patatin-like phospholipase domain-containing 3 (PNPLA3) I148M (rs738409) affects hepatic VLDL secretion in humans and in vitro. *J. Hepatol.* **57**, 1276–1282 (2012).

53. Sulaiman, S. A., Dorairaj, V. & Adrus, M. N. H. Genetic polymorphisms and diversity in nonalcoholic fatty liver disease (NAFLD): A mini review. *Biomedicines* **11**, 1–23 (2023).

54. Mancina, R., Matikainen, N. & Maglio, C. Paradoxical dissociation between hepatic fat content and de novo lipogenesis due to PNPLA3 sequence variant. *J. Clin. Endocrinol. Metab.* **100**, 821–825 (2015).

55. Gou, Y., Wang, L. & Zhao, J. PNPLA3-I148M Variant Promotes the Progression of Liver Fibrosis by Inducing Mitochondrial Dysfunction. *Int. J. Mol. Sci.* **24**, (2023).

56. Najafi, M., Rafiei, A., Ghaemi, A. & Hosseini, V. Association between rs738408, rs738409 and rs139051polymorphisms in PNPLA3 gene and non-alcoholic fatty liver disease. *Gene Rep.* **26**, (2022).

57. McCarthy, C., Carrea, A. & Diambra, L. Bicodon bias can determine the role of synonymous SNPS in human diseases. *BMC Genomics* **18**, (2017).

58. Buhr, F., Jha, S. & Thommen, M. Synonymous Codons Direct Cotranslational Folding toward Different Protein Conformations. *Mol. Cell* **61**, 341–351 (2016).

59. Tsai, C.-J., Sauna, Z. E. & Kimchi-Sarfaty, C. Synonymous Mutations and Ribosome Stalling Can Lead to Altered Folding Pathways and Distinct Minima. *J. Mol. Biol.* **383**, 281–291 (2008).

60. Santoro, N. *et al.* Hepatic Fat Accumulation Is Modulated by the Interaction between the rs738409 Variant in the PNPLA3 Gene and the Dietary Omega6/Omega3 PUFA Intake. *PLoS One* **7**, (2012).

61. Harayama, T. & Shimizu, T. Roles of polyunsaturated fatty acids, from mediators to membranes. *J. Lipid Res.* **61**, 1150–1160 (2020).

62. Mititelu, M. *et al.* Polyunsaturated Fatty Acids and Human Health: A Key to Modern Nutritional Balance in Association with Polyphenolic Compounds from Food Sources. *Foods* **14**, (2024).

63. Willis, S. A. *et al.* The role of hepatic lipid composition in obesity-related metabolic disease. *Liver Int.* **41**, 2819–2835 (2021).

64. Ariyama, H., Kono, N., Matsuda, S., Inoue, T. & Arai, H. Decrease in membrane phospholipid unsaturation induces unfolded protein response. *J. Biol. Chem.* **285**, 22027–22035 (2010).

65. Chen, Y.-F. *et al.* n-3 polyunsaturated fatty acids in phospholipid or triacylglycerol form attenuate nonalcoholic fatty liver disease via mediating cannabinoid receptor 1/adiponectin/ceramide pathway. *J. Nutr. Biochem.* **123**, (2024).

66. Qiu, B. *et al.* Phospholipids with two polyunsaturated fatty acyl tails promote ferroptosis. *Cell* **187**, 1177-1190.e18 (2024).

67. Li, J. *et al.* Ferroptosis: past, present and future. *Cell Death Dis.* **11**, (2020).

68. Sokol, K. *et al.* Lipid availability influences ferroptosis sensitivity in cancer cells by regulating polyunsaturated fatty acid trafficking. *Cell Chem. Biol.* **32**, 408–422 (2025).

69. Cui, S. & Ye, J. MAFLD: a ferroptotic disease. *Trends Mol. Med.* **32**, 284–294 (2026).

70. Peleman, C., Francque, S. & Berghe, T. Emerging role of ferroptosis in metabolic dysfunction-associated steatotic liver disease: revisiting hepatic lipid peroxidation. *eBioMedicine* **102**, (2024).

71. Liu, Y. *et al.* Involvement of ferroptosis in metabolic dysfunction-associated steatohepatitis-related liver diseases. *J. Mol. Med.* **103**, 1299–1315 (2025).

72. Liu, N. *et al.* Regulation of FSP1 myristoylation by NADPH: A novel mechanism for ferroptosis inhibition. *Redox Biol.* **73**, 103176 (2024).

73. Doll, S. *et al.* FSP1 is a glutathione-independent ferroptosis suppressor. *Nature* **575**, 693–698 (2019).

74. Sies, H. *et al.* Defining roles of specific reactive oxygen species (ROS) in cell biology and physiology. *Nat. Rev. Mol. Cell Biol.* **23**, 499–515 (2022).

75. Schieber & Chandel, N. ROS Function in Redox Signaling and Oxidative Stress. *Curr. Biol.* **24**, 453–462 (2015).

76. Allameh, A., Niayesh-Mehr, R., Aliarab, A., Sebastiani, G. & Pantopoulos, K. Oxidative Stress in Liver Pathophysiology and Disease. *Antioxidants* **12**, (2023).

77. Su, L.-J. *et al.* Reactive Oxygen Species-Induced Lipid Peroxidation in Apoptosis, Autophagy, and Ferroptosis. *Oxid. Med. Cell. Longev.* **2019**, 5080843 (2019).

78. Sharma, S., Khandelwal, R., Yadav, K., Ramaswamy, G. & Vohra, K. Effect of cooking food in iron-containing cookware on increase in blood hemoglobin level and iron content of the food: A systematic review. *Nepal J. Epidemiol.* **11**, 994–1005 (2021).

79. Puig, S., Ramos-Alonso, L., Romero, A. & Martinez-Pastor, M. The elemental role of iron in DNA synthesis and repair. *Metallomics* **9**, 1483–1500 (2017).

80. Roemhild, K. *et al.* Iron metabolism: Pathophysiology and Pharmacology. *Trends Pharmacol. Sci.* **42**, 640–656 (2021).

81. Wang, S., Guo, Q., Zhou, L. & Xia, X. Ferroptosis: A double-edged sword. *Cell Death Discov.* **10**, 265 (2024).

82. Zelber-Sagi, S. *et al.* Serum Malondialdehyde is Associated with Non-Alcoholic Fatty Liver and Related Liver Damage Differentially in Men and Women. *Antioxidants* **9**, (2020).

83. Dierge, E. *et al.* Peroxidation of n-3 and n-6 polyunsaturated fatty acids in the acidic tumor environment leads to ferroptosis-mediated anticancer effects. *Cell Metab.* **33**, 1701–1715 (2021).

84. Mortensen, M. S., Ruiz, J. & Watts, J. L. Polyunsaturated Fatty Acids Drive Lipid Peroxidation during Ferroptosis. *Cells* **12**, 804 (2023).

85. Qadri, S. *et al.* The PNPLA-I148M variant increases polyunsaturated triglycerides in human adipose tissue. *Liver Int.* **40**, 2128–2138 (2020).

86. Florentino, R. M. *et al.* PNPLA3-I148M genetic variant rewires lipid metabolism to drive programmed cell death in human hepatocytes. *JCI Insight* **10**, e193805 (2025).

87. TeSlaa, T., Ralser, M., Fan, J. & Rabinowitz, J. D. The pentose phosphate pathway in health and disease. *Nat. Metab.* **5**, 1275–1289 (2023).

88. Ting, K. *et al.* Measuring the rate of NADPH consumption by glutathione reductase in the cytosol and mitochondria. *PLoS One* **19**, (2024).

89. Covarrubias, A. J., Perrone, R., Grozio, A. & Verdin, E. NAD+ metabolism and its roles in cellular processes during ageing. *Nat. Rev. Mol. Cell Biol.* **22**, 119–141 (2021).

90. Zhang, J. *et al.* Emerging strategies, applications and challenges of targeting NAD+ in the clinic. *Nat. Aging* **5**, 1704–1731 (2025).

91. Mukherjee, S. *et al.* Nicotinamide adenine dinucleotide biosynthesis promotes liver regeneration. *Hepatol. Baltim. Md* **65**, 616–630 (2017).

92. Paolini, E. *et al.* The I148M PNPLA3 variant mitigates niacin beneficial effects: How the genetic screening in non-alcoholic fatty liver disease patients gains value. *Front. Nutr.* **10**, 1101341 (2023).

93. Basantani, M. K., Sitnick, M. T. & Cai, L. Pnpla3/Adiponutrin deficiency in mice does not contribute to fatty liver disease or metabolic syndrome. *J. Lipid Res.* **52**, 318–329 (2011).

94. Research, N. R. C. (US) and I. of M. (US) C. on the B. and B. A. of S. C. Embryonic Stem Cells. in *Stem Cells and the Future of Regenerative Medicine* (National Academies Press (US), 2002).

95. Takahashi, K. & Yamanaka, S. Induction of Pluripotent Stem Cells from Mouse Embryonic and Adult Fibroblast Cultures by Defined Factors. *Cell* **126**, 663–676 (2006).

96. Ishino, Y., Shinagawa, H., Makino, K., Amemura, M. & Nakata, A. Nucleotide sequence of the iap gene, responsible for alkaline phosphatase isozyme conversion in Escherichia coli, and identification of the gene product. *J. Bacteriol.* **169**, 5429–5433 (1987).

97. Bolotin, A., Quinquis, B., Sorokin, A. & Ehrlich, S. D. Clustered regularly interspaced short palindrome repeats (CRISPRs) have spacers of extrachromosomal origin. *Microbiology* **151**, 2551–2561 (2005).

98. Liao, C. & Beisel, C. L. The tracrRNA in CRISPR biology and technologies. *Annu. Rev. Genet.* **55**, 161–181 (2021).

99. Jinek, M. *et al.* A Programmable Dual-RNA–Guided DNA Endonuclease in Adaptive Bacterial Immunity. *Science* **337**, (2012).

100. Varble, A. & Marraffini, L. The CRISPR-Cas system of Streptococcus pyogenes: function and applications. in *Streptococcus pyogenes: Basic Biology to Clinical Manifestations* (eds. Ferretti, J. J., Stevens, D. L. & Fischetti, V. A.) (University of Oklahoma Health Sciences Center, Oklahoma City (OK), 2022).

101. Bialk, P., Rivera-Torres, N., Strouse, B. & Kmiec, E. B. Regulation of Gene Editing Activity Directed by Single-Stranded Oligonucleotides and CRISPR/Cas9 Systems. *PLoS ONE* **10**, e0129308 (2015).

102. Liao, H., Wu, J., VanDusen, N. J., Li, Y. & Zheng, Y. CRISPR-Cas9-mediated homology-directed repair for precise gene editing. *Mol. Ther. Nucleic Acids* **35**, 102344 (2024).

103. O'Brien, A. R., Wilson, L. O. W., Burgio, G. & Bauer, D. C. Unlocking HDR-mediated nucleotide editing by identifying high-efficiency target sites using machine learning. *Sci. Rep.* **9**, 2788 (2019).

104. Li, H., Bartke, R., Zhao, L., Verma, Y. & Hockemeyer, D. Functional annotation of variants of the BRCA2 gene via locally haploid pluripotent stem cells. *Nat. Biomed. Eng.* **8**, 165–176 (2023).

105. Krivec, N., Ghosh, M. S. & Spits, C. Gains of 20q11.21 in human pluripotent stem cells: Insights from cancer research. *Stem Cell Rep.* **19**, 11–27 (2023).

106. Gavril, O., Arhire, L. & Gavril, R. Correlations between PNPLA3 gene polymorphisms in type 2 diabetic patients. *Medicina (Mex.)* **57**, 1–11 (2021).

107. Ang, L. T., Tan, A. K. Y., Autio, M. I. & Goh, S. A Roadmap for Human Liver Differentiation from Pluripotent Stem Cells. *Cell Rep.* **22**, 2190–2205 (2018).

108. Qi, L., Groeger, M., Sharma, A. & Goswami, I. Adipocyte inflammation is the primary driver of hepatic insulin resistance in a human iPSC-based microphysiological system. *Nat. Commun.* **15**, (2024).

109. Kotulkar, M., Robarts, D. R. & Udayan, A. HNF4alpha in hepatocyte health and disease. *Semin. Liver Dis.* **43**, 234–244 (2023).

110. Roll, G. R. & Willenbring, H. Transplanted nonviable human hepatocytes produce appreciable serum albumin levels in mice. *Stem Cell Res.* **5**, (2010).

111. Wang, J., Ye, D., Li, S. & Lu, X. Generation of human induced pluripotent stem cells carrying albumin-sfGFP reporter. *Stem Cell Res.* **81**, (2024).

112. Komatsu, M. *et al.* NNMT activation can contribute to the development of fatty liver disease by modulating the NAD + metabolism. *Sci. Rep.* **8**, 8637 (2018).

113. Wright, M. H., Heal, W. P., Mann, D. J. & Tate, E. W. Protein myristoylation in health and disease. *J. Chem. Biol.* **3**, 19–35 (2009).